Master’s Thesis

Optimal Guidance and Control for Electromagnetic Formation Flying

（磁気フォーメーションフライトのための最適誘導・制御に関する研究）

August – 2019

Department of Electrical Engineering and Information Systems

The School of Engineering

The University of Tokyo

37-175073 Abdulla Ayyad

Supervisor: Prof. Tatsuaki Hashimoto

Abstract

Satellite Formation Flying (FF) is amongst the most enabling space technologies that would allow for a more flexible and functional design for future space missions. One active area of research in this field is maintaining formation stability and controllability without the use of propellants; in order to maximize mission lifetime and avoid thruster related problems. Among the most promising propellant-less FF technologies is Electromagnetic FF (EMFF). As the name suggests, EMFF refers to the concept of controlling the relative degrees of freedom in a formation by using superconducting electromagnets and harnessing the resultant magnetic interactions.

Despite the high potential and relative maturity of EMFF, several challenges still confine its actual deployment. For instance, the current state of superconducting electromagnets is a serious limitation in EMFF as they are still prone to faults and heating. This, in turn, jeopardizes the navigation and control capabilities of a formation. Additionally, the accumulation of electromagnetic torques can result in angular momentum build-up and the saturation of reaction wheels. This study aims to tackle these two shortcomings by incorporating them in the guidance and control processes in two different means. The first approach exploits the modulation of electromagnetic fields in phase and frequency to expand the range of possible magnetic interactions. The second method relies on finding optimal trajectories that would reconfigure a formation as desired while minimizing any undesired behavior.

In this thesis, the translational and rotational dynamics of an N-spacecraft orbiting electromagnetic formation are first investigated and summarized. Subsequently, appropriate control laws based on Lyapunov's direct method and dynamic inversion are constructed. These control laws are then adjusted to optimize EMFF performance in terms of the aforementioned problems. Afterward, optimal trajectory generation using Legendre Pseudospectral method is implemented to further enhance the EMFF reconfiguration problem. Closed-loop simulations were carried out to verify the validity and capability of the proposed approaches in improving EMFF performance. The results presented in this thesis confirm that enhanced guidance and control methods can be the key to realizing the fully propellant-less formation flying goal.

Acknowledgment

I would like to express my sincere appreciation to my supervisor Prof. Tatsuaki Hashimoto for his invaluable guidance and assistance over my two years stay in the Institute of Space and Astronautical Science. I am also grateful to all the member of the Spacecraft Control and Robotics lab for all the rich conversations and enlightening discussions. My gratitude also goes to the staff of the International Multidisciplinary Engineering program at the University of Tokyo for their constant support. Last but definitely not least, I would like to thank my parents for to them I attribute any success in my life.

Table of Contents

List of Figures

List of Tables

Chapter 1. Introduction

1.1. Motivation & Background

Formation Flying (FF) refers to the idea of flying multiple spacecrafts while maintaining a fixed or time-varying configuration. FF has gained much attention over the years as it can offer advantages in terms of functionality, efficiency and cost reduction [1, 2, 3]. Additionally, the distributed nature of FF allows for better adaptability, scalability, evolvability, maintainability and robustness [1]. Tens of FF missions in areas of space and planetary science, remote sensing and earth observation have been proposed and researched by several research institutions around the world [1, 2]. Figure 1 shows some of the well-known FF missions. ESA's Proba-3 for example is a coronagraph mission that creatively utilizes FF where one spacecraft covers the disc of the sun while the other images the sun corona [4]. The TPF-1 is multi-spacecraft interferometer suggested by NASA [5] and the XEUS is a long telescope concept proposed by ESA [6]. FF technologies can also be essential for spacecraft rendezvous as is the case with Caltech's AAReST [7].

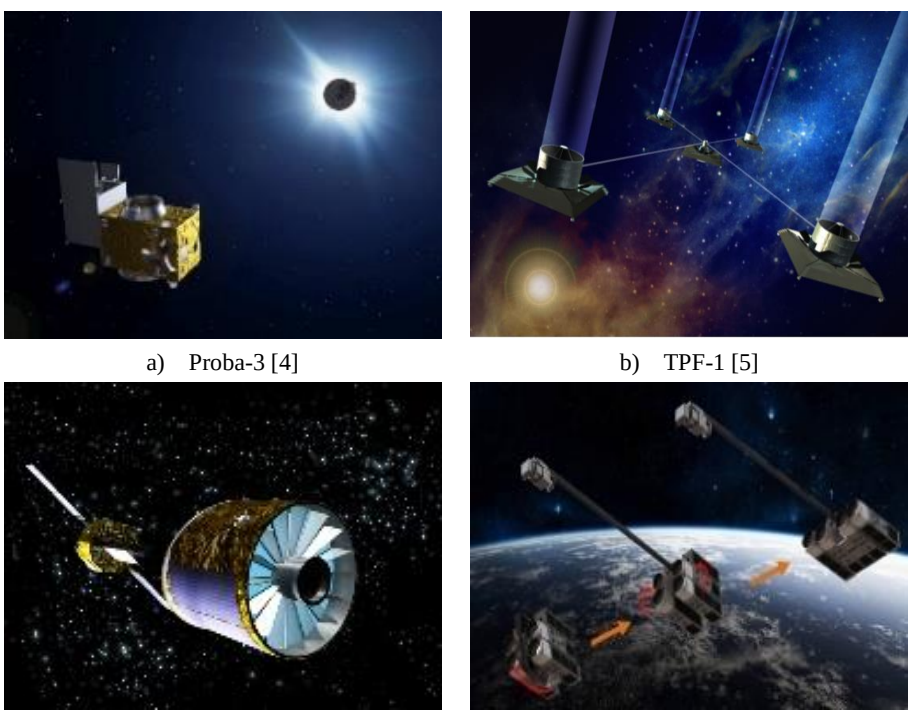

a) Proba-3 [4]

b) TPF-1 [5]

c) XEUS [6]

d) AAReST [7]

Figure 1. Proposed FF missions

The unstable nature of orbiting formations means that continuous control effort or thrust must be applied to maintain a desired formation [8]. Therefore, the lifetime of a conventional formation flying mission that relies on thrusters is significantly shortened due to finite fuel. Moreover, thruster-based FF has the problem of plume impingement which can cause disturbance forces, undue heating and particle contamination on the formation's spacecrafts, which in turn affects the accuracy and performance of the sensors installed in the system [9].

These problems with thruster-based FF have given rise to the need for propellant-less alternatives. One such alternative is Electrostatic (or Coulomb) FF, in which a group of satellites are controlled by relative electrostatic forces and torques, where these interactions are generated by regulating the charge on the surface of these spacecrafts [10]. Lorentz FF is another means of formation control which relies on electrostatic charge control. However, rather than exploiting the relative interactions between the formation's spacecrafts, Lorentz FF utilizes forces generated between charged vehicles and earth's magnetic field [11]. Other research investigates formations with physical tethers connecting the spacecrafts in what is known as Tethered FF [9]. Each of these methods offers certain advantages that can make them more suitable for specific scenarios. However, either their limited degree of controllability or low technology readiness level makes them a less attractive choice for a lot of the proposed FF missions.

Electromagnetic Formation Flying (EMFF), which is the main focus of this study, is another propellant less FF technology that mitigates a lot of the challenges faced by the aforementioned FF approaches. EMFF relies on utilizing High-Temperature Superconducting (HTS) electromagnets to generate strong magnetic dipoles at different spacecrafts of a formation, which would then interact yielding relative forces and torques affecting the dynamics of the formation. This concept allows for full controllability of either translational or rotational motion, and in specific cases, it can be sufficient to control both position and attitude. Moreover, HTS electromagnets are already being used in a variety of applications from Magnetic Resonance Imaging (MRI) [12] to magnetic levitation (Maglev) trains [13]. EMFF merely extends the use of HTS technology to space systems and employs it in satellite formation control. As such, EMFF offers a favorable balance between controllability, maturity and future potential and is considered to be among the most mature and promising propellant-less FF methods. Subsequently, EMFF has

been proposed to maintain and reconfigure formations in Low Earth Orbit (LEO) with separation distances up to tens of meters [14, 15, 16] without the need of any propellants.

The most common EMFF configuration equips each spacecraft with three orthogonal electromagnets to mimic a fully steerable magnetic dipole [15, 17]. These dipoles are utilized to generate controlled forces in any arbitrary direction to manipulate the translational degrees of freedom. This configuration also relies on reaction wheels to control the attitude and compensate for electromagnetic torques.

Controlling EMFF configurations have been studied extensively in the literature for deep space and orbiting constellations. Linear and non-linear control laws have been developed for many types of formations taking into consideration the highly nonlinear and coupled dynamics of EMFF [15, 17, 18, 19, 20]. EMFF was experimentally verified on a testbed on earth [21], as well as in an experiment abroad the ISS [22]. The testbed is a 2D model of EMFF consisting of two model spacecrafts. It was used to validate EMFF's concept and several associated control policies. On the other hand, the ISS experiment was implemented to simply verify the dynamic model of EMFF. Figure 2 shows the hardware setup for both experiments.

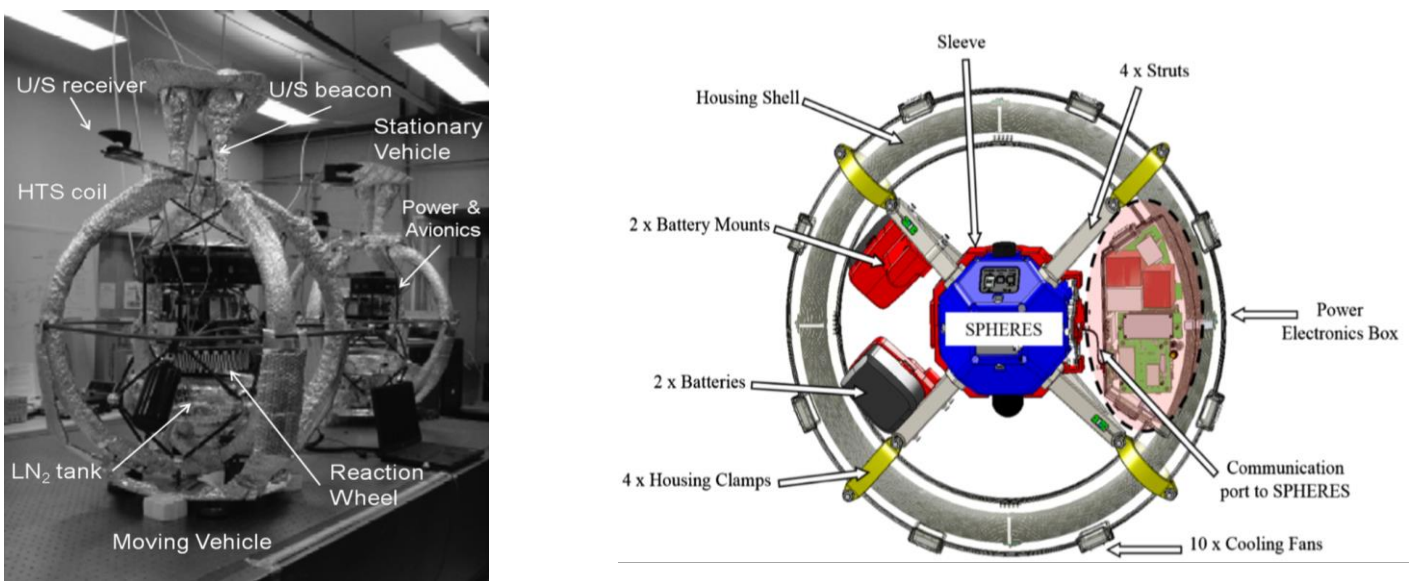

a) EMFF testbed [15]

b) EMFF experiment onboard the ISS [22]

Figure 2. Hardware setup for EMFF experiments

Despite the high potential and relative maturity, EMFF still faces several problems that are preventing functional deployment. One major challenge lies in the high number of electromagnets

required in EMFF, which significantly adds to the overall cost and mass of launching a formation. Furthermore, EMFF relies on HTS electromagnets which require to be cooled below a critical temperature to maintain a non-resistive state [23]. Consequently, overheating and thermal accumulation can terminate the operation of the respective electromagnet [24]. The loss or fault of an electromagnet can then jeopardize the controllability of the entire formation. Reference [25] attempted to tackle this issue by rotating the spacecrafts themselves to create steerable dipoles. This approach enables control of the translational degrees of freedom but sacrifices the ability to freely control the spacecrafts' attitude, which severely disturbs the objectives of launching a formation. Therefore, it is highly desirable to find means of controlling a formation with a minimal number of electromagnets without disturbing its functionality.

Another problem facing EMFF is angular momentum buildup in the formation's satellites. The strong magnetic interactions can cause undue torques that accumulate through time resulting in angular momentum buildup. These magnetic torques are either due either to the interactions between different electromagnets among each other or with earth's magnetic field. This buildup causes the reaction wheels to saturate and disables the attitude control functionality. One solution to this problem lies in optimizing the magnetic interactions between the formation's electromagnets to minimize the generated torque as suggested in ref. [16]. This technique can reduce the accumulated torque during the execution of maneuvers, but this reduction is limited and is not a sufficient solution on the long term. Another possible way to undermine this issue is periodically switching the polarity of all dipoles in the formation. This would keep the relative interactions between dipoles identical but eliminates the effect of the geomagnetic field. Based on the above solution, ref. [14] proposed exciting the electromagnets using sinusoidal current leading to alternating magnetic moments. The studies in refs. [26, 27] build on this by utilizing earth's magnetic field for angular momentum reduction. While promising results were obtained for alleviating this problem, it remains a serious concern for EMFF and further reduction methods are needed.

1.2. Research Objectives

It is apparent from the literature that several gaps still exist in EMFF research. For instance, few studies have considered the case where less than three electromagnets are available per spacecraft. Reducing the number of electromagnets installed on each spacecraft while maintaining 6-DoF controllability can ease cost and mass requirements for building and launching a cluster of spacecrafts to space. Therefore, it is highly advantageous to investigate and control such underactuated cases. This becomes more important when considering that in its current state, HTS electromagnets are prone to overheating faults which would restrict the limit of either the translational or rotational degrees of freedom in a formation. It can also be beneficial to develop control algorithms that prevent excessive thermal accumulation in any of the electromagnets.

Angular momentum buildup is another issue that requires further investigation in EMFF. While utilizing earth's magnetic field showed potential in addressing this problem, limitations still exist due to the restricted directions of torque the geomagnetic field can provide. It is possible that the effects of these limitations can be mitigated or alleviated if they were taken into consideration within the formation's guidance and control structure. This concept is still not studied in the literature and its effectiveness is yet to be evaluated.

Taking the above into account, this research aims to tackle the current shortcomings in EMFF identified as:

- EMFF control under minimal availability of superconducting electromagnets.
- Preventive thermal management of EMFF electromagnets.
- Angular momentum management for EMFF.

Two approaches were adopted to tackle the aforementioned challenges. The first approach lies in employing phase and frequency modulation of alternating magnetic fields to optimize magnetic interactions among the spacecrafts of the formation. Reference [14] demonstrated how varying the phase angle of alternating magnetic moments affects the forces in an EMFF formation, and presented a practical method of manipulating this phase angle in superconducting electromagnets. However, the advantages of such modulation were not exploited in that study. Reference [26] on the other hand utilized alternating magnetic moments at different frequencies to

decouple different EMFF satellites and simplify the control process. Other studies apply similar concepts as well [28], but none consider phase and frequency modulation for the purposes alleviating the EMFF problems discussed above. This thesis builds upon previous studies and aims to examine the additional advantages modulation can present for EMFF.

The second approach employs recent advancements in optimal control theory to generate trajectories that improve EMFF performance with respect to a target criterion. The coupled and nonlinear dynamics of orbiting electromagnetic formations make them very sensitive to trajectory variations. Therefore, it becomes essential to find the best possible path to reconfigure a formation given initial and target positions. For this purpose, a joint theoretical-computational approach referred to as Pseudo-spectral Optimal Control is utilized in this study due to its simplicity, accuracy, and applicability.

1.3. Thesis Overview

The remainder of this thesis thoroughly investigates electromagnetic formations to realize the objectives described in section 1.2. Chapter 2 first presents the translational and rotational dynamics associated with satellite formations in earth orbit. In the case of EMFF, the two main sources of forces and torques are the gravitational and electromagnetic effects, both of which are reviewed in that chapter. The equations of motion demonstrated in chapter 2 become the building blocks of all mathematical derivations and closed-loop simulations presented in the following sections of the study.

Chapter 3 utilizes the reviewed system dynamics to develop control laws for the relative position and attitude of N-spacecraft formations. For position control, a combination of terminal sliding mode control and dynamic inversion is applied to effectively employ superconducting electromagnets to reconfigure the formation. On the other hand, Lyapunov's direct method is applied to the classical configuration of three orthogonal reaction wheels to control the attitude of each satellite separately. Simulations results are then presented to validate the proposed control approach.

Chapter 4 tackles the first EMFF problem within the objectives of this research: formation control under minimal availability of electromagnets. It augments the control scheme of chapter 3 with the ability to modulate electromagnetic fields in phase and frequency to increase the diversity of possible electromagnet interactions. This added diversity becomes the key to undermine the effects of removing several electromagnets from the formation's satellites. Following a similar approach, chapter 5 optimizes electromagnetic interaction to alleviate the other two shortcomings of EMFF: angular momentum buildup and thermal accumulation.

Chapter 6 adopts a different approach to enhance EMFF operation by optimizing trajectories for formation reconfiguration problems. The strong relationship between electromagnetic interactions and separation distances translates into the high sensitivity of EMFF to the reference paths or trajectories. This feature is exploited and a Pseudospectral optimal control method is employed for this objective. Finally, chapter 7 summarizes the results and findings of this study and provides recommendations for future work.

Chapter 2. EMFF Dynamics

The process of controlling or enhancing a dynamical system always starts with understanding the equations of motion governing its behavior. This chapter reviews and presents the dynamics of spacecraft formations in an earth orbit. These equations become the basis of developing guidance and control strategies later in this study, as well as establishing numerical simulations to verify these strategies. First, the effects of orbital dynamics on the relative translational motion of a formation are examined and demonstrated. Then, Electromagnetic interactions, along with the idea of modulating magnetic fields are investigated. Afterward, the rotational properties of each satellite in the formation are thoroughly analyzed to be later used in attitude control. External effects such as the geomagnetic field and gravity gradient torques are also briefly summarized in this chapter. Finally, a realistic spacecraft design is presented to ensure the sensibility of the upcoming stages of this study.

2.1. Dynamics of Orbiting Satellite Formations

Orbital dynamics play a dominant part in the relative motion of orbiting satellite formations. As such, it is crucial to incorporate orbital effects in the analysis of FF systems. This section examines the translational dynamics of satellite formations in a near-earth orbit as in Figure 3.

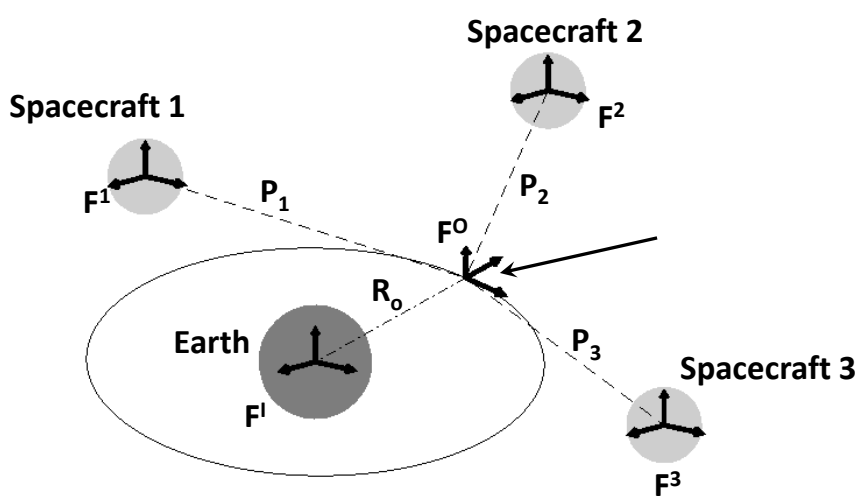

Figure 3. In orbit spacecraft formation

First, an Earth Centered Inertial (ECI) frame F^I is defined as:

$$F^I: \{\hat{I}, \hat{J}, \hat{K}\}. \tag{1.}$$

Where $\hat{I}$ points towards the vernal equinox, $\hat{K}$ points towards the geographic north pole and $\hat{J}$ completes the right-hand system.

Introducing the vector $\vec{R}_i$ as the position of the ith spacecraft of the formation relative to Earth's center, the equation of motion of this spacecraft can be represented as:

$$\ddot{\vec{R}}_i = \vec{g}\left(\vec{R}_i\right) + \vec{J}_2\left(\vec{R}_i\right) + \frac{\vec{f}_i^C + \vec{f}_i^D}{m_i}. \tag{2.}$$

Where $g\left(\vec{R}_i\right)$ is the gravitational acceleration due to a spherical earth, $\vec{J}_2\left(\vec{R}_i\right)$ is the acceleration due to the J_2 earth oblateness potential, $\vec{f}_i^C$ represents control forces and $\vec{f}_i^D$ corresponds to other disturbance forces. $g\left(\vec{R}_i\right)$ and $\vec{J}_2\left(\vec{R}_i\right)$ can be calculated as presented in Eqs. (3) and (4) [29] respectively:

$$\vec{g}\left(\vec{R}_i\right) = \left(\frac{\mu_g}{R_i^3}\right)\vec{R}_i. \tag{3.}$$

$$\vec{J}_2\left(\vec{R}_i\right) = -\left(\frac{3}{2}\right)\left(\frac{J_2\mu_g R_e^2}{R_i^4}\right)\left[(1 - 3\,sin^2\,i_o\,sin^2\,\theta)\hat{\boldsymbol{x}}_{ref} + (2\,sin^2\,i_o\,sin\,\theta\,cos\,\theta)\hat{\boldsymbol{y}}_{ref} + (2\,sin\,i_o\,cos\,i_o\,sin\,\theta)\hat{\boldsymbol{z}}_{\boldsymbol{ref}}\right]. \tag{4.}$$

Where $\mu_g \approx 3.986 \times 10^{14}\ m^3/s^2$ is the standard gravitational parameter of earth, $J_2 = 1.082 \times 10^{-3}$ is the second zonal harmonics coefficient of earth's gravitational field, $R_e = 6.371 \times 10^6\ m$ is the mean radius of earth, i_o is the orbit inclination, θ is the argument of latitude. Finally, the coordinates $\{\hat{\boldsymbol{x}}_{ref}, \hat{\boldsymbol{y}}_{ref}, \hat{\boldsymbol{y}}_{ref}\}$ are defined as a Local vertical local horizontal (LVLH) coordinate system assuming a reference orbit not affected by the J_2 perturbations [29]. The $\hat{\boldsymbol{x}}_{ref}$ vectors points in the orbit radial direction, $\hat{\boldsymbol{z}}_{ref}$ is the orbit normal vector with the same direction as the angular momentum vector, and $\hat{\boldsymbol{y}}_{ref}$ completes the right-handed coordinate system.

In formation flying, the main objective is usually to control the relative position between different satellites rather than the absolute location of each spacecraft separately. The relative position of the ith spacecraft $\vec{p}_i$ can be described in reference to the center of mass of the entire formation $\vec{R}_o$ as:

$$\vec{p}_i = \vec{R}_i - \vec{R}_o \,. \tag{5.}$$

Controlling $\vec{p}_i$ is quite challenging using the equations of motions presented in Eq. (2). Therefore, several studies have targeted simplifying the representation of the relative dynamics in an orbiting satellite formation. Two common simplifications are the Hill-Clohessy-Wiltshire (HCW) equations and the Tschauner-Hempel (TH) equations [11]. The HCW equations represent the linearized relative dynamics in a circular orbit, while the TH equations extend the formulation to include elliptical orbits. It must be noted that neither the HCW nor the TH equations take earth's oblateness into account and simply treat the J_2 effects as disturbances.

Prior to examining these equations, an orbital frame F^O centered at the formation's center of mass is defined as:

$$F^O : \{\hat{x}, \hat{y}, \hat{z}\} \,. \tag{6.}$$

where $\hat{x}$ points opposite of the along-track direction, $\hat{y}$ points towards the orbit radial direction and $\hat{z}$ completes the right-handed coordinate system.

Considering the time derivate of the relative position vector with respect to F^O: $\frac{{}^{F^O}d}{dt}(\vec{p}_i) = \left\{\dot{p}_{i_x}, \dot{p}_{i_y}, \dot{p}_{i_z}\right\}$, the TH equations describe the relative equations of motion of each spacecraft as [11]:

$$\frac{{}^{F^O}d^2}{dt^2}(\vec{p}_i) + \begin{bmatrix} 0 & -2\dot{u} & 0 \\ 2\dot{u} & 0 & 0 \\ 0 & 0 & 0 \end{bmatrix} \frac{{}^{F^O}d}{dt}(\vec{p}_i) + \begin{bmatrix} -\dot{u}^2 + \frac{\mu}{R_o^3} & -\ddot{u} & 0 \\ \ddot{u} & -\dot{u}^2 - 2\frac{\mu}{R_o^3} & 0 \\ 0 & 0 & \frac{\mu}{R_o^3} \end{bmatrix} \vec{p}_i = \frac{\vec{f}_i^C + \vec{f}_i^D}{m_i} \,. \tag{7.}$$

Where u is the true anomaly of the orbit.

In the case of circular orbits, $\dot{u}$ becomes equal to the orbital frequency: $\omega_o = \sqrt{\mu_g / R_o^3}$ and $\ddot{u} = 0$. Equation (7) then simplifies to the well-known Hill-Clohessy-Wiltshire (HCW) equations which can be simply written as [18]:

$$\frac{{}^{F^O}d^2}{dt^2}(\vec{p}_i) + \vec{c}_i\left(\omega_o, \frac{{}^{F^O}d}{dt}(\vec{p}_i)\right) + \vec{g}_i(\omega_o, \vec{p}_i) = \frac{\vec{f}_i^C + \vec{f}_i^D}{m_i} \ . \tag{8.}$$

Where $\vec{c}_i$ and $\vec{g}_i$ represent a coriolis-like term and the gravitational term respectively and can be calculated as:

$$\vec{c}_i\left(\omega_o, \frac{{}^{F^O}d}{dt}(\vec{p}_i)\right) = \begin{bmatrix} 0 & -2\omega_o & 0 \\ 2\omega_o & 0 & 0 \\ 0 & 0 & 0 \end{bmatrix} \frac{{}^{F^O}d}{dt}(\vec{p}_i) \ , \tag{9.}$$

$$\vec{g}_i(\omega_o, \vec{p}_i) = \begin{bmatrix} 0 & 0 & 0 \\ 0 & -3\omega_o & 0 \\ 0 & 0 & \omega_o \end{bmatrix} \vec{p}_i \ . \tag{10.}$$

2.2. Magnetic Forces & Torques

The essential concept behind EMFF falls in generating magnetic dipoles with strong magnetic moments μ from superconducting electromagnets as governed by Eq. (11).

$$\mu = N_t \, A \, i_c \, . \tag{11.}$$

Where N_t is the number of coil turns, A is the cross-sectional area of the coil and i_c is the current running through the electromagnet.

A magnetic dipole generates a magnetic field as governed by Eq. (12), where $\vec{r}$ correspond to the displacement from the dipole and μ_o is the magnetic permeability.

$$\vec{B} = \frac{\mu_o}{4\pi}\left[\frac{3\,\vec{r}\,(\vec{\mu}\cdot\vec{r})}{r^5} - \frac{\vec{\mu}}{r^3}\right]. \tag{12.}$$

Different magnetic dipoles, as shown in Figure 4, would then interact yielding forces and torques which can be calculated using the far field approximation in by Eqs. (13) and (14).

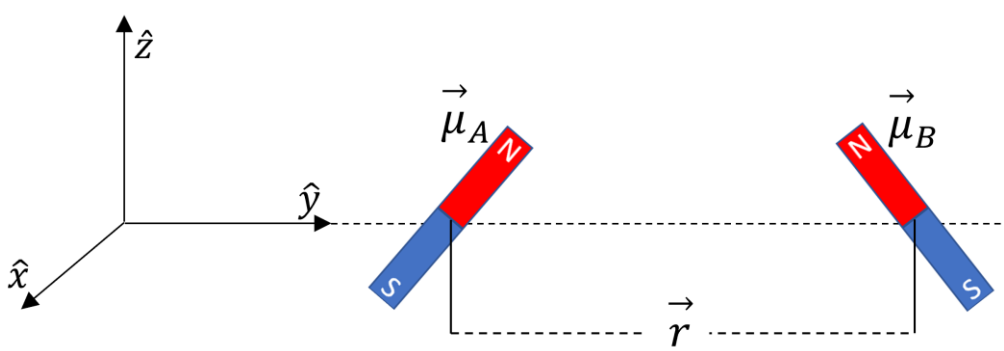

Figure 4. Magnetic dipoles' interaction

$$\vec{f}_M\left(\vec{\mu}_A,\vec{\mu}_B\right) = \frac{3\mu_o}{4\pi}\left(-\frac{\vec{\mu}_A\cdot\vec{\mu}_B}{r^5}\vec{r} - \frac{\vec{\mu}_A\cdot\vec{r}}{r^5}\vec{\mu}_B - \frac{\vec{\mu}_A\cdot\vec{r}}{r^5}\vec{\mu}_A + 5\frac{(\vec{\mu}_A\cdot\vec{r})(\vec{\mu}_B\cdot\vec{r})}{r^7}\vec{r}\right), \tag{13.}$$

$$\vec{\tau}_M\left(\vec{\mu}_A,\vec{\mu}_B\right) = \vec{\mu}_A \times \frac{\vec{\mu}_o}{4\pi}\left(\frac{\vec{\mu}_B}{r^3} + 3\frac{\vec{\mu}_B\cdot\vec{r}}{r^5}\vec{r}\right). \tag{14.}$$

Where

$$\vec{f}_M\left(\vec{\mu}_A,\vec{\mu}_B\right) = -\vec{f}_M\left(\vec{\mu}_B,\vec{\mu}_A\right). \tag{15.}$$

But

$$\vec{\tau}_M\left(\vec{\mu}_A,\vec{\mu}_B\right) \neq -\vec{\tau}_M\left(\vec{\mu}_B,\vec{\mu}_A\right) \ . \qquad (16.)$$

The concept of EMFF can be simply explained as artificially generating magnetic moments $\vec{\mu}$ at different satellites and harnessing the resultant interactions. The control of electromagnetic formations becomes the problem of finding appropriate magnetic moments for all the spacecrafts in that would result in desired forces or torques.

In order to guarantee full position controllability considering only this phenomenon, an electromagnetic formation must be capable of generating forces in unrestrained directions. To do so, the magnetic dipoles must be fully steerable in 3D, such that it is possible to assign any arbitrary magnetic moment vector $\vec{\mu}$ to any spacecraft in the formation. The most straightforward method of creating such a steerable dipole is utilizing three orthogonal electromagnets as shown in Figure 5. Where by controlling the strength of these orthogonal dipoles, an equivalent inclined dipole is yielded. Additionally, reaction wheels can be augmented to compensate for the disturbance electromagnetic torques effectively control the attitude.

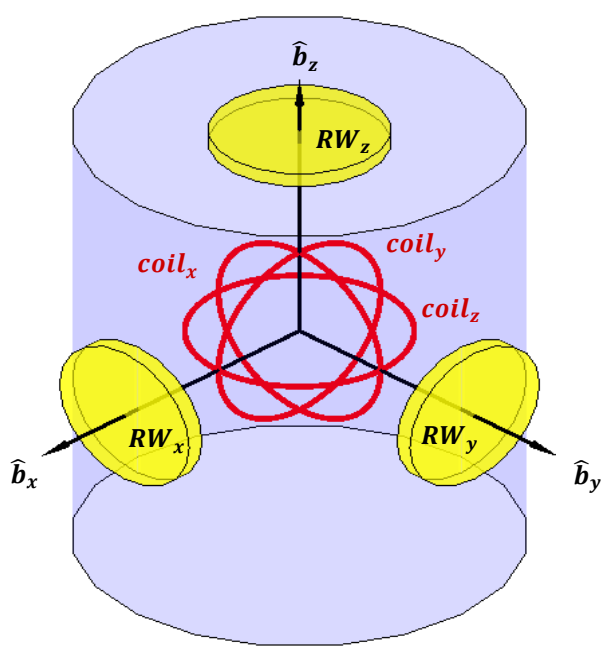

Figure 5. EMFF spacecraft configuration

2.3. Phase & Frequency Modulation of Alternating Magnetic Moments

The use of alternating magnetic moments for EMFF was first proposed to decouple earth's magnetic field from the formation [14]. This is done by exciting the superconducting electromagnets with sinusoidal current, leading to sinusoidal magnetic moments. The magnetic moment of an electromagnet in the formation can then be written as:

$$\vec{\mu}_A(t) = \vec{\mu}_A \, cos\left(\omega_{f_A} t + \phi_A\right) \ . \tag{17.}$$

In addition to decoupling earth's magnetic field, this allows for a higher level of manipulation by varying the frequency ω_f and phase ϕ. Sections 2.3.1 and 2.3.2 illustrate how modulating this phase and frequency affects the interactions between multiple magnetic moments.

2.3.1. Phase Modulation

As the name suggests, phase modulation is concerned with varying the phase ϕ of alternating magnetic moments. By varying the phase of multiple magnetic moments, the interactions between these moments is affected. Considering the case of two electromagnets producing different alternating magnetic moments: $\vec{\mu}_A(t)$ and $\vec{\mu}_B(t)$, each with their own phase ϕ_A and ϕ_B, but the same frequency ω_f. Following the far field dipole model in Eq. (13), the force between these two electromagnets can be calculated as:

$$\vec{f}_{AB}(t) = \vec{f}_M\left(\vec{\mu}_A, \vec{\mu}_B\right) \cdot cos\left(\omega_f t + \phi_A\right) \cdot cos\left(\omega_f t + \phi_B\right) \ . \tag{18.}$$

Using trigonometric identities and taking the average along one sinusoidal cycle, the average force between μ_A and μ_B becomes:

$$\vec{f}_{AB_{avg}} = 0.5\vec{f}_M\left(\vec{\mu}_A, \vec{\mu}_B\right) \cdot \cos(\phi_A - \phi_B) \ . \tag{19.}$$

It can be easily inferred from Eq. (19) that the force between two electromagnets differs by varying the phase of their sinusoidal excitation. For instance, if the phase difference is 90°, the average resultant force would be zero and the two magnetic moments would be decoupled.

An easier way to deal with such controlled coupling when more than two magnetic moments are involved, is to divide alternating magnetic moments into sine and cosine components as in Eqs. (20). The force between two magnetic moments can then be thought of as the sum of the sine components force and cosine components force as illustrated in Eq. (21). The same idea can also be extended to electromagnetic torques similar to Eq. (22).

$$\vec{\mu}_A(t) = \vec{\mu}_{A_{sin}} \, sin(\omega_f t) + \vec{\mu}_{A_{cos}} \, cos(\omega_f t) \ , \tag{20.}$$

$$\vec{f}_{AB_{avg}} = 0.5 \left[\vec{f}_M \left(\vec{\mu}_{A_{sin}}, \vec{\mu}_{B_{sin}} \right) + \vec{f}_M \left(\vec{\mu}_{A_{cos}}, \vec{\mu}_{B_{cos}} \right) \right] \ . \tag{21.}$$

$$\vec{\tau}_{AB_{avg}} = 0.5 \left[\vec{\tau}_M \left(\vec{\mu}_{A_{sin}}, \vec{\mu}_{B_{sin}} \right) + \vec{\tau}_M \left(\vec{\mu}_{A_{cos}}, \vec{\mu}_{B_{cos}} \right) \right] \ . \tag{22.}$$

Equations (21) and (22) show that electromagnetic interactions now rely on two orthogonal sine and cosine components, allowing for an additional means of regulating how electromagnets affect each other. For instance, if one electromagnet disturbs the dynamics of the formation, this electromagnet can be easily decoupled by setting it 90° out of phase.

Reference [14] presents and experimentally verifies a practical method of controlling the phase of sinusoidally excited superconducting electromagnets by applying voltage pulses at different times as shown in Figure 6. This concept opens the door for more possible magnetic interactions that can be utilized to enhance EMFF operation as discussed in later sections of this thesis.

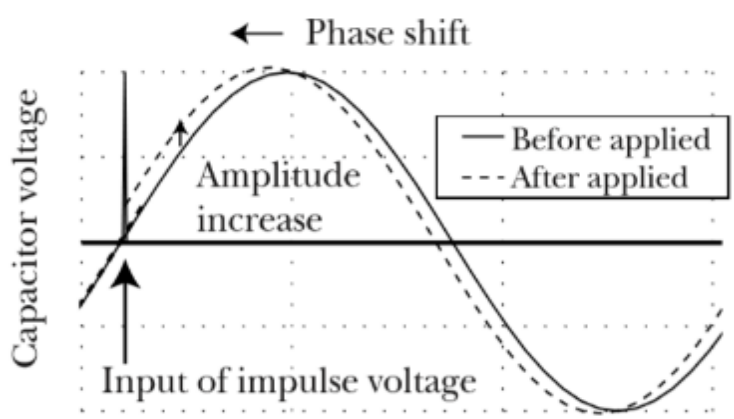

Figure 6. Phase control in superconducting electromagnets [14]

2.3.2. Frequency Modulation

Similar to phase modulation, varying the frequency ω_f also affects the interactions between alternating magnetic moments as electromagnets excited at different frequencies are decoupled. Furthermore, while in phase modulation only two decoupled sets can be achieved, frequency modulation offers a theoretically unlimited number of sets. Practically, the number of decoupled sets would be limited by the range of feasible frequencies. This range can be confined by hardware capabilities or frequencies of external magnetic fields such as the geomagnetic field in low earth orbits.

Taking the case of two alternating magnetic moments $\vec{\mu}_A(t)$ and $\vec{\mu}_B(t)$ with different frequencies but an identical phase. The force between $\vec{\mu}_A(t)$ and $\vec{\mu}_B(t)$ can be written as:

$$\vec{f}_{AB}(t) = \vec{f}_M\left(\vec{\mu}_A, \vec{\mu}_B\right) \cdot cos\left(\omega_{f_A} t\right) \cdot cos\left(\omega_{f_B} t\right) \ . \tag{23.}$$

Due to the orthogonality of sinusoids at different frequencies, the average force across one cycle becomes:

$$\vec{f}_{AB_{avg}} = \begin{cases} 0.5\vec{f}_M\left(\vec{\mu}_A, \vec{\mu}_B\right), & \omega_{f_A} = \omega_{f_B} \\ 0 & otherwise \end{cases} \ . \tag{24.}$$

Equation (24) shows that electromagnets operating at different frequencies have zero net effect on each other, and are hence decoupled. This again provides additional freedom in the control of an EMFF formation as unwanted magnetic interactions can be eliminated.

The main advantage frequency modulation holds over phase modulation is the theoretically unlimited number of decoupled sets. However, practical means of controlling the phase in a superconducting electromagnet have already been developed and tested. On the other hand, the practicality of controlling the frequency in a superconducting electromagnet, or operating the same electromagnet at the different frequencies simultaneously is yet to be investigated. For the remainder of this study, such functionality is assumed in both phase and frequency.

2.4. Rotational Dynamics

The attitude of the formation's spacecrafts can be of high importance considering the proposed applications of FF. For this objective, each spacecraft is equipped with three orthogonal reaction wheels aligned with the axes of the principal coordinate frame as shown in Figure 7. This section studies the rotational dynamics of such configuration to be later used for attitude control. For simplicity, the spacecraft mass is assumed to be distributed evenly across its rigid body.

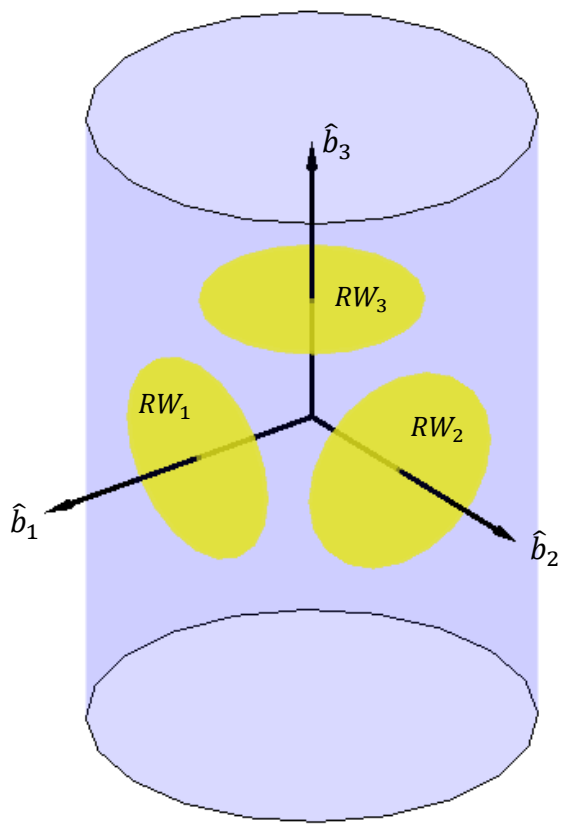

Figure 7. Spacecraft with 3 reaction wheels

First, defining the spacecraft's body-fixed coordinate frame F^B and moment of inertia matrix $[I_B]$ as:

$$F^B: \{\hat{b}_1, \hat{b}_2, \hat{b}_3\}. \tag{25.}$$

$$^{F^B}[I_B] = \begin{bmatrix} I_{B_1} & 0 & 0 \\ 0 & I_{B_2} & 0 \\ 0 & 0 & I_{B_3} \end{bmatrix}. \tag{26.}$$

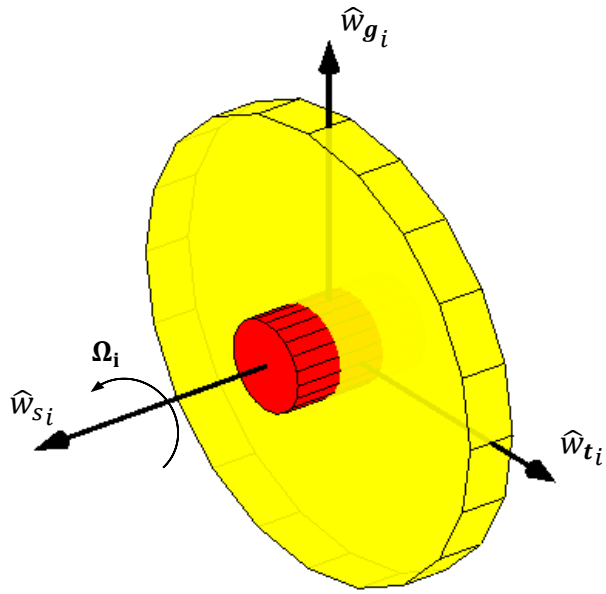

Figure 8. Reaction wheel configuration

Similarly, for each reaction wheel as shown in Figure 8, a wheel coordinate frame F^{W_i} is defined as:

$$F^{W_i}: \left\{\widehat{w}_{s_i}, \widehat{w}_{t_i}, \widehat{w}_{g_i}\right\}. \tag{27.}$$

Where i corresponds to the index of the reaction wheel (1, 2, or 3), $\widehat{w}_{s_i}$ is the rotation axis, $\widehat{w}_{t_i}$ is a transverse axis and $\widehat{w}_{g_i}$ completes the right-hand coordinates convention. The reaction wheels' moment of inertia matrix $\left[I_{W_i}\right]$ becomes:

$$^{F^{W_i}}\left[I_{W_i}\right] = \begin{bmatrix} I_{s_i} & 0 & 0 \\ 0 & I_{t_i} & 0 \\ 0 & 0 & I_{t_i} \end{bmatrix}. \tag{28.}$$

Each reaction wheel's rotation with respect to the spacecraft can be described by $\vec{\omega}_{W_i/B}$:

$$\vec{\omega}_{W_i/B} = \Omega_i \widehat{w}_{s_i}. \tag{29.}$$

The total angular momentum of the system can be considered as the vector sum of angular momentums of the spacecraft and each of its reaction wheels as indicated by Eq. (30).

Subsequently, Eqs. (31) and (32) show how to calculate the angular momentum of each component independently where $\vec{\omega}_{B/N}$ denotes the spacecraft's rotation with respect to an inertial frame F^N.

$$\vec{H} = \vec{H}_B + \sum_{i=1}^{3} \vec{H}_{W_i} . \tag{30.}$$

$$\vec{H}_B = [I_B]\, \vec{\omega}_{B/N} . \tag{31.}$$

$$\vec{H}_{W_i} = [I_{W_i}](\vec{\omega}_{B/N} + \vec{\omega}_{W_i/B}) . \tag{32.}$$

Plugging Eqs. (31), (32) and (30) into Eq. (22) yields the following:

$$\begin{aligned} \vec{H} &= \left([I_B] + \sum_{i=1}^{3}[I_{W_i}]\right)\vec{\omega}_{B/N} + \sum_{i=1}^{3}[I_{W_i}]\, \vec{\omega}_{W_i/B} \\ &= \left([I_B] + \sum_{i=1}^{3}[I_{W_i}]\right)\vec{\omega}_{B/N} + \sum_{i=1}^{3}[I_{W_i}]\Omega_{\mathrm{i}}\widehat{w}_{s_i} . \end{aligned} \tag{33.}$$

Defining I_{sum}:

$$[I_{sum}] = \left([I_B] + \sum_{i=1}^{3}[I_{W_i}]\right). \tag{34.}$$

And using the following property:

$$[I_{W_i}]\widehat{w}_{s_i} = I_{s_i}\widehat{w}_{s_i}. \tag{35.}$$

The total system angular momentum becomes:

$$\vec{H} = [I_{sum}]\, \vec{\omega}_{B/N} + \sum_{i=1}^{3} I_{s_i}\Omega_{\mathrm{i}}\widehat{w}_{s_i} . \tag{36.}$$

For the sake of simplicity, the remainder of this study assumes the three reaction wheels are identical in terms of dimensions, mass, and inertia, such that $I_{s_1} = I_{s_2} = I_{s_3} = I_s$ and $I_{t_1} = I_{t_2} = I_{t_3} = I_t$. This simplifies the angular momentum expression $\vec{H}$:

$$\vec{H} = [I_{sum}]\, \vec{\omega}_{B/N} + I_s \sum_{i=1}^{3} \Omega_{\mathrm{i}}\widehat{w}_{s_i} . \tag{37.}$$

An aggregate reaction wheel angular velocity vector $\vec{\Omega}$ can be defined as:

$$\vec{\Omega} = \sum_{i=1}^{3} \Omega_i \hat{w}_{s_i}. \tag{38.}$$

Considering that the three reaction wheels are orthogonal, they can be aligned with the principal axes of the spacecraft's body-fixed frame, such that $\hat{w}_{s_1} = \hat{b}_1$, $\hat{w}_{s_2} = \hat{b}_2$, and $\hat{w}_{s_3} = \hat{b}_3$. This allows $\vec{\Omega}$ to be expressed in the body-fixed frame as follows:

$${}^{F^B}\vec{\Omega} = \begin{pmatrix} \Omega_1 \\ \Omega_2 \\ \Omega_3 \end{pmatrix}. \tag{39.}$$

Additionally, aligning the reaction wheels this way causes the moment of inertia matrix of each reaction wheel in the body fixed frame to take one of three possible values depending on which body frame axis the wheel is aligned with:

$${}^{F^B}[I_{W_i}] = \begin{bmatrix} I_s & 0 & 0 \\ 0 & I_t & 0 \\ 0 & 0 & I_t \end{bmatrix}, or \begin{bmatrix} I_t & 0 & 0 \\ 0 & I_s & 0 \\ 0 & 0 & I_t \end{bmatrix}, or \begin{bmatrix} I_t & 0 & 0 \\ 0 & I_t & 0 \\ 0 & 0 & I_s \end{bmatrix}. \tag{40.}$$

Since the reaction wheels are orthogonal, each wheel takes a different value from Eq. (40). This concurrently simplifies I_{sum} to the following:

$${}^{F^B}[I_{sum}] = \begin{bmatrix} I_{B_1} + I_s + 2I_t & 0 & 0 \\ 0 & I_{B_2} + I_s + 2I_t & 0 \\ 0 & 0 & I_{B_3} + I_s + 2I_t \end{bmatrix}. \tag{41.}$$

As a result, the angular momentum vector of the setup in Figure 7 can be described by Eq. (42):

$$\vec{H} = [I_{sum}]\,\vec{\omega}_{B/N} + I_s\,\vec{\Omega}\ . \tag{42.}$$

Once the angular momentum vector is defined, Euler's second law of motion can be used to derive the rotational dynamics of the system. Euler's second law states that the rate of change of the angular momentum of a system with respects to an inertial frame equals the sum of external torques acting on the system:

$$\frac{{}^{F^N}d\vec{N}}{dt} = \dot{\vec{H}} = \vec{\tau}_e \,. \tag{43.}$$

Using transport theorem to calculate the inertial derivatives of the angular momentum vector in Eq. (42) results in Eq. (44):

$$\dot{\vec{H}} = [I_{sum}]\,\dot{\vec{\omega}}_{B/N} + \vec{\omega}_{B/N} \times [I_{sum}]\,\vec{\omega}_{B/N} + I_s \frac{{}^{F^B}d\vec{\Omega}}{dt} + \vec{\omega}_{B/N} \times I_s\,\vec{\Omega}\,. \tag{44.}$$

Where $I_s \frac{{}^{F^B}d\vec{\Omega}}{dt}$ are the reaction wheels' torques as observed from the body frame.

Taking all into consideration, the rotational dynamics of the system can be simply described by the below equation:

$$[I_{sum}]\,\dot{\vec{\omega}}_{B/N} = \vec{\tau}_e - \vec{\omega}_{B/N} \times [I_{sum}]\,\vec{\omega}_{B/N} - I_s \frac{{}^{F^B}d\vec{\Omega}}{dt} - \vec{\omega}_{B/N} \times I_s\,\vec{\Omega}. \tag{45.}$$

Finally, the Modified Rodrigues Parameters (MRP) vector $\vec{\sigma} = \{\sigma_1, \sigma_2, \sigma_3\}^T$ is used to represent the attitude of the formation's satellites [30]. Eq. (46) shows the definition of the MRP vector with respect to unit quaternions and Eq. (47) relates the rate of change of $\vec{\sigma}$ with the angular velocity vector $\vec{\omega}_{B/N}$ [30].

$$\sigma_i = \frac{q_i}{1 + q_0} \qquad i = 1,2,3\,. \tag{46.}$$

$$\dot{\vec{\sigma}} = \frac{1}{4}\left[\left(1 - \vec{\sigma}^T\vec{\sigma}\right)E_{3\times3} + 2\left[\vec{\sigma}^{\times}\right] + 2\vec{\sigma}\vec{\sigma}^T\right]\vec{\omega}_{B/N}\,. \tag{47.}$$

Where $\left[\vec{\sigma}^{\times}\right]$ is the skew-symmetric cross-product matrix defined as:

$$\left[\vec{\sigma}^{\times}\right] = \begin{bmatrix} 0 & -\sigma_3 & \sigma_2 \\ \sigma_3 & 0 & -\sigma_1 \\ -\sigma_2 & \sigma_1 & 0 \end{bmatrix}. \tag{48.}$$

2.5. Earth's Magnetic Field

As the concept of EMFF heavily relies on magnetic interactions, external magnetic interference can play a crucial role in the success or failure of a mission. As such they must be taken into consideration when designing and operating an electromagnetic formation. In earth orbits, the most impactful external magnetic field becomes that of earth. Several detailed models exist for the geomagnetic field based on experimental measurements from years of study, such as the International Geomagnetic Reference Field (IGRF) from the International Association of Geomagnetism and Aeronomy (IAGA). Simpler models also exist that provide satisfactory estimates of the geomagnetic field for most locations around earth. One such model is the dipolar approximation, which approximates the magnetic properties of earth as that of a magnetic dipole with a moment of $\mu_e \approx 8.1 \times 10^{22}\ A \cdot m^2$ and tilted around 11° from geographical poles [31]. Incorporating this model into the EMFF configuration of this study would result in an overall system as shown in Figure 9, where the magnetic moments of the satellites are controlled while the magnetic moment of earth is fixed and acts as a disturbance source.

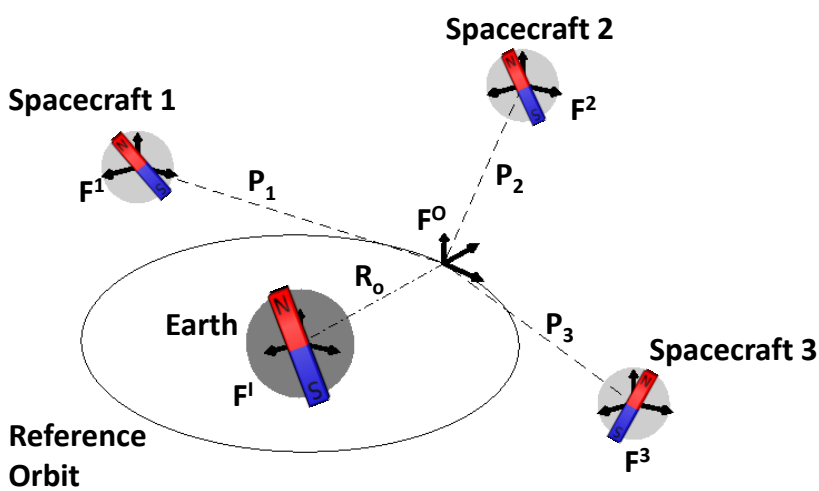

Figure 9: EMFF with the geomagnetic field

The dipole model is adopted throughout this study to represent interactions with the geomagnetic field. For further simplification without loss of generality, the 11° tilt is ignored and the magnetic moment of earth is considered to be aligned with the geographical poles. The magnetic interactions caused by earth on each of the spacecrafts of the formations can then be

calculated from Eqs. (13) and (14). Forces caused by earth's magnetic field are often negligible compared to the intra-formation forces, as electromagnetic force is inversely proportional to the fourth power of the separation distance. However, electromagnetic torques are less sensitive to distances and the rotational effect of the geomagnetic field is non-trivial. Section 2.3 discussed using alternating magnetic moments for formation control, which would eliminate any net effect of the geomagnetic field. Nonetheless, the geomagnetic field might still cause transient disturbances and vibrations and must be incorporated into EMFF simulations. Furthermore, external magnetic fields can be utilized in a beneficial manner for EMFF, as is later presented in section 3.4.

2.6. Gravity Gradient Torque

In terms of the rotational dynamics for satellites in LEO, one of the most impactful external effects is the gravity gradient torque. The differences in the gravitational force exhibited on different parts of the spacecraft can yield torques that in turn affect the spacecraft's attitude. While these torques can be used to stabilize the attitude in certain configurations, they can also severely deteriorate the rotational behavior of a system. Therefore, it is important to consider these torques in numerical simulations and possibly take them into account when designing the attitude controller. Although gravity gradient effects might sound complex to compute at first, they can be accurately approximated using the most common form as [30]:

$$\vec{\tau}_G = 3\frac{\mu_g}{R^5}\left[\vec{R} \times [I]\,\vec{R}\right] \tag{49.}$$

Where μ_g is the gravitational parameter, $\vec{R}$ is the global position of the target body and $[I]$ is its inertia matrix.

2.7. Spacecraft Design

To simulate and validate the concepts that are developed later in this thesis, it is crucial to consider reasonable specifications for the spacecrafts of the formation. As shown in Figure 5, each spacecraft is equipped with three electromagnets for position control and three reaction wheels for attitude control. Spacecrafts would also be equipped with other equipment for the scientific objective of the mission. While practically the satellites would have different requirements according to their role in the formation, the formation's satellites are considered to be identical in this study for simplicity.

For effective position control, the electromagnets in the formation should be capable of generating strong magnetic moments. Considering separation distances of tens of meters, a maximum momentarily magnetic moment of $3 \times 10^5\ A \cdot m^2$ would be more than sufficient to provide the desired forces. Table 1 shows the sensible specifications of an HTS electromagnet capable of providing the target magnetic moment. These specifications are inspired by the testbed developed in ref. [21] and the analysis of ref. [14]. Each spacecraft incorporates three of these electromagnets arranged orthogonally. For cooling purposes, satellites are also equipped with 25kg of liquid nitrogen (LN_2).

Table 1. Specifications of a superconducting electromagnet

Radius	Turns	Max Current	Mass	Critical Temperature
0.7 m	1000	200 A	25 kg	110 k

As for attitude control, the properties of each of the three orthogonal reaction wheels are summarized in Table 2. These specifications would allow a single reaction wheel to hold a maximum angular momentum of around $30\ N \cdot m \cdot s$.

Table 2. Specifications of a single reaction wheel

Radius	Thickness	Mass	Max speed	Max torque
0.25 m	0.1 m	10 kg	100 rad/s	$1\ N \cdot m$

Finally, to accommodate the control actuators and any additional scientific equipment, a cylindrical spacecraft shape is assumed. Table 3 presents a comprehensive overview of the spacecraft's specifications. As mentioned previously, all satellites are equipped with the same

configuration and have identical properties throughout the remainder of this study unless specifically stated otherwise.

Table 3. Specifications of the formation's satellites

Shape	Cylinder
Radius	1.2 m
Height	2 m
Mass of scientific mission equipment	70 kg
Mass of electromagnets' configuration + cooling	100 kg
Mass of reaction wheels' system	30 kg
Total mass	200 kg

Chapter 3. Development of EMFF Control Policy

Following the summary of EMFF dynamics in the previous chapter, this chapter investigates the control of electromagnetic formations to enable their use in scientific missions. The overall control scheme developed in this chapter can be seen in Figure 10. The position controller calculates a target force on each spacecraft to reconfigure the formation as desired. Afterward, the dipole inversion and modulation process assigns magnetic moments on all the electromagnets to yield this target forces. Phase and frequency modulation can take place during this step in order to benefit from the additional possible interactions they offer. The attitude controller handles orienting each of the satellites using reaction wheels. Finally, the angular momentum management utilizes the geomagnetic field to desaturate the reaction wheels. Each of these components is explained in detail in sections 3.1. through 3.4. Finally, section 3.5 presents results obtained from closed-loop simulations to validate the proposed control approach.

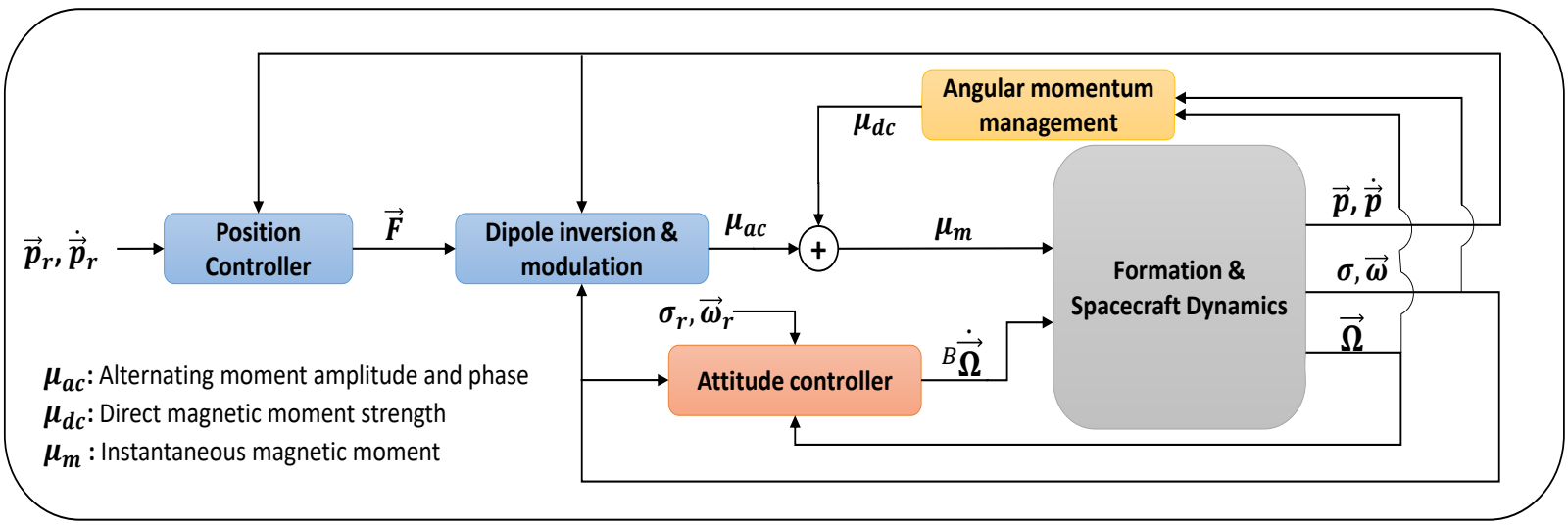

Figure 10. Formation control scheme

3.1. Translational Control of EMFF

As illustrated in Figure 10, the position controller is responsible for determining a target force that would reconfigure each spacecraft of the formation as desired. A Terminal Sliding Mode (TSM) controller is developed in this section for this purpose. TSM controllers have been popular

for FF applications due to their robustness and relatively easy implementation [18, 32]. At this stage, perfect knowledge of all the global and relative positions of all the spacecrafts along with their velocities is assumed as state estimation is beyond the scope of this study.

The main objective of the controller is to regulate the relative position $\vec{p}$ of each spacecraft in the formation to follow a designated reference position $\vec{p}_r$. It must be noted that since EMFF only generates internal forces within the formation, the reference trajectories for all satellites should take into consideration that the center of mass of the entire formation cannot be changed with electromagnetic forces.

Following the equations of motion and coordinate frame definitions presented in section 2.1, an error function can be defined for each spacecraft as:

$$\vec{S}_i = \left(\frac{{}^{F^O}d}{dt}\left(\vec{p}_{r_i}\right) - \frac{{}^{F^O}d}{dt}\left(\vec{p}_i\right) \right) + [\lambda]\left(\vec{p}_{r_i} - \vec{p}_i\right) . \tag{50.}$$

Where $[\lambda]$ is a positive definite gain matrix.

By using the relative dynamics of a formation expressed by the HCW equations, the rate of change of the error function relative to the orbital frame F^O can be written as:

$$\begin{aligned} \frac{{}^{F^O}d}{dt}\left(\vec{S}_i\right) &= \left(\frac{{}^{F^O}d^2}{dt^2}\left(\vec{p}_{r_i}\right) - \frac{{}^{F^O}d^2}{dt^2}\left(\vec{p}_i\right) \right) + [\lambda]\left(\frac{{}^{F^O}d}{dt}\left(\vec{p}_{r_i}\right) - \frac{{}^{F^O}d}{d}\left(\vec{p}_i\right) \right) \\ &= \left[\left(\frac{{}^{F^O}d^2}{dt^2}\left(\vec{p}_{r_i}\right) + \vec{c}_i + \vec{g}_i - \frac{\vec{f}_i^{\,C} + \vec{f}_i^{\,d}}{m_i} \right) + [\lambda]\left(\frac{{}^{F^O}d}{dt}\left(\vec{p}_{r_i}\right) - \frac{{}^{F^O}d}{dt}\left(\vec{p}_i\right) \right) \right]. \end{aligned} \tag{51.}$$

In order to find control forces $\vec{f}_i^{\,C}$ on each spacecraft that would drive this error function to zero and perform the target trajectories, a positive definite Lyapunov function is introduced as:

$$V_i = \frac{1}{2}\vec{S}_i^{\,T}\vec{S}_i \ , \tag{52.}$$

The rate of change of this Lyapunov function can be expressed as in Eq. (53):

$$\dot{V}_i = \left[\frac{{}^{F^O}d}{dt}\left(\vec{S}_i\right)\right]^T \vec{S}$$
$$= \left[\left(\frac{{}^{F^O}d^2}{dt^2}\left(\vec{p}_{r_i}\right) + \vec{c}_i + \vec{g}_i - \frac{\vec{f}_i^C + \vec{f}_i^d}{m_i}\right) + [\lambda]\left(\frac{{}^{F^O}d}{dt}\left(\vec{p}_{r_i}\right) - \frac{{}^{F^O}d}{dt}\left(\vec{p}_i\right)\right)\right]^T \vec{S}_i \,. \tag{53.}$$

By selecting the control force on each spacecraft $\vec{f}_i^C$ using Eq. (54), the Lyapunov function's rate of change becomes negative definite as demonstrated in Eq. (55), where $[K]$ is a positive definite gain matrix. This indicates the asymptotic stability of the system [33].

$$\vec{f}_i^C = -\vec{f}_i^d + m_i\left\{\frac{{}^{F^O}d^2}{dt^2}\left(\vec{p}_{r_i}\right) + \vec{c}_i + \vec{g}_i + [\lambda]\left(\frac{{}^{F^O}d}{dt}\left(\vec{p}_{r_i}\right) - \frac{{}^{F^O}d}{dt}\left(\vec{p}_i\right)\right) + [K]\vec{S}_i\right\}, \tag{54.}$$

$$\dot{V}_i = -\vec{S}_i^{\,T}\,[K]\vec{S}_i \tag{55.}$$

The controller formulation so far only provides intuition regarding the stability of the system but does not provide guidelines on selecting the gain matrices $[\lambda]$ and $[K]$ for tuning the performance. However, by simply plugging the controller structure from Eq. (54) into the equation of relative motion from Eq. (8), a linear second-order differential equation is yielded as shown below:

$$\left(\frac{{}^{F^O}d^2}{dt^2}\left(\vec{p}_{r_i}\right) - \frac{{}^{F^O}d^2}{dt^2}\left(\vec{p}_i\right)\right) + ([\lambda] + [K])\left(\frac{{}^{F^O}d}{dt}\left(\vec{p}_{r_i}\right) - \frac{{}^{F^O}d}{dt}\left(\vec{p}_i\right)\right)$$
$$+ [K][\lambda]\left(\vec{p}_{r_i} - \vec{p}_i\right) = 0 \,. \tag{56.}$$

$[\lambda]$ and $[K]$ can then be easily tuned to provide the desired response in terms of damping, overshoot and settling time.

3.2. Dipole Inversion

Once target forces are determined, magnetic moments are assigned to all the available electromagnets in the system to achieve this force. This assignment can be referred to as "dipole inversion", and a magnetic moment assignment that results in the target force can be called a "dipole solution". As coupling usually exists between all the spacecrafts in the formation, this process should be done in a centralized manner taking all spacecrafts into consideration. This problem can be represented as finding the magnetic moments $\vec{\mu}$ of all the spacecrafts in the formation that would achieve these target forces from the position controller as indicated below:

$$\vec{f}_i^C = \sum_j^N \vec{f}_M\left(\vec{\mu}_j, \vec{\mu}_i\right), \qquad for\ i = 1,2, \ldots\ldots N\ . \tag{57.}$$

Where N represents the number of satellites in the formation.

This corresponds to a set of nonlinear system equations which can be solved using a variety of numerical algorithms. Throughout this study, the "Levenberg-Marquardt" algorithm is used to solve such problems using MATLAB's "fsolve" package.

The dipole inversion process is part of the feedback control scheme which is iteratively applied as time progresses. Implementing the dipole inversion process at each time step might seem computationally expensive and time-consuming upon initial inspection. However, by initializing the non-linear solver with the solution from the previous time step, convergence time is significantly reduced making this approach reasonable for real-time implementation.

3.2.1. Dipole Inversion with Modulation

The dipole inversion process can be extended to make use of phase and frequency modulation as discussed in section 2.3. Modulation enables controlled decoupling between the magnetic interactions of different satellites. For instance, electromagnets operated at different frequencies are considered decoupled as the net resultant forces and torques would be zero. Therefore, if two electromagnets are excited with multiple frequencies at the same time, the net force between these electromagnets would be the linear sum of forces between the matching

frequency components. The same concept can be extended to phase modulation where sine and cosine components are orthogonal and decoupled. The dipole inversion problem in this case grows larger as it becomes important to account for all the decoupled sets.

When modulation takes place, the magnetic moment of each spacecraft in the formation can be thought of as the sum of orthogonal components $\left\{ {}^{1}\vec{\mu}, {}^{2}\vec{\mu}, {}^{3}\vec{\mu}, \ldots \right\}$ created from modulation as:

$$\vec{\mu} = {}^{1}\vec{\mu} + {}^{2}\vec{\mu} + {}^{3}\vec{\mu} + \cdots = \sum_{O=1}^{N_O} {}^{O}\vec{\mu} \tag{58.}$$

Where each of these orthogonal components is either at a unique frequency or 90° out of phase from other components and N_O is simply the number of orthogonal components created through modulation.

The force between two satellites becomes the sum of the forces between the matching components of magnetic moments as:

$$\vec{f}_M\left(\vec{\mu}_A, \vec{\mu}_B\right) = \sum_{O=1}^{N_O} \vec{f}_M\left({}^{O}\vec{\mu}_A, {}^{O}\vec{\mu}_B\right). \tag{59.}$$

Taking this into account, the inversion problem becomes finding suitable values for each decoupled set ${}^{O}\vec{\mu}$ of the magnetic moment $\vec{\mu}$ for every satellite in the formation that would result in the target force. This translates into transforming the set of nonlinear equations in Eq. (44) as follows:

$$\vec{f}_i^{\,C} = \sum_{j}^{N} \sum_{O=1}^{N_O} \vec{f}_M\left({}^{O}\vec{\mu}_j, {}^{O}\vec{\mu}_i\right), \qquad for\ i = 1,2, \ldots\ldots N. \tag{60.}$$

Comparing Eq. (60) to Eq. (57), it becomes clear that modulation increases the complexity of the dipole inversion process. Nonetheless, modulation also offers more freedom in terms of magnetic moments assignment. This freedom is exploited in chapters Chapter 4 and Chapter 5 of this thesis to enhance EMFF operation by minimizing the number of electromagnets in a formation, optimizing thermal accumulation, and reducing the buildup of angular momentum.

3.2.2. Optimal Dipole Inversion

Multiple solutions of magnetic moments might result in the same net force. This is especially the case when modulation is applied as more variant electromagnetic interactions are achievable. This opens the door to selecting an optimal dipole solution that enhances EMFF operation with respect to a specified criterion. Assuming the optimization criterion can be characterized by a cost function J, the dipole inversion process can then be represented as a constrained nonlinear optimization problem as shown in Eq. (61).

$$\textbf{Minimize}: \mathrm{J},$$

$$\textbf{Subject to}: \quad \vec{f}_i^{\,C} = \sum_j^N \vec{f}_M\left(\vec{\mu}_j, \vec{\mu}_i\right), \quad for\ i = 1,2, \ldots\ldots N\,. \tag{61.}$$

This constrained optimization problem can be solved by a variety of nonlinear programming algorithms. A Sequential Quadratic Programming (SQP) approach using MATLAB's "fmincon" package was adopted in this study. Since this optimization problem is repeated at every time increment, the solution from the previous timestep can be used to initialize the nonlinear solver to minimize convergence time.

3.3. Attitude Control of EMFF Satellites

In formation flying and space systems in general, a spacecraft's orientation is crucial to the success of a mission. Therefore, attitude control is a priority when designing and operating such systems. For this purpose, this study equips each spacecraft in the formation with three orthogonal reaction wheels as shown in Figure 7. The dynamics of this configuration were derived in section 2.4. This section builds upon the summarized dynamics and uses Lyapunov's Direct Method to develop a control law for controlling the attitude and its rate of change. The attitude control law developed in this study is decentralized in which each satellite is controlled separately.

First, to represent the desired attitude, a target reference frame F^R is defined with reference angular velocity vector $\vec{\omega}_{R/N}$. A velocity error vector is then introduced as:

$$\delta\vec{\omega} = \vec{\omega}_{B/N} - \vec{\omega}_{R/N} \ . \tag{62.}$$

The MRP attitude representation vector $\vec{\sigma}$ is redefined to describe the difference in attitude between the spacecraft frame F^B and the reference frame F^R. The rate of change of $\vec{\sigma}$ becomes:

$$\dot{\vec{\sigma}} = \frac{1}{4}\left[\left(1 - \vec{\sigma}^T\vec{\sigma}\right)E_{3\times3} + 2\left[\vec{\sigma}^{\times}\right] + 2\vec{\sigma}\vec{\sigma}^T\right]\delta\vec{\omega} \ . \tag{63.}$$

Based on $\delta\vec{\omega}$ and $\vec{\sigma}$, a positive definite Lyapunov function is developed as presented in Eq. (64):

$$V(\vec{\sigma}, \delta\vec{\omega}) = \frac{1}{2}\delta\vec{\omega}^T[I_{sum}]\delta\vec{\omega} + 2K_a \ln\left(1 + \vec{\sigma}^T\vec{\sigma}\right) \ , \tag{64.}$$

Where K_a is a positive gain scalar.

The rate of change of this Lyapunov function can be calculated as:

$$\dot{V}(\vec{\sigma}, \delta\vec{\omega}) = \delta\vec{\omega}^T[I_{sum}]\delta\dot{\vec{\omega}} + K_a\left(\frac{\vec{\sigma}^T}{1 + \vec{\sigma}^T\vec{\sigma}}\right)\left[\left(1 - \vec{\sigma}^T\vec{\sigma}\right)E_{3\times3} + 2\left[\vec{\sigma}^{\times}\right] + 2\vec{\sigma}\vec{\sigma}^T\right]\delta\vec{\omega} \ . \tag{65.}$$

By expanding the second term of Eq. (65) into its matrix form and applying the associated linear algebra, the term simplifies to the following:

$$K_a\left(\frac{\vec{\sigma}^T}{1+\vec{\sigma}^T\vec{\sigma}}\right)\left[\left(1-\vec{\sigma}^T\vec{\sigma}\right)E_{3\times3}+2\left[\vec{\sigma}^{\times}\right]+2\vec{\sigma}\vec{\sigma}^T\right]\delta\vec{\omega}=K_a\vec{\sigma}^T\delta\vec{\omega}=K_a\delta\vec{\omega}^T\vec{\sigma}\,. \tag{66.}$$

Plugging this result back to Eq. (65):

$$\begin{aligned}\dot{V}\left(\vec{\sigma},\delta\vec{\omega}\right)&=\delta\vec{\omega}^T[I_{sum}]\delta\dot{\vec{\omega}}+K_a\delta\vec{\omega}^T\vec{\sigma}=\delta\vec{\omega}^T\left([I_{sum}]\delta\dot{\vec{\omega}}+K_a\vec{\sigma}\right)\\&=\delta\vec{\omega}^T\left([I_{sum}]\dot{\vec{\omega}}_{B/N}-[I_{sum}]\dot{\vec{\omega}}_{R/N}+K_a\vec{\sigma}\right).\end{aligned} \tag{67.}$$

Substituting $[I_{sum}]\dot{\vec{\omega}}_{B/N}$ by the dynamics of the system from Eq. (45):

$$\begin{aligned}\dot{V}\left(\vec{\sigma},\delta\vec{\omega}\right)=\delta\vec{\omega}^T\Bigg(&\vec{\tau}_e-\vec{\omega}_{B/N}\times[I_{sum}]\,\vec{\omega}_{B/N}-I_s\,{}^{F^B}\frac{d\,\vec{\Omega}}{dt}\\&-\vec{\omega}_{B/N}\times I_s\,\vec{\Omega}-[I_{sum}]\dot{\vec{\omega}}_{R/N}+K_a\vec{\sigma}\Bigg).\end{aligned} \tag{68.}$$

Finally, by accelerating the reaction wheel following Eq. (69), the Lyapunov function's rate becomes negative definite as indicated by Eq. (70). This indicates the asymptotic stability of the attitude and its rate of change [33].

$$I_s\,{}^{F^B}\frac{d\,\vec{\Omega}}{dt}=\vec{\tau}_e-\vec{\omega}_{B/N}\times[I_{sum}]\,\vec{\omega}_{B/N}-\vec{\omega}_{B/N}\times I_s\,\vec{\Omega}-[I_{sum}]\dot{\vec{\omega}}_{R/N}+K_a\vec{\sigma}+[\lambda_a]\delta\vec{\omega}\ , \tag{69.}$$

$$\dot{V}\left(\vec{\sigma},\delta\vec{\omega}\right)=-\delta\vec{\omega}[\lambda_a]\delta\vec{\omega}\ . \tag{70.}$$

Where $[\lambda_a]$ is a positive definite gain matrix.

3.4. Angular Momentum Management Using the Geomagnetic Field

Section 2.5 introduced a simple model of the geomagnetic field which can interact with the electromagnets of the formations. While exciting the electromagnets with sinusoidal current as discussed eliminates any net effect of earth's magnetic field, such an external field might still be of benefit in controlling the formation if taken into account during the formation control process. Ref. [26] proposed using the geomagnetic field for angular momentum management (AMM) of EMFF. It relies on assigning direct magnetic moments to the electromagnets of the formation in order to generate controlled torques from interactions with earth's magnetic field. These torques can be generated in directions that counter the angular momentum buildup, thus desaturating the reaction wheels.

The direct magnetic moments used for this purpose are inherently decoupled from the alternating magnetic moments utilized for formation control. As such, they do not affect the forces between the different spacecrafts and can be assigned independently from the relative motion control system. This step should however be applied for one spacecraft at a time to prevent different direct magnetic moments from interacting. A simple illustration of this process can be seen in Figure 11.

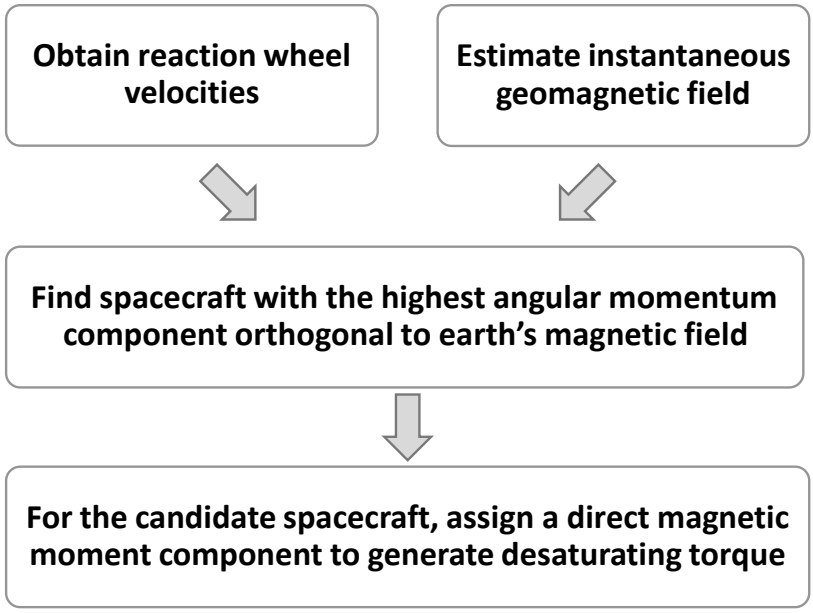

Figure 11. Angular momentum management algorithm

Following this procedure, any electromagnet can be excited by an alternating and a direct component as in Eq. (71). The $\vec{\mu}_{ac}$ element is used for the relative interactions between the formation's satellites while the $\vec{\mu}_{dc}$ component is used for angular momentum management. The magnitude of direct component can either be zero or a pre-set value μ_{AMM} as demonstrated in Eq. (72), depending on whether it is the designated satellite's turn to desaturate its reaction wheels.

$$\vec{\mu} = \vec{\mu}_{ac} + \vec{\mu}_{dc} \,. \tag{71.}$$

$$\|\vec{\mu}_{dc}\| = \begin{cases} \mu_{AMM} & , \quad during\ RW\ desaturation\ phase \\ 0 & , \quad otherwise \end{cases} \,. \tag{72.}$$

The main shortcoming of this method is the limited directions of torques that can be generated from earth's magnetic field. As a result, this technique cannot fully eliminate angular momentum buildup but can only undermine this problem.

3.5. Simulation & Results

In order to validate the control strategies presented in this chapter, a numerical simulation was constructed using MATLAB. The simulation was carried out for a seven-spacecraft formation in a circular LEO using the dynamics presented in chapter Chapter 2. Six of the spacecrafts rotate around a central satellite as demonstrated in Figure 12. Such trajectories are useful for data collection in space interferometry. All spacecrafts start from rest as observed from the orbital coordinate frame. All the seven vehicles are identical with three orthogonal electromagnets and three orthogonal reaction wheels. The spacecraft specifications from section 2.7 were adopted in this simulation. Other simulation related parameters are shown in Table 4 and Table 5 while Table 6 specifies the control parameters. It must be noted that disturbance factors such as J2 perturbations, the geomagnetic field and gravity gradient torques were taken into account in the simulations.

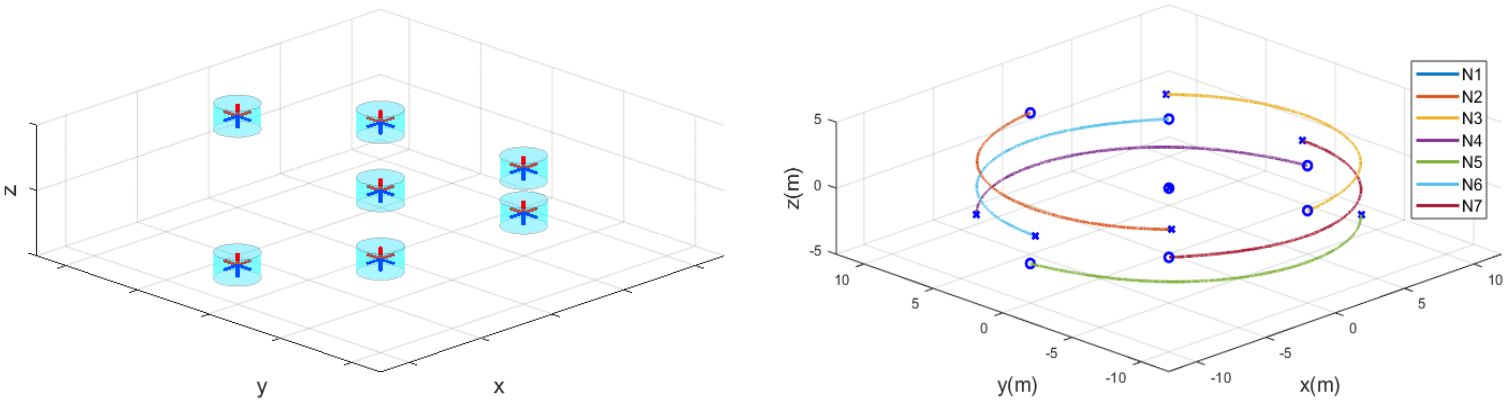

a) Configuration b) Trajectory

Figure 12. Configuration for the simulation of a 7-spacecraft formation

Table 4. Simulation parameters

Simulation time	1500 seconds
Timestep	0.1 s
Integrator	4'th order Runge-Kutta
Position control frequency	2 Hz
Alternating magnetic moments' frequency	2 Hz
Attitude control frequency	10 Hz

Table 5. Orbit properties

Orbit Type	Circular LEO
Altitude	900 km
Orbit inclination	0°

Table 6. Control parameters for the 7-spacecraft rotation simulation

$[\boldsymbol{K}]$	$[\boldsymbol{\lambda}]$	$[\boldsymbol{k_a}]$	$[\boldsymbol{\lambda_a}]$	$\boldsymbol{\mu_{AMM}}$
$0.0125 \times [I]$	$0.0125 \times [I]$	$10 \times [I]$	$15 \times [I]$	$5 \times 10^4\ A \cdot m^2$

First, the relative positions of the satellites with respects to the formation's center of mass are considered. The center of mass of the entire formation is only affected by earth's gravitational field, and not the intra-formation electromagnetic forces as they would sum up to zero. Nonetheless, electromagnetic interactions are used to control the relative configuration of the formation following the procedure described in sections 3.1 and 3.2 and the control parameters in Table 6. Figure 13 shows the relative positions of the formation's satellites in the orbital coordinates. The dotted lines indicate the reference trajectories for the rotation maneuver while the continuous lines represent the simulation results. It can be clearly seen that the satellites follow their designated trajectories with small average errors as shown in Table 7. These errors are considered to be tolerable as they are two orders of magnitude less than the target separation distances. All of which validates the position control strategy introduced in this chapter.

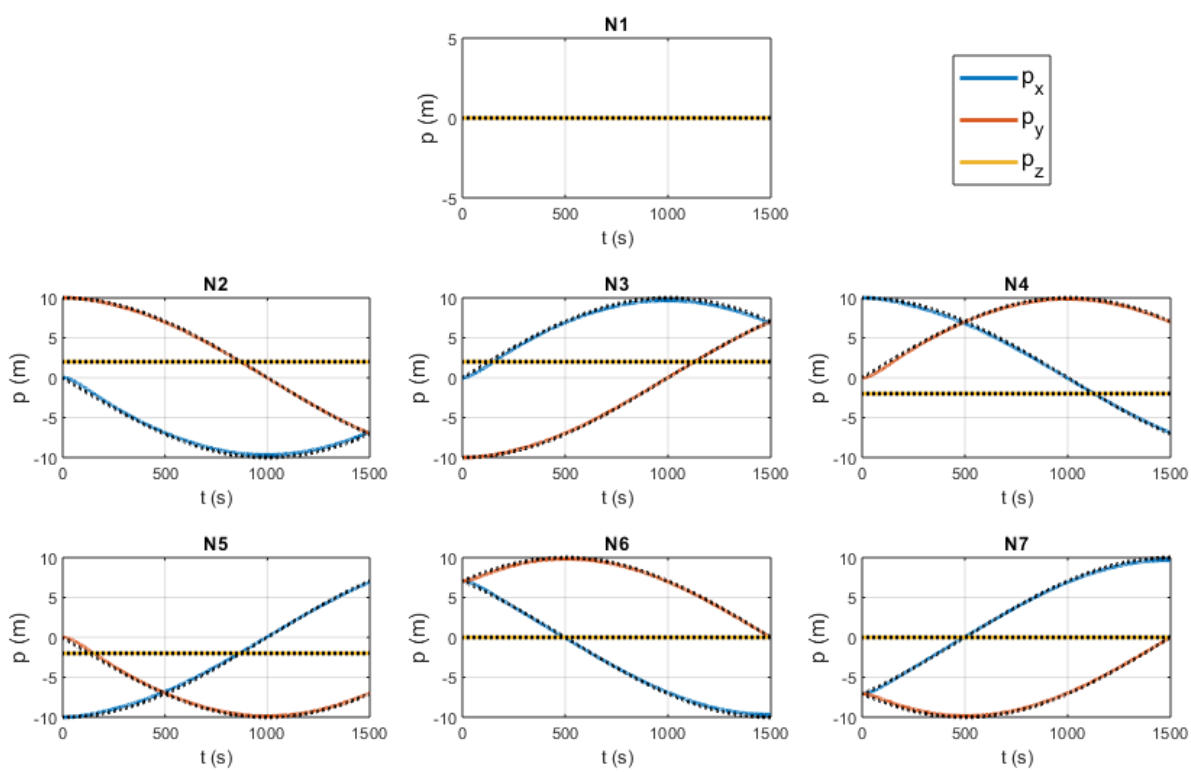

Figure 13. 7-spacecraft rotation simulation results – relative position

Table 7. Average position errors for the simulation of the 7-spacecraft rotation simulation

Spacecraft:	**1**	**2**	**3**	**4**	**5**	**6**	**7**
Average Error (m):	0.0007	0.2916	0.2916	0.2416	0.2413	0.2262	0.2265

Figure 14 displays the time history of the controls resulting in the above translational motion. These controls are depicted as the magnitude of the alternating magnetic moments assigned to the electromagnets of the formation.

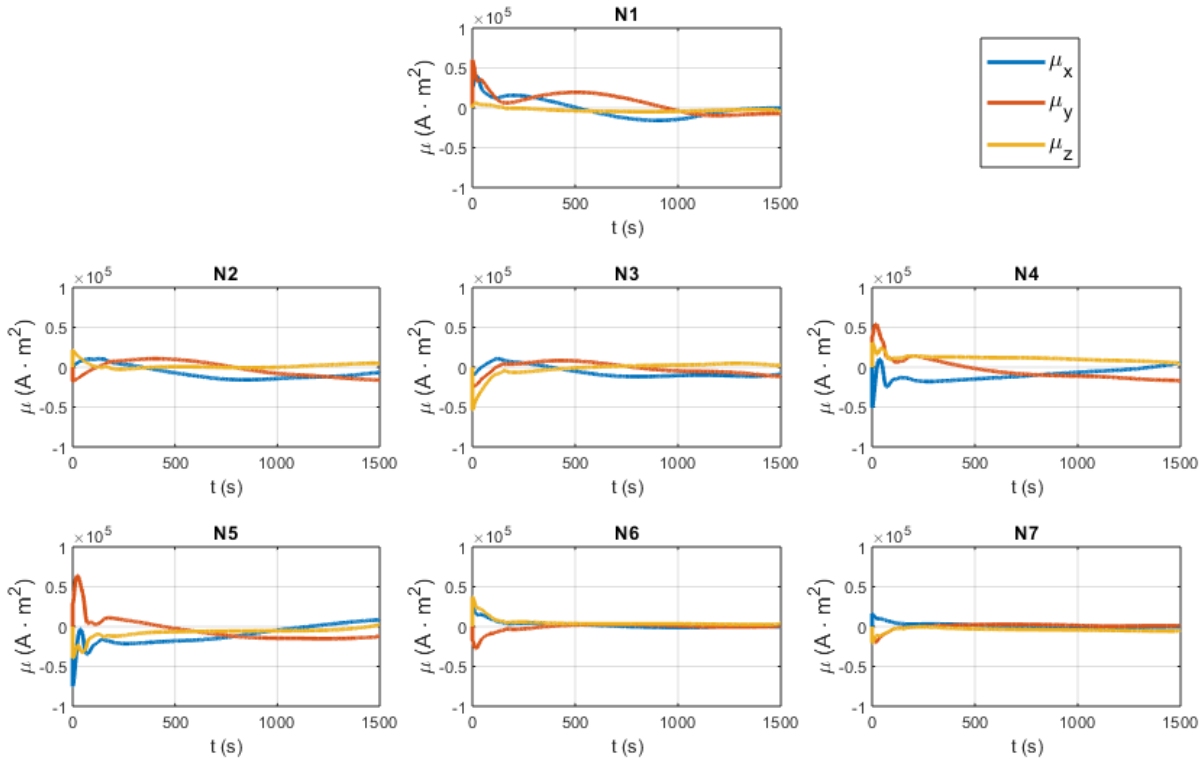

Figure 14. Control time history for the 7-spacecraft rotation simulation

As for the rotational dynamics, reaction wheels are used to control the attitude of all the satellite and align them with the ECI frame following the analysis of section 3.3. Figure 15 shows the quaternions corresponding to the relative attitude of each spacecraft and the ECI frame. As the scalar component of the quaternions q_0 remains at almost exactly unity throughout the trajectory, it can be deduced the attitude control system using reaction wheels adequately serves its purpose.

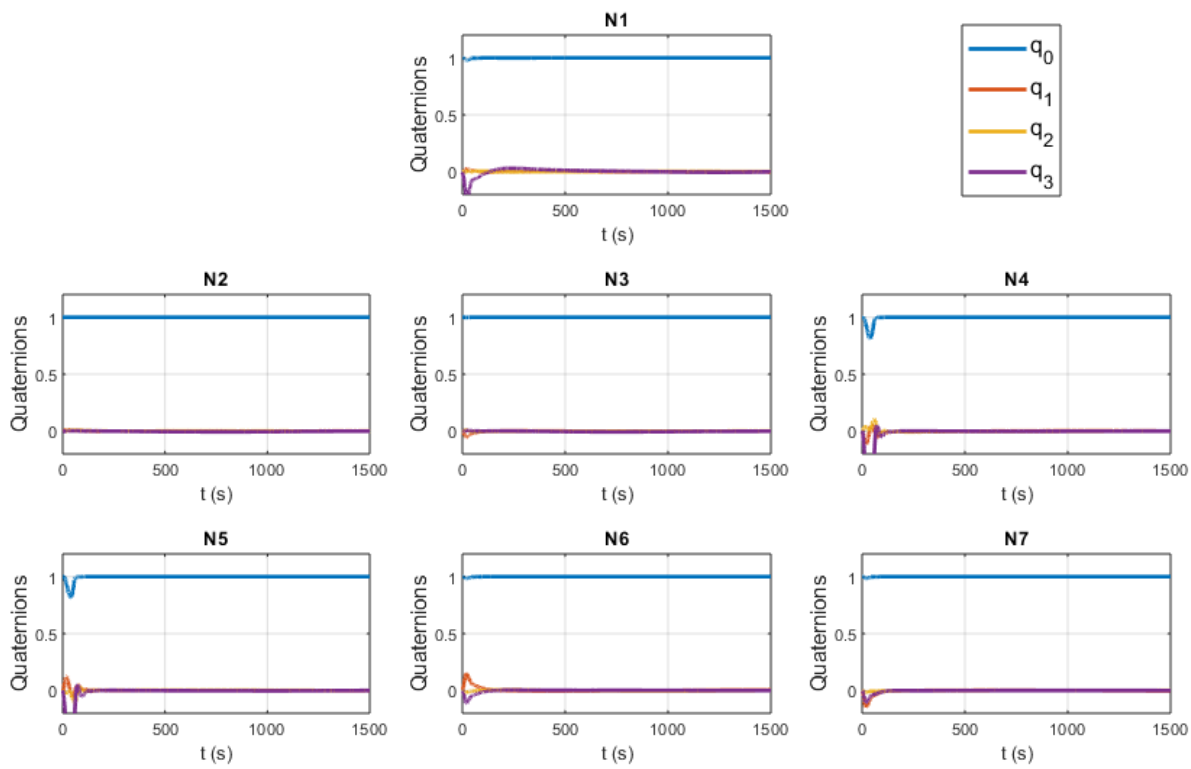

Figure 15. 7-spacecraft rotation simulation results – attitude

To analyze the problem of angular momentum accumulation in the reaction wheels, the simulation was repeated twice: with and without applying the geomagnetic angular momentum management approach of section 3.4. Both simulations exhibit similar behavior in terms of relative position and attitude but differ significantly in terms of the angular momentum stored in the reaction wheels. Figure 16 shows the reaction wheel velocities with and without applying the angular momentum management algorithm and Figure 17 displays the direct magnetic moments used for the reaction wheel desaturation process. For easier analysis, Figure 18 compares the aggregate reaction wheels' angular momentum for each spacecraft considering both cases. It is apparent that accumulated angular momentum is noticeably lower with the geomagnetic AMM, which in turn proves the effectiveness of this process.

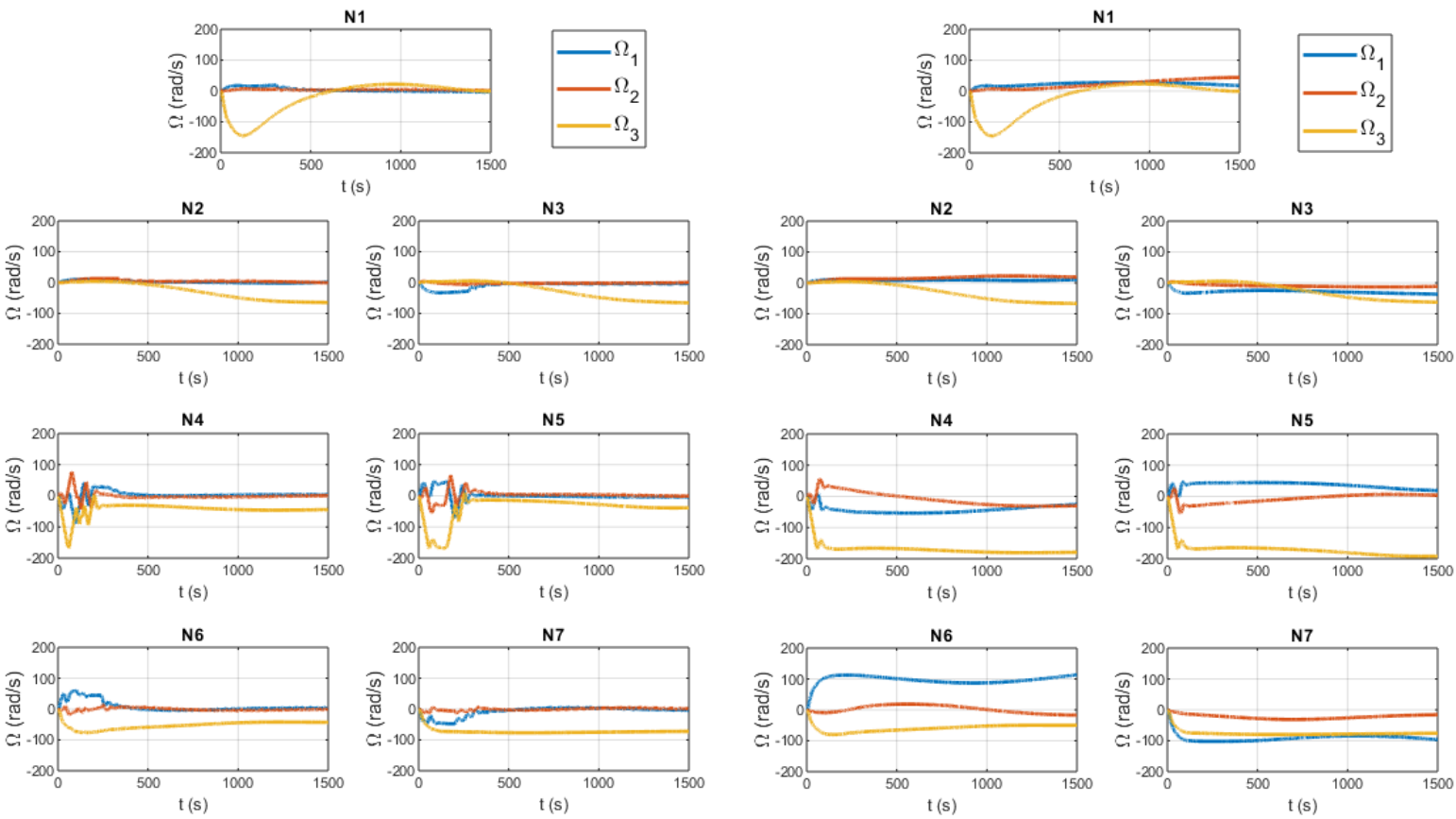

a) With AMM

b) Without AMM

Figure 16. 7-spacecraft rotation simulation results – RW velocities

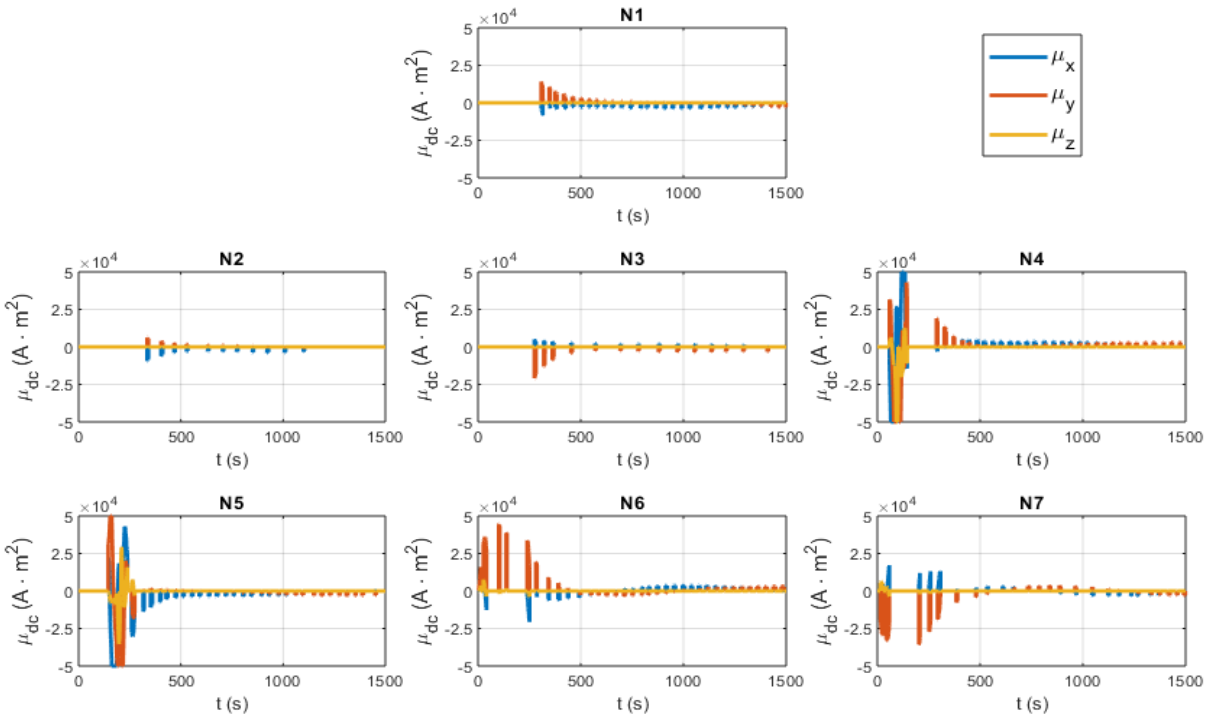

Figure 17. Direct magnetic moments time history for AMM of the 7-spacecraft rotation simulation

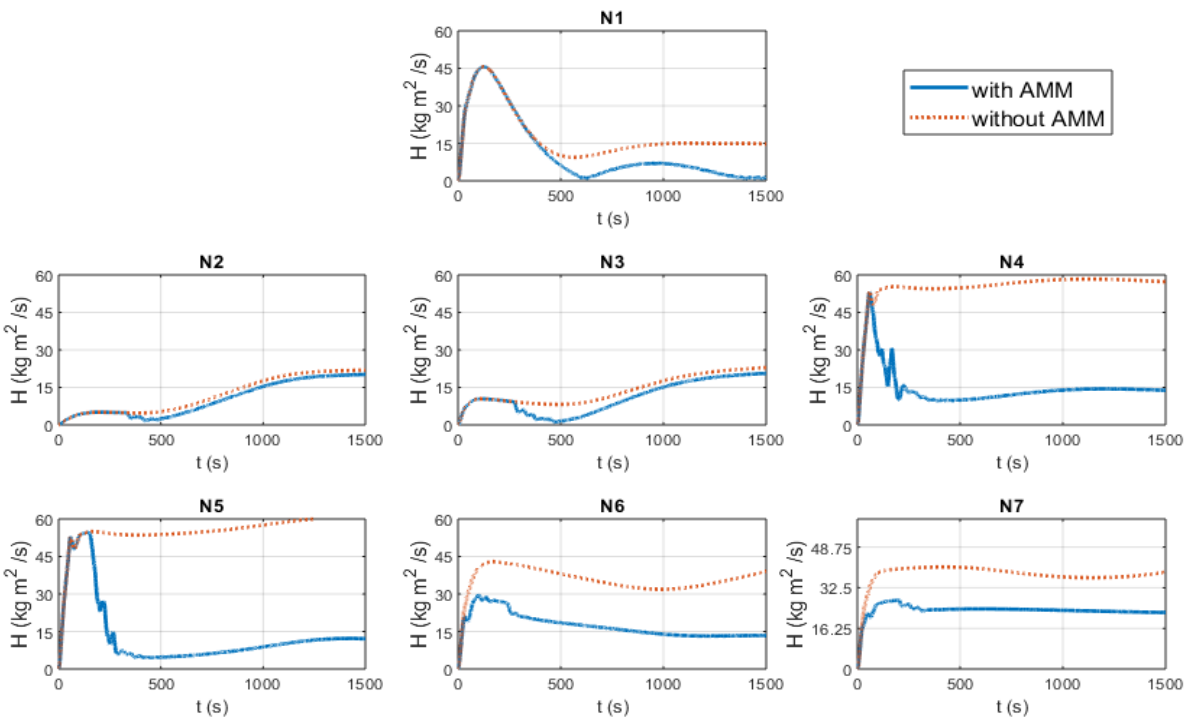

Figure 18. 7-spacecraft rotation simulation results – angular momentum

All in all, the simulation results presented in this section validate the EMFF control concepts developed in the entire chapter. These results enforce the potential of EMFF for future space missions and demonstrate the capabilities of the proposed configurations and conceptions. Later chapters in this thesis improve and build upon these concepts to optimize performance and tackle EMFF shortcomings.

Chapter 4. Control of Underactuated Electromagnetic Formations

As discussed and presented in earlier sections, most studies consider equipping each spacecraft in an EMFF formation with three electromagnets. This high requirement of electromagnets translates into a higher overall mass and cost of launching a formation. Therefore, the ability to control an EMFF formation with a lower number of electromagnets is substantially advantageous as it results in more efficient EMFF launching and operation. Furthermore, the ability to maintain formation controllability with fewer electromagnets adds redundancy to EMFF operation in the case of an electromagnet fault or overheating, which can be a serious concern due to the quenching effect in High-Temperature Superconducting electromagnets [24].

Previous attempts to tackle this issue restrict the ability to freely control the attitude of the formation's spacecraft [25]. In this section, a different approach is proposed in which phase and frequency modulation of alternating magnetic moments are employed to control an EMFF formation with less than three electromagnets per spacecraft. Section 4.1 explains the intuition behind using modulation in tackling the underactuated EMFF case with a simple illustrative example in 2D. Subsequently, section 4.2 describes how the approach can be generalized to any EMFF formation. Finally, section 4.3 presents simulation results that validate the proposed approach and verify the potential of modulation in minimizing the number of electromagnets required to control an EMFF formation.

4.1. Concept Overview

This sub-section aims to build an intuitive understanding of how modulation can be used to undermine the high requirement of electromagnets. To simplify the analysis, formations are assumed to be in 2D. Analogous to 3D formations, each spacecraft in a 2D formation should be equipped with two electromagnets to be able to generate arbitrary forces. However, there is a small tweak to this requirement. For instance, taking the two-spacecraft formation in 2D shown in Figure 19. One spacecraft denoted as the "Leader" spacecraft has two orthogonal electromagnets while

the other "Follower" spacecraft has a single electromagnet. Despite the minimization in the number of electromagnets in the follower spacecraft, the leader spacecraft is still able to exert any force on the follower spacecraft by controlling the strength of its two orthogonal electromagnets.

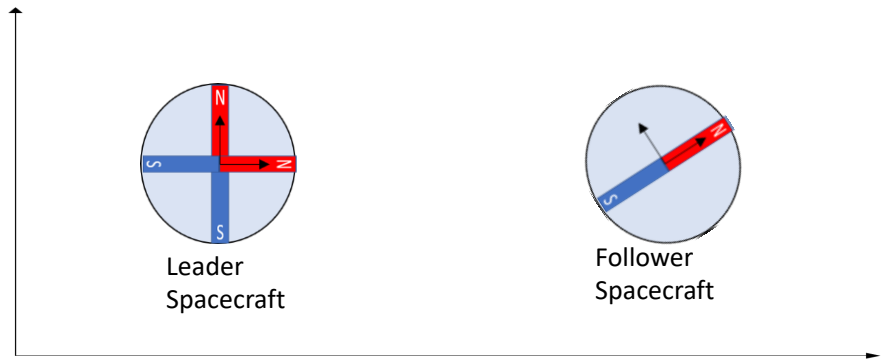

Figure 19. Two spacecraft electromagnetic formation in 2D

As such, the required number of electromagnets for a formation in 2D would be represented as $2N - 1$, where N is the number of satellites. In 3D, this expression becomes $3N - 1$.

It should be noted that regardless of the number of electromagnets, electromagnetic forces are internal and the net resultant force on all the spacecraft would sum to zero. This means that the force exerted on the follower due to the leader is always equal in magnitude and opposite in sign to the force exerted on the leader from the follower. This is a constraint that always exists in EMFF.

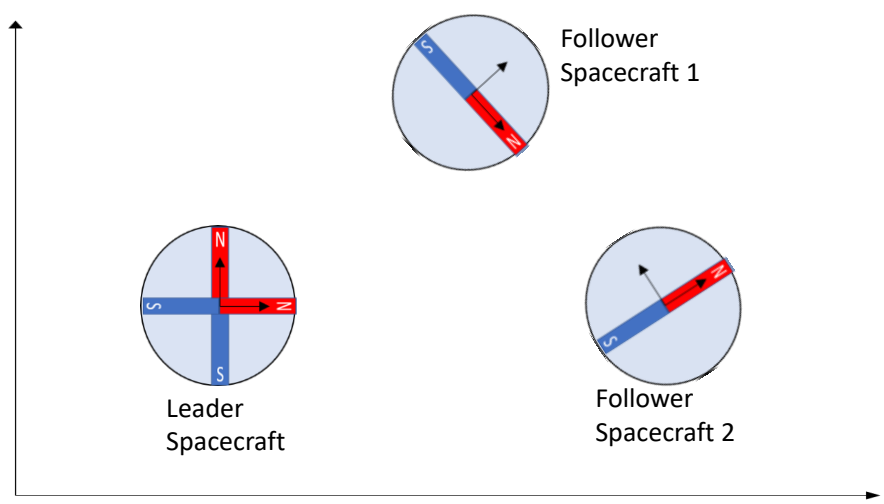

Figure 20. Three spacecraft electromagnetic formation in 2D

Taking the case of a three-spacecraft formation as in Figure 20. Compared to the previous formation, an additional follower spacecraft with a single electromagnet is added to the formation. In this case, due to the coupling between all the spacecrafts, the possible forces that can be generated on the follower spacecrafts are limited. Arbitrary forces can be exerted on only a single follower spacecraft while the direction of the force on the second spacecraft would be restricted.

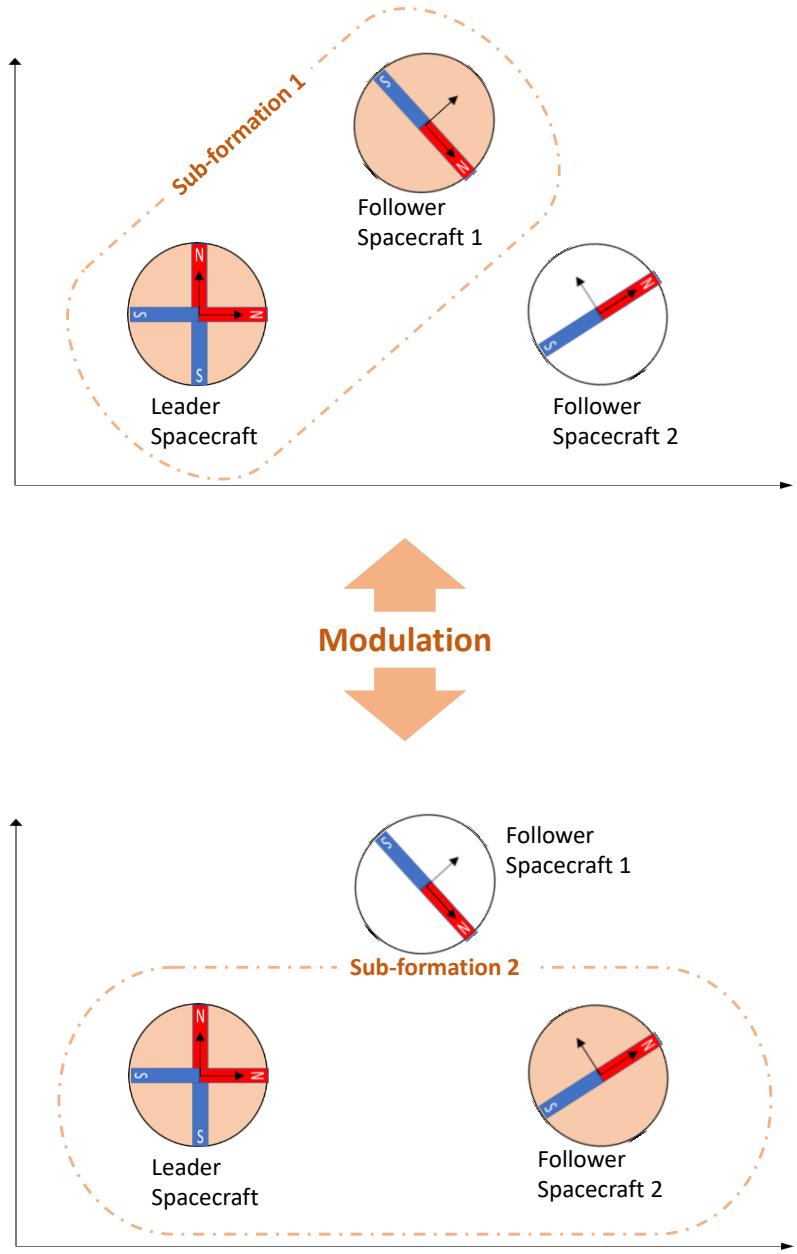

Figure 21. Dividing formation into sub-formations using modulation

Such cases are when modulation can be of benefit. Using the modulation concepts discussed in section 2.3, the three-spacecraft formation can be divided into two sub-formations; each consisting of the leader spacecraft and a single follower spacecraft as shown in Figure 21. Each of the sub-formations would utilize magnetic fields at different frequencies or 90° out of phase, making them decoupled. Each sub-formations is now equivalent to the two-spacecraft formation in Figure 19; which allows for generating unrestrained forces on the follower spacecraft. This translates into the capability of generating arbitrary forces on both the follower spacecrafts.

This highlights how creating additional decoupled sets using modulation can be used to minimize the number of required electromagnets for formation control. These decoupled sets can be generated either by phase or frequency modulation. In a general sense, given the number of decoupled sets $\mathrm{N_D}$ created using modulation, the total number of required electromagnets required to control a formation in 2D becomes:

$$Number\ of\ Required\ Electromagnets = 2N - N_D\ . \qquad (73.)$$

Similarly, in 3D the number would be:

$$Number\ of\ Required\ Electromagnets = 3N - N_D\ . \qquad (74.)$$

One restriction remains however as the number of decoupled sets should be less than the number of spacecrafts in the formation ($\mathrm{N_D} < N$). Having more decoupled sets than the number of spacecrafts does not offer advantages in terms of reducing the number of required electromagnets. Also, each spacecraft should have at least a single electromagnet as otherwise, it would be impossible to generate electromagnetic interactions on that spacecraft.

4.2. Extension to 3D

The previous section showed how creating decoupled sets of magnetic interactions using modulation allows for better controllability of a 2D formation with a lower number of electromagnets. In order to effectively expand this idea to larger formations in 3D, it is desirable to augment the modulation process in the control algorithm to enable it to automatically divide the formation into sub-formations during operation time. The main reason for applying modulation during operation is that the configuration of the formation can change with time and failures can occur unforeseeably. While this might seem challenging at first, it can be easily transformed into a numerical problem incorporated in the process of dipole inversion explained in section 3.2.1. This section shows how the dipole inversion process can be adjusted to account for any reduction in electromagnets in the formation.

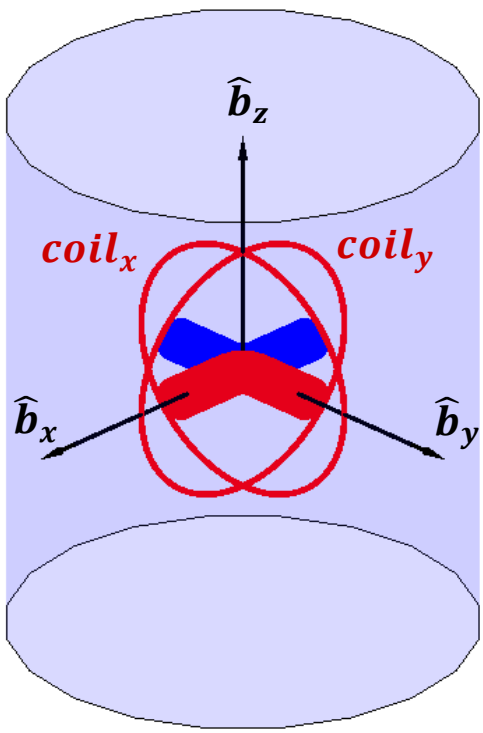

Figure 22. Underactuated EMFF spacecraft in 3D

Considering the case of a spacecraft in 3D with only two orthogonal electromagnets as shown in Figure 22. Logically, the spacecraft would not be able to generate a magnetic moment in

the $\hat{b}_z$ direction as it does not have an electromagnet aligned in that direction. Denoting a unit vector $\hat{K}$ as the direction of the missing electromagnet of the spacecraft, the relationship between feasible magnetic moments $\vec{\mu}$ and $\hat{K}$ becomes as follows:

$$dot(\vec{\mu}, \hat{K}) = 0 . \tag{75.}$$

In the case of a formation, $\hat{K}_i$ represents removed or faulty electromagnets in the ith spacecraft. If a spacecraft is fully actuated, $\hat{R}_i$ can be set to zero in which the property in Eq. (75) always holds. Incorporating this concept into the dipole inversion process, the set of dipole inversion equations to solve numerically becomes:

$$\vec{f}_i^C = \sum_j^N \vec{f}_M \left(\vec{\mu}_j, \vec{\mu}_i\right), \qquad dot\left(\vec{\mu}_i, \hat{K}_i\right) = 0 , \qquad for\ i = 1,2, \ldots\ldots N . \tag{76.}$$

It is apparent from Eq. (76) that an electromagnet loss represents an additional constraint in finding appropriate magnetic moments, which can jeopardize the formation controllability by restraining the ability to generate desired forces. As explained earlier, this can problem can be compensated for by phase and frequency modulation by offering additional freedom in magnetic moment assignments. Following the process explained in section 3.2.1, Eq. (76) can be modified to take advantage of modulation as:

$$\vec{f}_i^C = \sum_j^N \sum_{O=1}^{N_O} \vec{f}_M \left({}^o\vec{\mu}_j, {}^o\vec{\mu}_i\right) \qquad dot\left(\vec{\mu}_i, \hat{K}_i\right) = 0 , \qquad for\ i = 1,2, \ldots\ldots N . \tag{77.}$$

The only remaining design choice comes in determining the number of orthogonal or decoupled sets N_O. The higher the number of decoupled sets, the greater the freedom in the magnetic moment assignment process, which allows operating a formation with a reduced number of electromagnets.

4.3. Simulation & Results

For the purposes of testing the capabilities of phase and frequency modulation in providing control solutions to underactuated EMFF satellites, the simulation in section 3.5 was repeated but with a fewer number of electromagnets. Six of the seven spacecrafts in the formation were equipped with only two electromagnets in a similar manner to Figure 22. Only the central satellite was fully equipped with three electromagnets. To examine the benefits of modulating alternating magnetic fields, the simulation was carried out twice: with and without employing modulation.

4.3.1. Without modulation

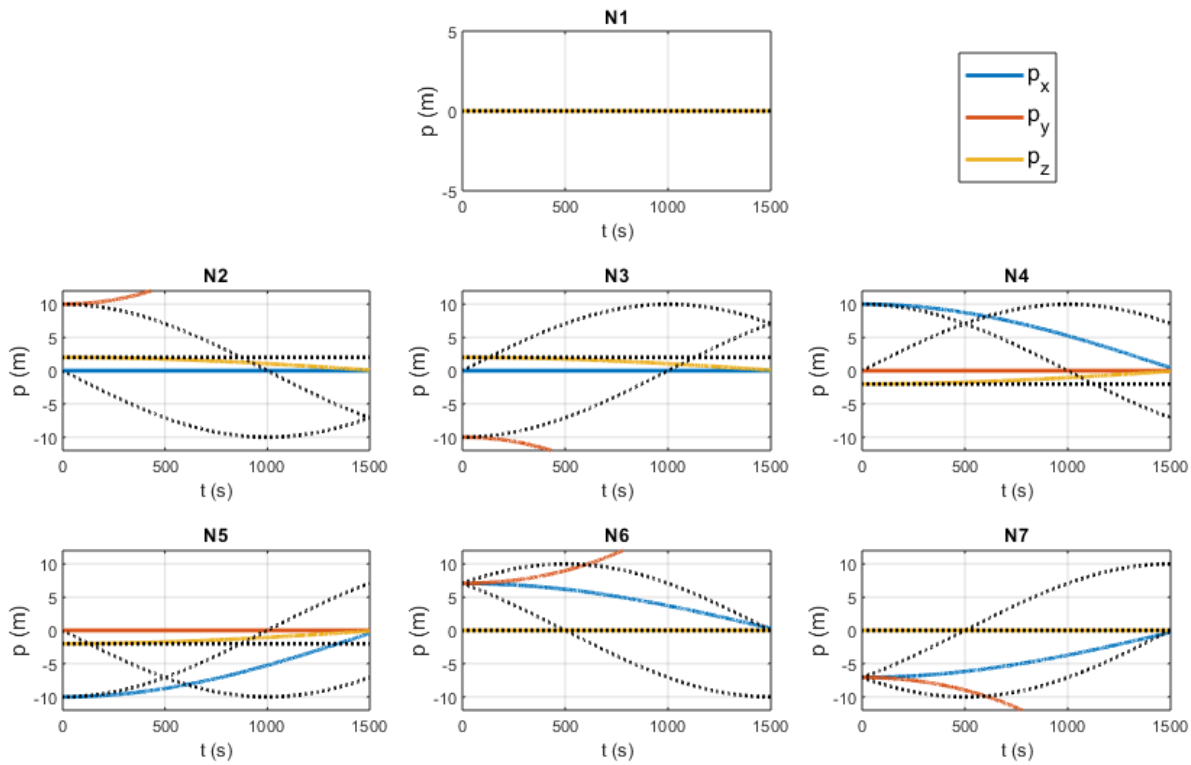

Figure 23. Underactuated 7-spacecraft rotation simulation results without modulation – relative position

First, the simulation was carried out without employing modulation and using the numerical dipole inversion method of Eq. (76). In contrast to the results of section 3.5, the reduction in electromagnets results in the inability of the dipole inversion process of generating the target forces from the position controller. Simply put, no magnetic moments' assignment

results in forces that would adjust the formation as desired. This ultimately results in satellites diverging away from their target positions as demonstrated in Figure 23, where the dotted lines indicate the reference trajectories.

4.3.2. With modulation

For the second simulation, modulation was applied in both frequency and phase. As discussed previously, modulation increases the variety of the possible magnetic interactions, which can undermine the reduction in electromagnets. For this case, modulation is done in two frequency values $f_1 = 2\,Hz$ and $f_2 = 4\,Hz$, with each of these frequencies being modulated in phase as well. This leads to four decoupled sets of magnetic interactions in total. Theoretically, this would allow for the removal of four electromagnets from the formation, which is still less than the six electromagnets removed for the purpose of this simulation. Nonetheless, there is still additional decoupling between distant spacecrafts as electromagnetic force is inversely proportional to the fourth power of separation distance.

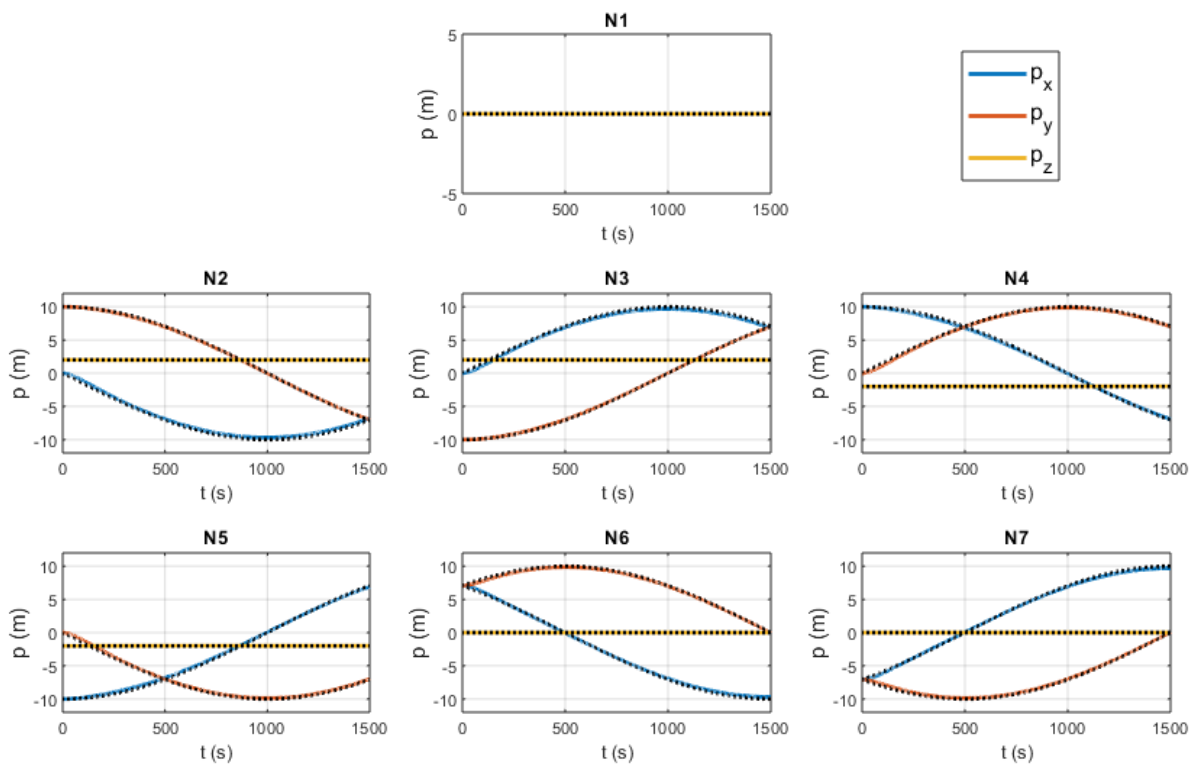

Figure 24. Underactuated 7-spacecraft rotation simulation results with modulation – relative position

Simulation results in terms of relative positions can be observed in Figure 24. The dotted lines show the reference trajectories, which the satellites are now capable of following in spite of the reduction in electromagnets. The average position errors are presented in Table 8. These errors are comparable to the errors in Table 7, which were obtained without the removal of electromagnets. This confirms the capabilities of modulation in undermining the effects of losing or reducing electromagnets. The profile of the magnitude of magnetic moments reconfiguring the formation is presented in Figure 25. It is apparent that the μ_z component of the magnetic moments is zero for most spacecrafts, indicating the faulty or removed electromagnets. Finally, the stable behavior of the satellites' attitude can be perceived in quaternions in Figure 26.

Table 8. Average position errors for the simulation of the underactuated 7-spacecraft rotation simulation

Spacecraft:	**1**	**2**	**3**	**4**	**5**	**6**	**7**
Average Error (m):	0.0031	0.2922	0.2914	0.2414	0.2402	0.2273	0.2267

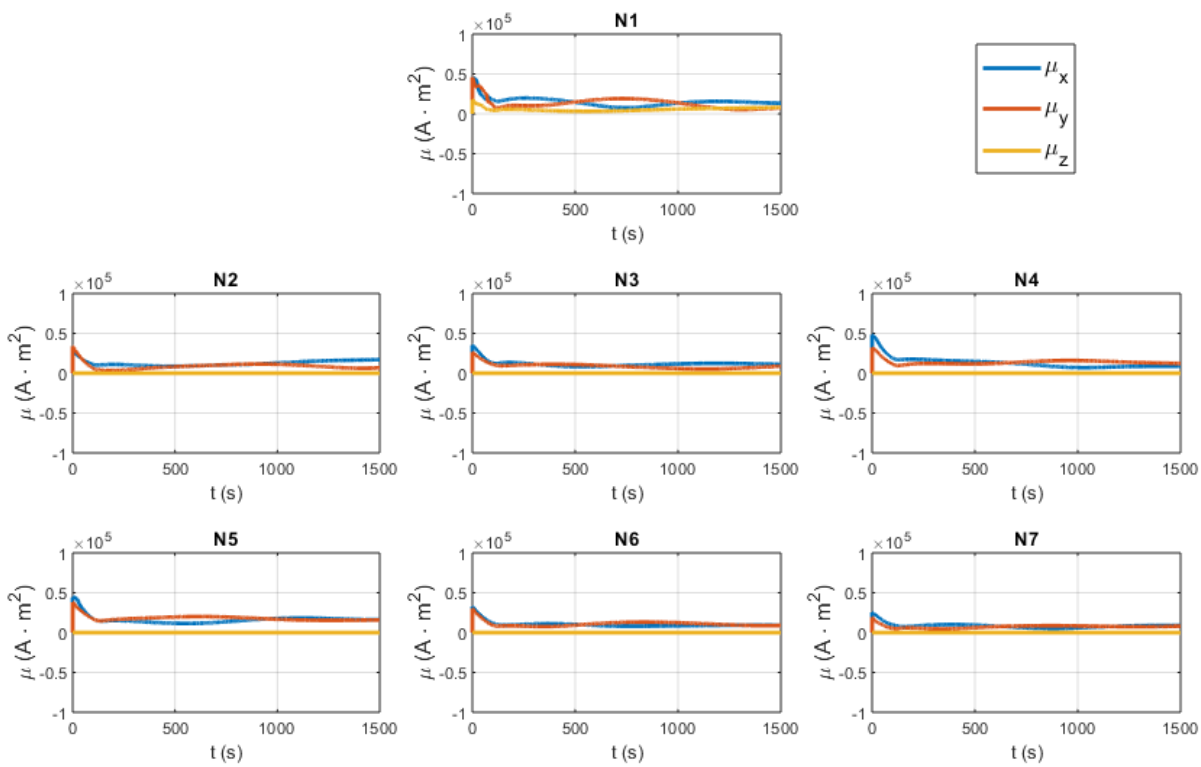

Figure 25. Control time history for the underactuated 7-spacecraft rotation simulation

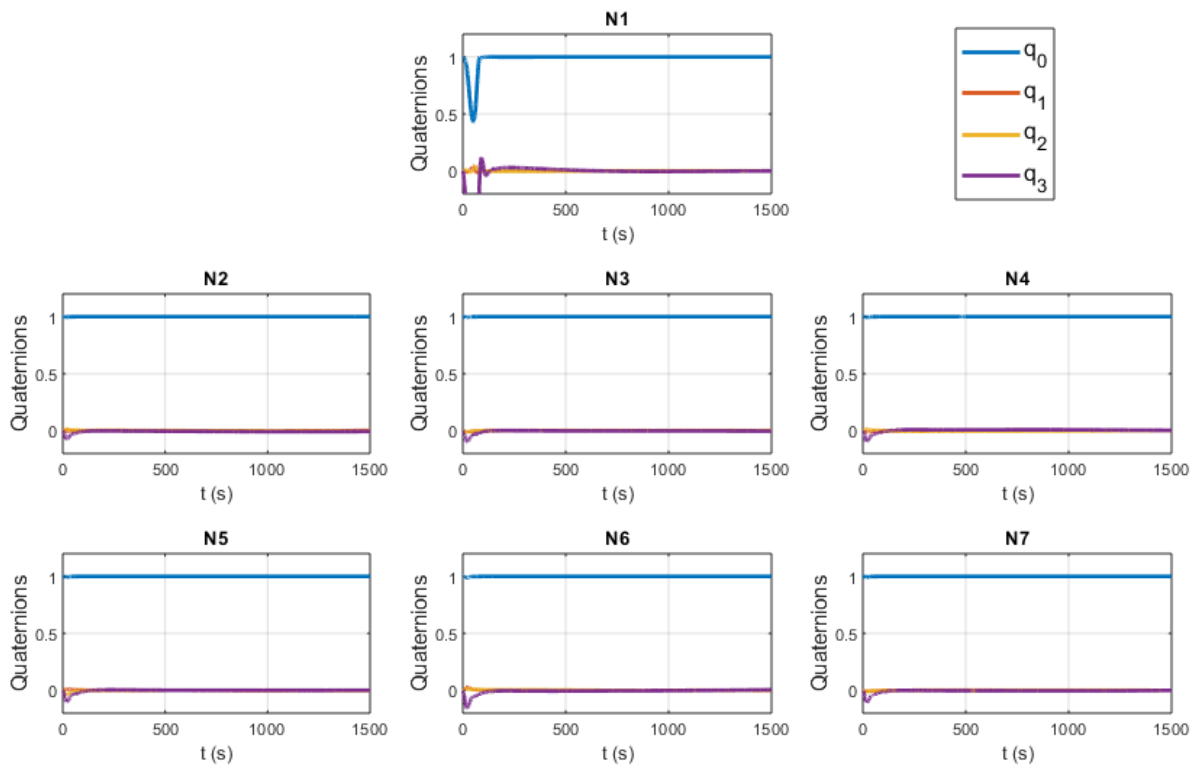

Figure 26. Underactuated 7-spacecraft rotation simulation results with modulation – attitude

In summary, results show that all spacecrafts follow their designated trajectory while maintaining their target attitude. This confirms the validity of the proposed approach of utilizing modulation to control EMFF formations with severe minimization in electromagnets. Conceptually, this would enable the design of EMFF missions with lower costs and mass. It also adds redundancy to EMFF operation by enabling formation control under several electromagnets' faults or overheating.

The main shortcoming of modulating alternating magnetic field is added computational complexity. The dipole inversion process finds appropriate magnetic moments' by numerically solving a set of nonlinear equations. Every additional set of decoupled interactions results in additional decision variables for the numerical problem, which in turn requires additional computational time. Table 9 shows the difference in the computation time for several iterations of the dipole inversion process between the simulations in section 3.5 and the simulations in this section. The dipole inversion equations were solved using MATLAB's "fsolve" package on a 3.6

GHz desktop computer. After the first iteration, the inversion problem is initialized with the solution from the previous timestep leading to lower computation times. As seen in the table, the computation time when modulation is employed is considerably higher for all the iterations. Depending on the frequency of the position controller, this might be a serious limiting factor in utilizing modulation for EMFF.

Table 9. Computation time of the dipole inversion process

Iteration:		**1**	**2**	**3**	**4**	**5**
Computation time (s)	**- Without modulation**	0.242	0.037	0.030	0.028	0.093
	- With modulation	0.534	0.177	0.181	0.182	0.191

Chapter 5. Optimization of Angular Momentum & Thermal Buildup

EMFF in its current form still faces some challenges that complicate and obscure practical implementation. One important concern lies in the buildup of angular momentum in the spacecrafts of the formation. The accumulation of torques resulting from electromagnetic interactions could lead to the saturation of the reaction wheels over time. Another serious problem is the thermal buildup and heating in the superconducting electromagnets used to control the formation. While HTS electromagnets should theoretically have zero resistance, this property might be lost as a result of imperfections and faults. This in turn damages the electromagnets and jeopardizes the controllability of the formation.

Several approaches were proposed to tackle the aforementioned problems in EMFF through better system design and mission planning. Another possible solution stems from enhancing the control process of electromagnetic formations by optimizing magnetic interactions. A variety of magnetic moments' combinations might result in the same forces and translational behavior in a formation while yielding different outcomes in terms of torques and heat generation. It then becomes advantageous to select the most optimal set of magnetic moments to avoid any undesired behavior and enhance overall performance. This concept can be referred to as optimal dipole inversion and has been briefly examined in section 3.2.2. Moreover, modulation of alternating magnetic moments induces more variety in the possible magnetic solutions, which can be beneficial in the optimal dipole inversion process. This chapter examines the effectiveness of optimal dipole inversion in alleviating the angular momentum buildup and thermal accumulation problems in sections 5.1 and 5.2 respectively.

5.1. Angular Momentum Minimization

5.1.1. Concept & Approach

Angular momentum buildup is a critical problem facing EMFF. The continuous accumulation of electromagnetic torques can have severe consequences on the attitude control functionality. Electromagnetic forces and torques are usually coupled; thus, when the formation is reconfigured, rotational behavior is often exhibited. Taking a closer look at Eqs. (13) and (14) reveals that electromagnetic torques are inversely proportional to the third power of the separation distance, while forces are inversely proportional to the fourth power of the distance. This leads to distant magnetic moments or spacecrafts having higher rotational impact on each other rather than a translational effect as shown in Figure 27. However, as the purpose of using electromagnets in most configurations of EMFF is to exclusively control the translational degrees of freedom, such rotational impact is considered to be undesirable as it would only accumulate angular momentum without positively contributing to formation reconfiguration.

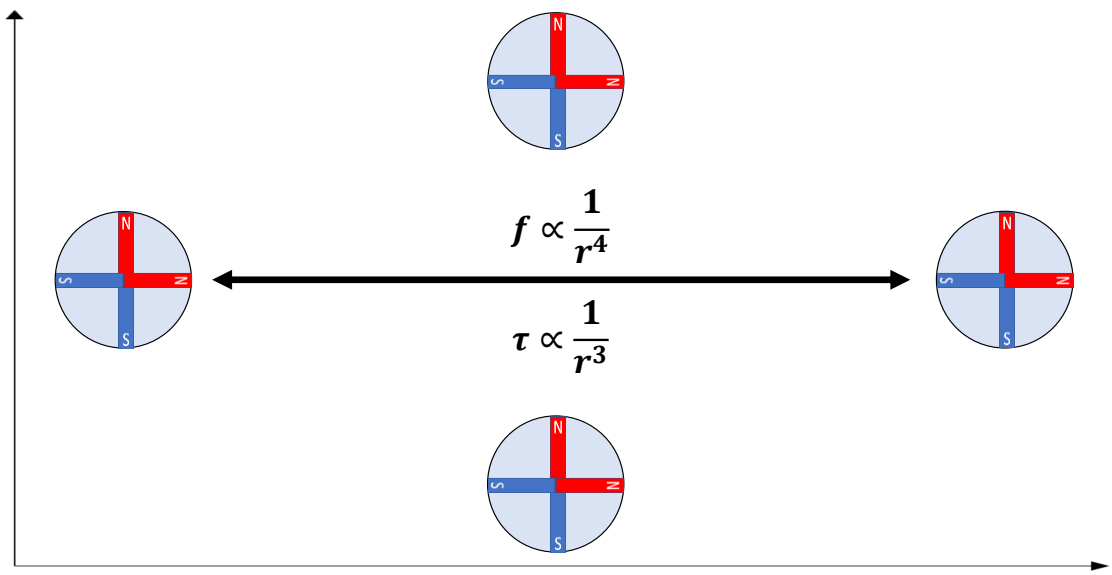

Figure 27. Electromagnetic forces and torques between distant spacecrafts

The intuition of using phase and frequency modulation stems from such cases of electromagnetic interactions, where torques are generated without beneficial forces. Modulation can be used to eliminate these interactions by decoupling the associated magnetic moments.

Selecting which magnetic moments to decouple and when to decouple is quite challenging to do manually; therefore, it is important to develop means of automatically harnessing the benefits modulation offers in minimizing angular momentum. The remainder of this section develops a framework to augment this optimization problem in the dipole inversion process of formation control. The framework developed here generally benefits from any freedom in assigning the magnetic moments and does not necessarily require modulation. Nonetheless, since modulation offers more freedom in magnetic moments' assignment, it is hence more advantageous to incorporate it in the overall optimization scheme as demonstrated later in the results section.

Section 3.2.2 presented a means of optimizing the selection of magnetic moments to minimize a cost function while achieving the desired forces. The goal now is to develop a cost function the represents the angular momentum optimization criteria. First, defining a $3N \times 1$ vector τ concatenating the electromagnetic torques in all the spacecrafts of the formation as:

$$\tau = \begin{bmatrix} \vec{\tau}_1 \\ \vec{\tau}_2 \\ \vdots \\ \vec{\tau}_N \end{bmatrix}. \tag{78.}$$

The most straightforward cost function to minimize torques is a quadratic function as:

$$J = \tau^T [W] \tau \,. \tag{79.}$$

Where $[W]$ is a positive definite weighting matrix.

While this cost function minimizes instantaneous torque at a given timestep of applying the control scheme, it does necessarily optimize the accumulated torque across several timesteps. Especially since the generated torques can sometimes actually counter the accumulation of angular momentum and desaturate the reaction wheels; at which case it becomes desirable to maximize such torques. To incorporate this feature, another $3N \times 1$ vector Ω is introduced to concatenate the reaction wheels velocities in all the satellites as:

$$\Omega = \begin{bmatrix} \vec{\Omega}_1 \\ \vec{\Omega}_2 \\ \vdots \\ \vec{\Omega}_N \end{bmatrix}. \tag{80.}$$

A new cost function that directly counters the accumulated angular momentum in the reaction wheels is then formulated as:

$$J = \tau^T [W_1] \tau - W_2 \, dot(\tau, \Omega) \, . \tag{81.}$$

Where W_2 is a weighing scalar.

The overall dipole inversion process then becomes:

$$\begin{gathered} \textbf{Minimize}: \mathrm{J} = \tau^T [W_1] \tau - W_2 \, dot(\tau, \Omega) \, , \\ \textbf{Subject to}: \vec{f}_i^{\,C} = \sum_j^N \vec{f}_M \left(\vec{\mu}_j, \vec{\mu}_i \right), \quad for \; i = 1,2, \ldots \ldots N \, . \end{gathered} \tag{82.}$$

One possible improvement that can be augmented is accounting for the geomagnetic field. As explained in section 3.4, earth's magnetic field can be used to generate desaturation torques and alleviate the torque accumulation problem. The shortcoming of that approach was that it cannot counter angular momentum parallel to the geomagnetic field. Therefore, the optimal dipole inversion process in Eq. (82) can be adjusted to specifically target and minimize angular momentum components parallel to earth's magnetic field. To do so, a $3N \times 1$ vector B is defined to represent earth's magnetic field $\vec{b}_{e_i}$ at each of the formation's N spacecrafts as:

$$B = \begin{bmatrix} \vec{b}_{e_1} \big/ \left\| \vec{b}_{e_1} \right\| \\ \vec{b}_{e_2} \big/ \left\| \vec{b}_{e_2} \right\| \\ \vdots \\ \vec{b}_{e_N} \big/ \left\| \vec{b}_{e_N} \right\| \end{bmatrix} . \tag{83.}$$

The exclusive penalization of angular momentum components parallel to B transfers the optimal dipole inversion problem in Eq. (82) to the following:

$$\begin{gathered} \textbf{Minimize}: \mathrm{J} = \tau^T [W_1] \tau - W_2 \, dot(\tau, dot(\Omega, \mathrm{B}) \cdot B) \, , \\ \textbf{Subject to}: \vec{f}_i^{\,C} = \sum_j^N \vec{f}_M \left(\vec{\mu}_j, \vec{\mu}_i \right), \quad for \; i = 1,2, \ldots \ldots N \, . \end{gathered} \tag{84.}$$

Finally, as mentioned earlier, phase and frequency modulation can offer additional advantages in this process by introducing more variant electromagnetic interactions and expanding the freedom in assigning magnetic moments. Following the guidelines of section 3.2.1 on incorporating modulation in the dipole inversion process, the optimization problem in Eq. (84) is modified to incorporate the N_o decoupled sets as:

$$\textbf{Minimize}: \mathrm{J} = \tau^T[W_1]\tau - W_2\, dot(\tau, dot(\Omega, \mathrm{B}) \cdot B)\,,$$

$$\textbf{Subject to}: \vec{f}_i^C = \sum_{j}^{N} \sum_{O=1}^{N_O} \vec{f}_M\left({}^{O}\vec{\mu}_j, {}^{O}\vec{\mu}_i\right), \quad for\ i = 1,2, \ldots\ldots N\,. \tag{85.}$$

5.1.2. Simulation & Results

To validate the torque optimized dipole inversion process proposed in this section, a closed-loop simulation was carried out for a three-spacecraft reconfiguration maneuver as shown in Figure 28. The overall control scheme still follows the guidelines of chapter 3 with the exception of the dipole inversion process. The simulation was repeated three times, with the details of the dipole inversion process being different for each simulation. First, the dipole inversion process was not optimized to take torque accumulation into account. The second simulation incorporates angular momentum buildup in the dipole inversion process as described by Eq. (84), but does not employ modulation of magnetic moments. The final simulation takes advantage of modulating magnetic moments in the optimized dipole inversion process as indicated by Eq. (85). Modulation is only applied in phase, leading to two decoupled sets of magnetic interactions ($N_O = 2$).

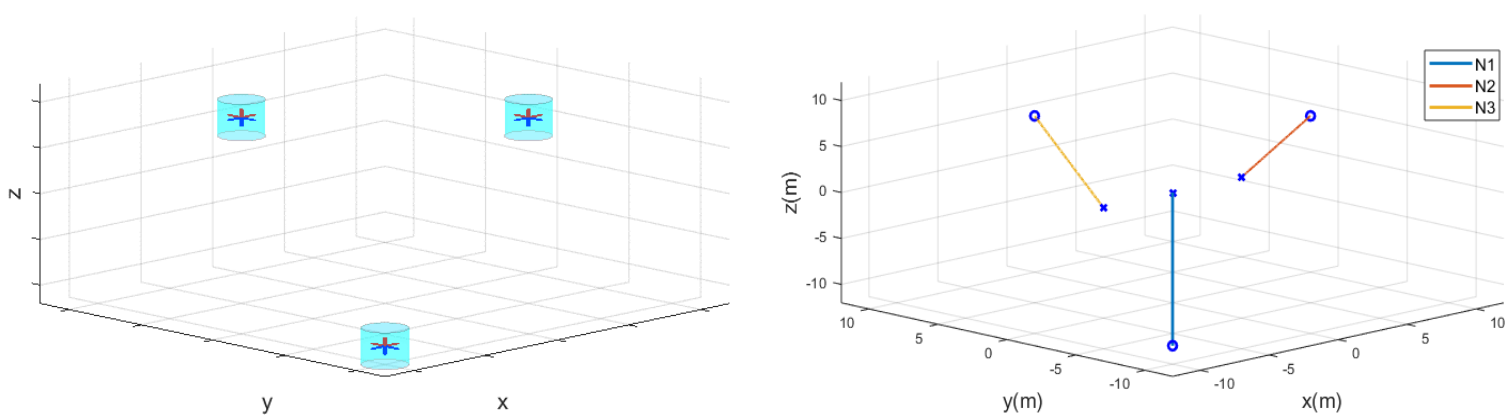

a) Configuration b) Trajectory

Figure 28. Configuration for the simulation of a 3-spacecraft formation

The design and specifications of each of the formation's satellites follow the description in section 2.7. Other simulation and control parameters can be observed in Table 10 to Table 12. It should be noted that the geomagnetic angular momentum management algorithm of section 3.4 is applied for all the three simulations.

Table 10. Simulation parameters

Simulation time	1500 seconds
Time step	0.1 s
Integrator	4'th order runge-kutta
Position control frequency	2 Hz
Alternating magnetic moments frequency	2 Hz
Attitude control frequency	10 Hz

Table 11. Orbit and formation properties

Orbit Type	Circular LEO
Altitude	900 km
Orbit inclination	0°
Initial relative positions (m)	$p_1 = \{-10, -10, -10\}$ $p_2 = \{10, 0, -5\}$ $p_3 = \{0, 10, -5\}$
Final relative positions (m)	$p_1 = \{0, 0, 0\}$ $p_2 = \{5, 0, 0\}$ $p_3 = \{-5, 0, 0\}$

Table 12. Control parameters for the 3-spacecraft reconfiguration simulation

$[\boldsymbol{K}]$	$[\boldsymbol{\lambda}]$	$[\boldsymbol{k_a}]$	$[\boldsymbol{\lambda_a}]$	$\boldsymbol{\mu_{AMM}}$	**Weighing Values**	
					$\mathbf{W_1}$	$\mathbf{W_2}$
$0.0125 \times [I]$	$0.0125 \times [I]$	$10 \times [I]$	$15 \times [I]$	$5 \times 10^4\ A \cdot m^2$	$10^4 \times [I]$	500

Since the position and attitude controllers were the same for all the three cases, almost identical results were obtained in the simulations. These results can be seen in Figure 29 and Figure 30. The position of all the spacecrafts clearly converges to the target indicated by the dotted line, while the scalar component of attitude quaternions q_o remains around unity for all satellites. This again proves the validity of the overall control scheme.

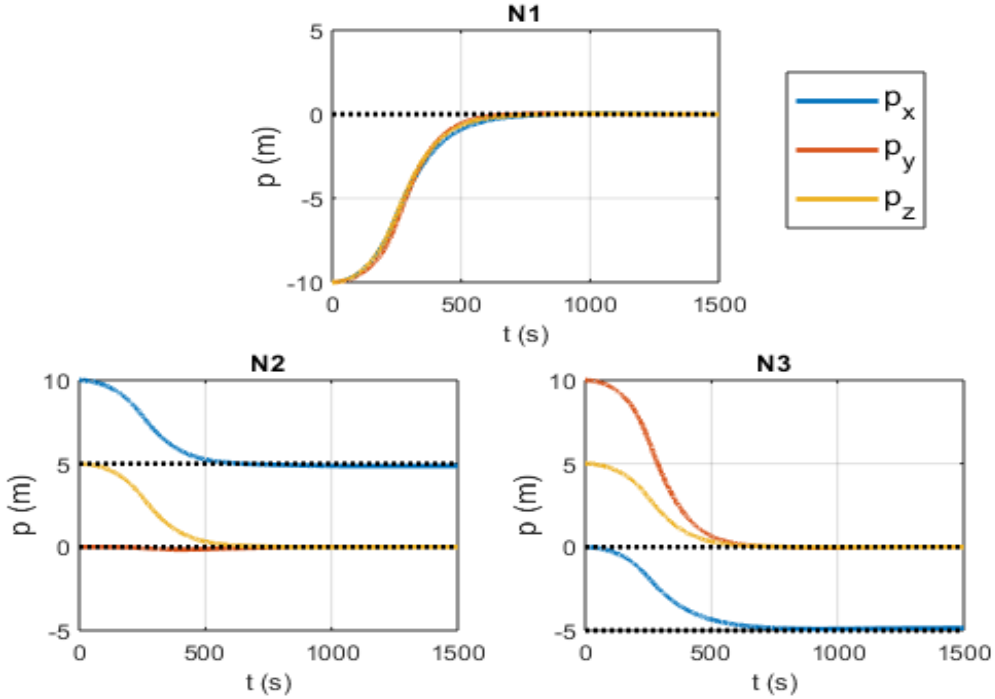

Figure 29. 3-spacecraft reconfiguration with torque optimization simulation results – relative position

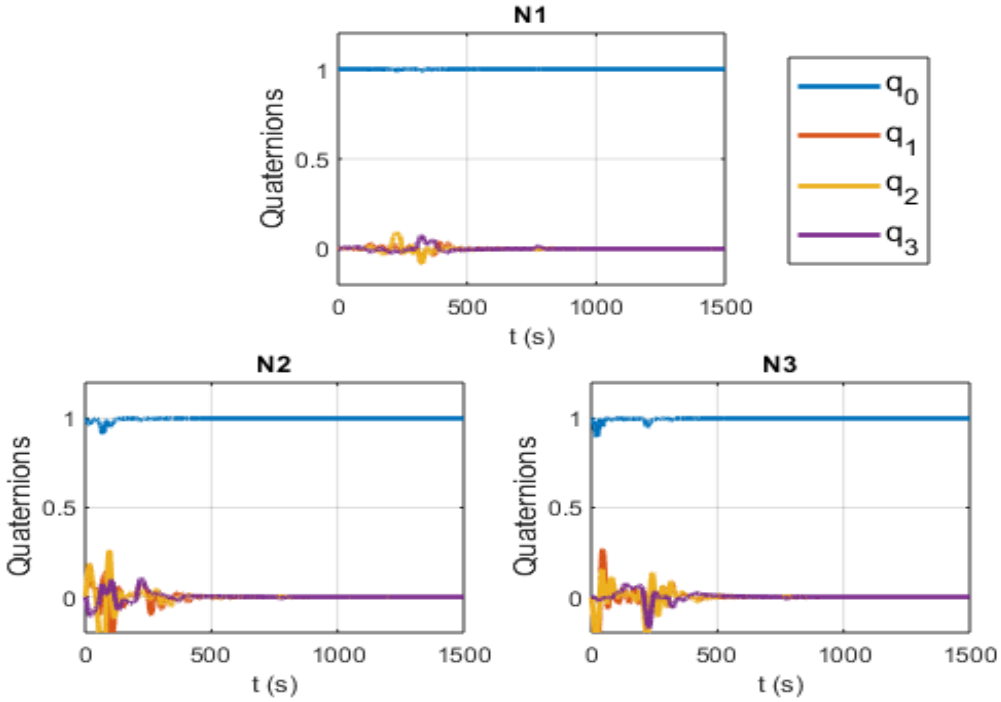

Figure 30. 3-spacecraft reconfiguration with torque optimization simulation results– attitude

The main differences between the three simulations manifest in the assignment of magnetic moments used to reconfigure the formation. Since the dipole inversion process differs in each case, the profile of control magnetic moments differs as well. Figure 31 shows the time history of the magnitude of magnetic moments for each electromagnet in the formation. The objective of manipulating these magnetic moments was to change the torque accumulation behavior in the formation. This would manifest in the response of the reaction wheels in the system. Figure 32 displays the angular velocity of the reaction wheels on each satellite of the formation. It is apparent that significant differences exist between the different simulations.

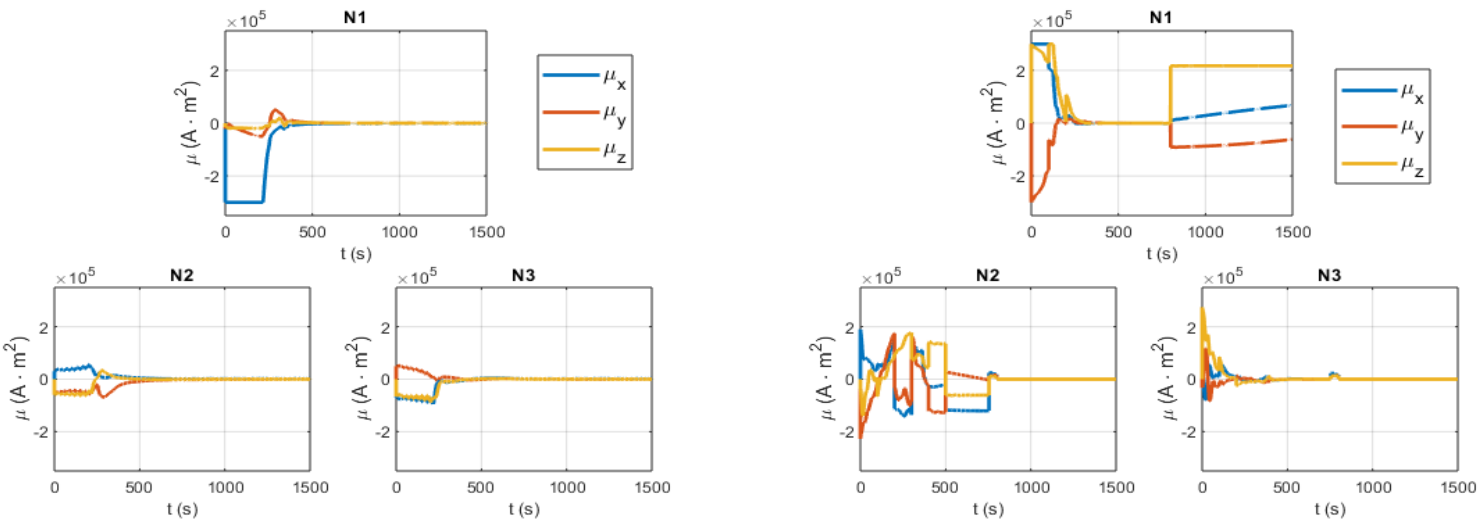

a) without optimization

b) with optimization – no modulation

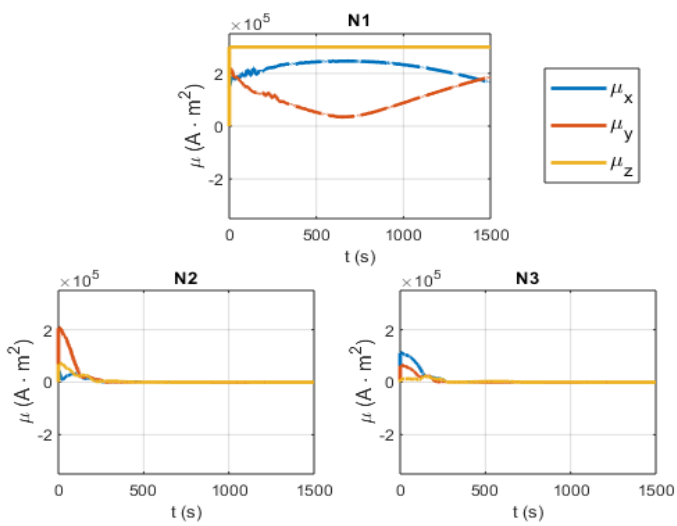

c) with optimization & modulation

Figure 31. Control time history for the 3-spacecraft reconfiguration simulation with torque optimization

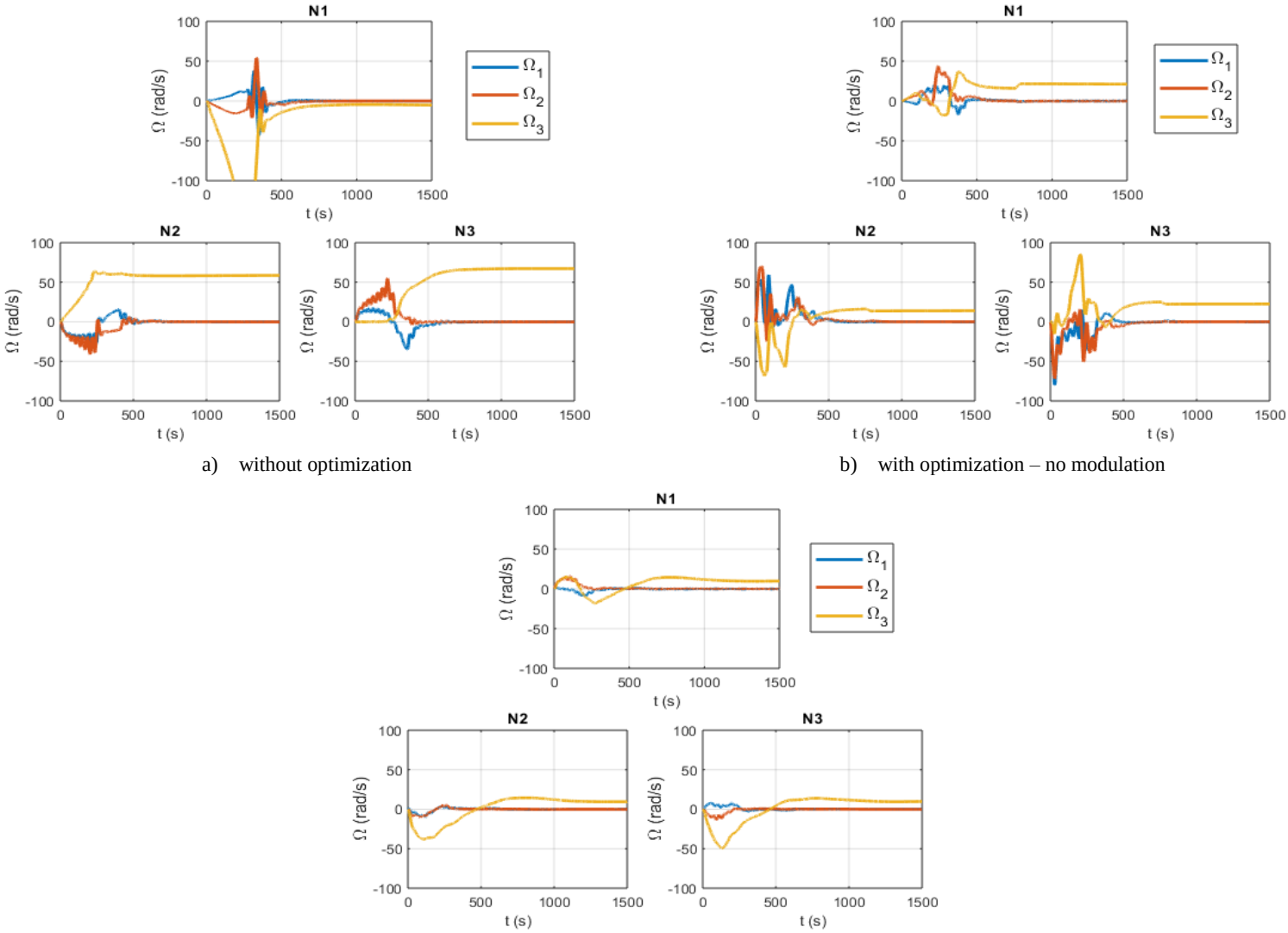

a) without optimization

b) with optimization – no modulation

c) with optimization & modulation

Figure 32. 3-spacecraft reconfiguration with torque optimization simulation results – reaction wheel velocity

It can be observed that in all the simulations, the x and y components of the reaction wheels' rotation die out as a result of the geomagnetic angular momentum algorithm. The target differences then become the z components of reaction wheels' angular velocity. For simpler analysis, Figure 33 demonstrates the accumulated angular momentum in each spacecraft for the three simulation cases. First, optimizing the dipole inversion process significantly reduces the accumulated angular momentum for the second and third satellites, but results in a slightly higher angular momentum for the first satellite. All in all, it results in a more uniform distribution of angular momentum which reduces the chance of a reaction wheel saturation and alleviates the

torque buildup problem. Furthermore, further reductions in angular momentum can be obtained when modulation is applied. Table 13 easily demonstrates these results numerically in terms of the terminal angular momentum in each satellite. These results confirm the effectiveness of optimal dipole inversion in mitigating the problem of torque accumulation in EMFF and validate the concepts presented in this section.

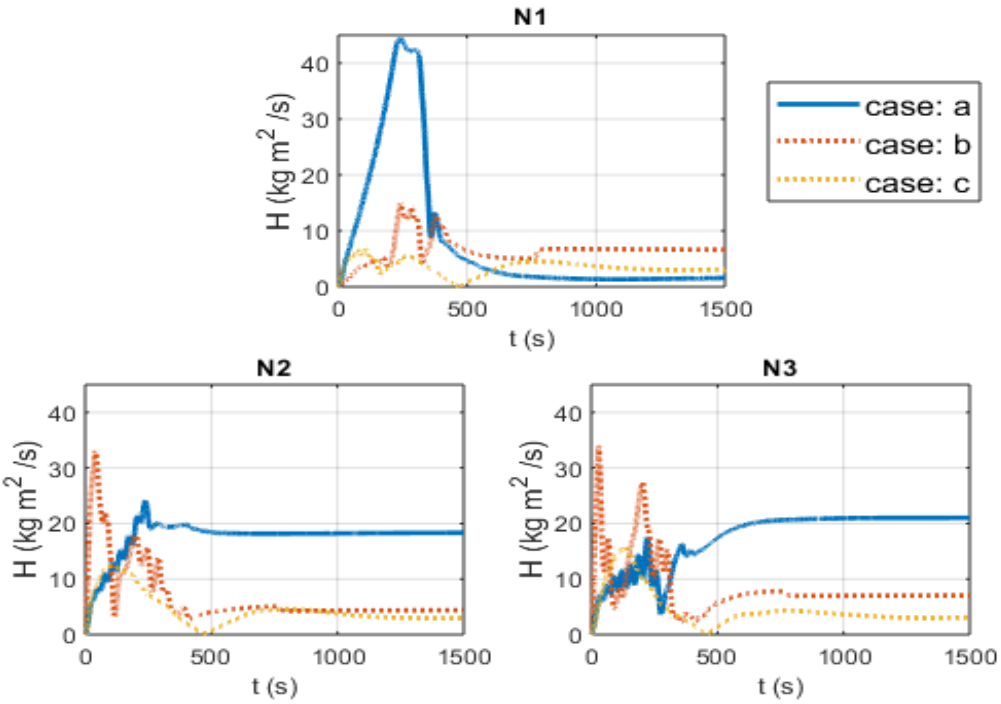

Figure 33. 3-spacecraft reconfiguration with torque optimization simulation results – angular momentum

Table 13. Terminal reaction wheels' angular momentum

Spacecraft:		**N1**	**N2**	**N3**	**Total**
Terminal Angular Momentum ($\mathbf{kg \cdot m^2/s}$):	**- Without optimization**	1.576	18.337	21.016	40.930
	- With optimization **- Without modulation**	6.626	4.388	7.050	18.064
	- With optimization **- With modulation**	3.059	2.999	3.071	9.129

These improvements, however, come at the cost of additional computational time. Table 14 shows the required time for several iterations of the dipole inversion process for each of the three cases. In the first case, the dipole inversion process was a numerical problem to solve a set of nonlinear equations. However, for the other two simulations, the dipole inversion problem became a constrained nonlinear optimization problem, which is more complex and demands more computational time. Applying modulation also increases the computational time as it corresponds to additional decision variables. The computing times in the below table were obtained from using MATLAB's "fmincon" package on a 3.6 GHz desktop computer.

Table 14. Computation time of the torque optimized dipole inversion process

Iteration:		**1**	**2**	**3**	**4**	**5**
Computation time (s)	**- Without optimization**	0.188	0.021	0.019	0.013	0.007
	- With optimization **- Without modulation**	0.245	0.104	0.0727	0.083	0.068
	- With optimization **- With modulation**	0.366	0.179	0.109	0.104	0.102

5.2. Thermal Accumulation Minimization

5.2.1. Concept & Approach

The previous section optimized the dipole inversion process to alleviate the angular momentum buildup problem. The same approach can be utilized to tackle another problem facing EMFF: the thermal accumulation in electromagnets. EMFF utilizes high-temperature superconducting electromagnets to generate very strong magnetic moments that interact yielding translational and rotational movement. These electromagnets require cooling below a critical temperature to maintain a non-resistive state [23]. While in theory a non-resistive state would mean that no heat would be generated, imperfections or faults in the electromagnets can accumulatively raise the temperature in the coils [24]. Consequently, heating would either prevent the generation of strong magnetic moments or permanently damage the electromagnets, both of which jeopardize formation controllability. While the most upfront approach of solving this problem is enhancing the electromagnet cooling mechanism, such negative consequences can also be averted by taking thermal accumulation into account when assigning magnetic moments into the electromagnets of the formation. This sub-section follows the second approach by modifying the dipole inversion process to target strong magnetic moments away from heating electromagnets; giving them a chance to cool down and leading to a better overall distribution of the thermal accumulation.

First, defining a $3N \times 1$ vector U to concatenate the magnetic moments $\vec{\mu}_i$ of all the N spacecrafts of the formations, and a $3N \times 3N$ diagonal matrix $[T]$ to represent the temperature of all the electromagnets of the formation:

$$U = \begin{bmatrix} \vec{\mu}_1 \\ \vec{\mu}_2 \\ \vdots \\ \vec{\mu}_N \end{bmatrix}. \tag{86.}$$

$$[T] = \begin{bmatrix} T_{1_x} & & & & & & & \\ & T_{1_y} & & & 0 & & \cdots & & 0 \\ & & T_{1_z} & & & & & & \\ & & & T_{2_x} & & & & & \\ & 0 & & & T_{2_y} & & & & \vdots \\ & & & & & T_{2_z} & & & \\ & \vdots & & & & & \ddots & & 0 \\ & & & & & & & T_{N_x} & \\ & 0 & & & \cdots & & 0 & & T_{N_y} \\ & & & & & & & & & T_{N_z} \end{bmatrix}. \qquad (87.)$$

Where T_{i_x}, T_{i_y} and T_{i_z} represent the temperatures in Kelvin for each of the three electromagnets installed on the ith spacecraft of the formation.

A simple quadratic cost function can then be constructed to penalize magnetic moments at heating electromagnets as $J = U^T[T]U$. This transforms the optimal dipole inversion to the formulation in Eq. (88). This cost function would favor generating magnetic moments at electromagnets with low temperature, while minimizing the utilization of heating electromagnets.

$$\textbf{Minimize}: \mathrm{J} = U^T[T]U\,,$$

$$\textbf{Subject to}: \vec{f}_i^{\,C} = \sum_j^N \vec{f}_M\left(\vec{\mu}_j, \vec{\mu}_i\right), \quad for\ i = 1,2,\ldots\ldots N\,. \qquad (88.)$$

This optimization technique can be applied without necessarily using modulation. But again, the additional freedom modulation offers in assigning magnetic moments can be of benefit in directing magnetic moments away from heating coils. Modulation can be easily incorporated in the optimal dipole inversion problem as explained in section 3.2.1.

5.2.2. Simulation & Results

Analogous to the previous chapters, closed-loop simulations are used to verify the ideas suggested in this section. The same simulation configuration and parameters from section 5.1 are used here with the only difference being the objectives of optimizing the dipole inversion process. The objective here is to minimize the thermal accumulation in electromagnets and reduce their risk of overheating by taking these criteria into account when finding solutions to the magnetic moments' assignment process. Again, the simulation is carried out three times: once without

optimizing the dipole inversion process, once with the optimal dipole inversion concept but without employing modulation, and finally, once with utilizing phase modulation in the optimization problem.

As the purpose of these simulations is to evaluate improvements in the thermal build-up problem, it is necessary to consider the thermal properties of the electromagnets. Although superconducting electromagnets should ideally have zero resistance and thus generate no heat at all, a relatively small resistance values of $\mathrm{R} = 2\,\Omega$ was assumed for each electromagnet to account for imperfections and possible quenching. Additionally, a specific heat of $\mathrm{C} = 6.2 \times 10^4\ j/k$ is considered for the coil and liquid-nitrogen combination. The heating rate $\frac{dT}{dt}$ in can then be calculated depending on the magnitude of the assigned magnetic moment μ as shown in Eq. (89). Where additional parameters such as the coil's number of turns N_t and cross-sectional area A are carried over from section 2.7.

$$\frac{dT}{dt} = \frac{p}{C} = \frac{(i^2 R)}{C} = \left(\frac{\mu^2 R}{N_t^2 A^2 C}\right) = \frac{R}{N_t^2 A^2 C}\mu^2 \approx 1 \times 10^{-11}\,\mu^2\ \ (k/s)\ . \tag{89.}$$

In regard to the simulation results, the three simulation exhibit identical response in position and attitude as the same controllers were used for these objectives. As demonstrated in Figure 34 and Figure 35, all spacecrafts converge to the desired position indicated by the dotted line while maintaining a stable attitude. The difference between the three cases lies in the magnetic moments that cause these maneuvers. Figure 36 shows the magnitude of magnetic moments on each satellite throughout the maneuver. The objective of manipulating the assignment of magnetic moments is to alter the thermal accumulation behavior in electromagnets. The time history of the temperature of each electromagnet can be observed in Figure 37 for the three simulations. Each electromagnet starts from a $0\,K$ temperature and any concurrent heating is caused by the assignment of magnetic moments as per Eq. (89). The dotted line in these figures indicates the critical temperature of the electromagnets, after which the coils lose their superconductive state and can be considered to be faulty. However, the operation of an electromagnet is not terminated upon reaching the critical temperature in these simulations as the objective is merely investigating the heating behavior.

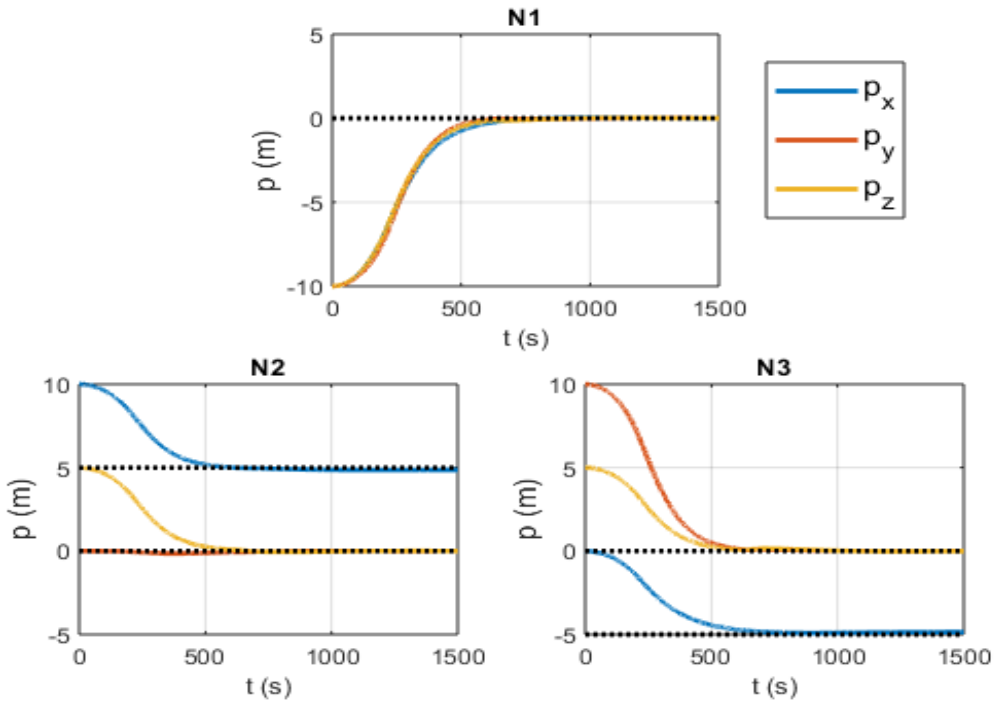

Figure 34. 3-spacecraft reconfiguration with thermal optimization simulation results – relative position

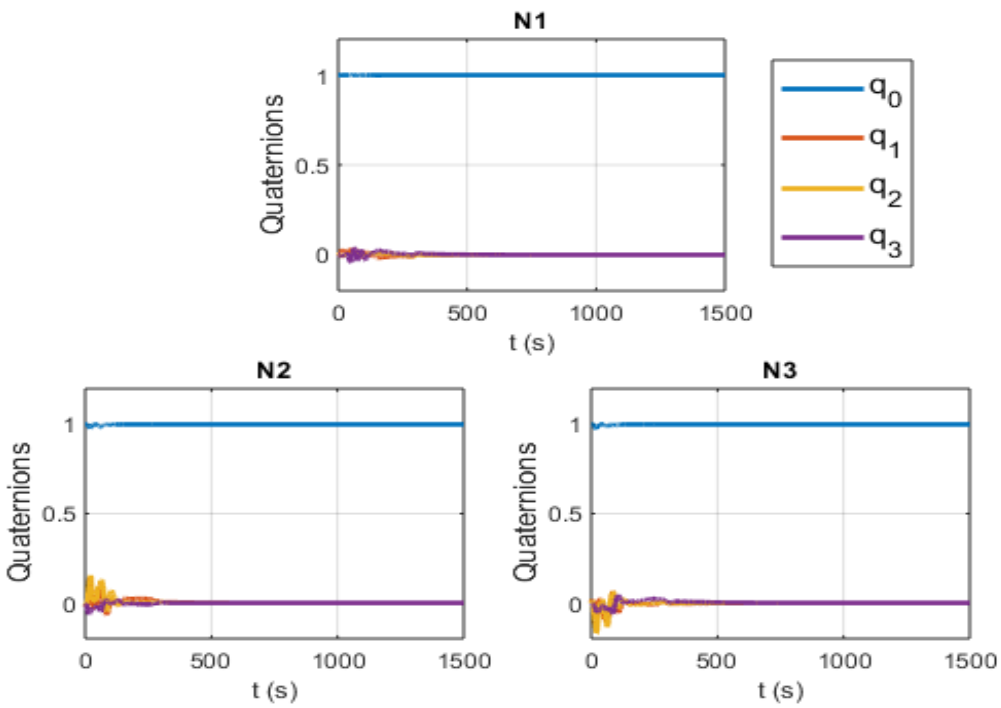

Figure 35. 3-spacecraft reconfiguration with thermal optimization simulation results – attitude

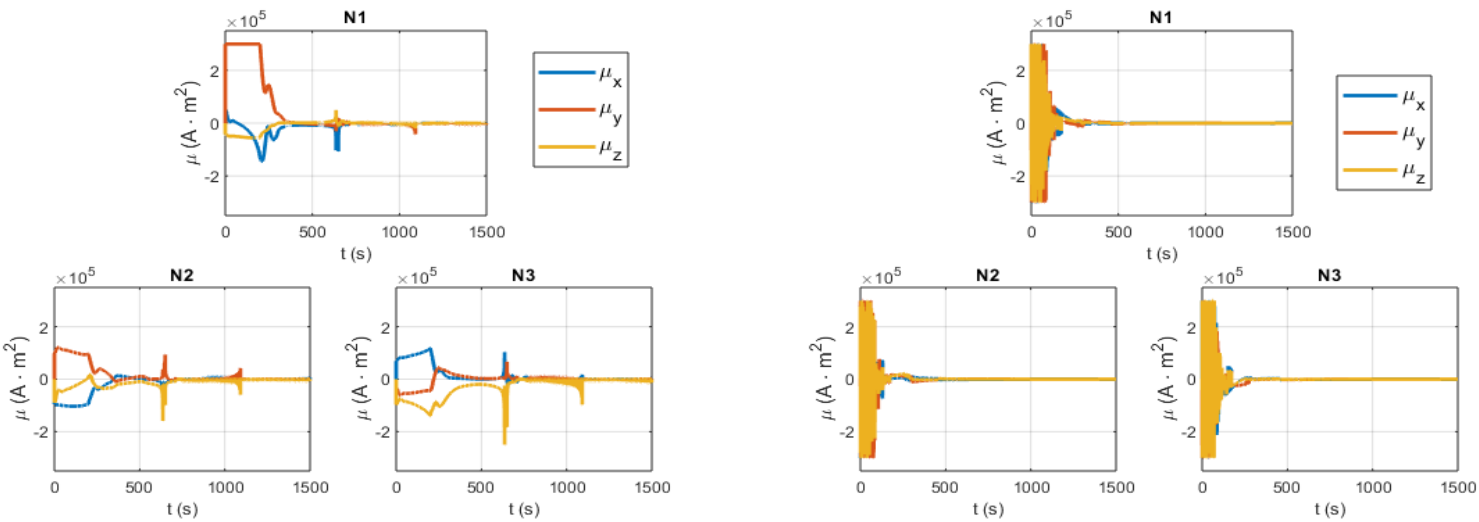

a) without optimization

b) with optimization – no modulation

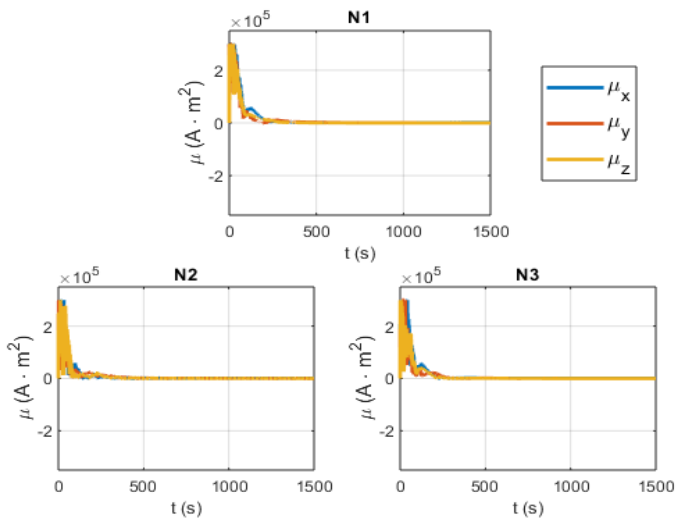

c) with optimization & modulation

Figure 36. Control time history for the 3-spacecraft reconfiguration simulation with thermal optimization

For the first scenario, it can be seen in Figure 37–a that one electromagnet exceeds the critical temperature, which can cause faults and jeopardize the controllability of the formation. This is because the thermal properties of each coil are not taken into account when assigning magnetic moments. For the second and third cases however, the dipole inversion process tries to minimize the utilization of electromagnets that are heating up. This leads to a more uniform distribution of heat across the electromagnets as observed in Figure 37-b and Figure 38-c. This reduces the chance of overheating and results show that none of the electromagnets exceeds the critical temperature.

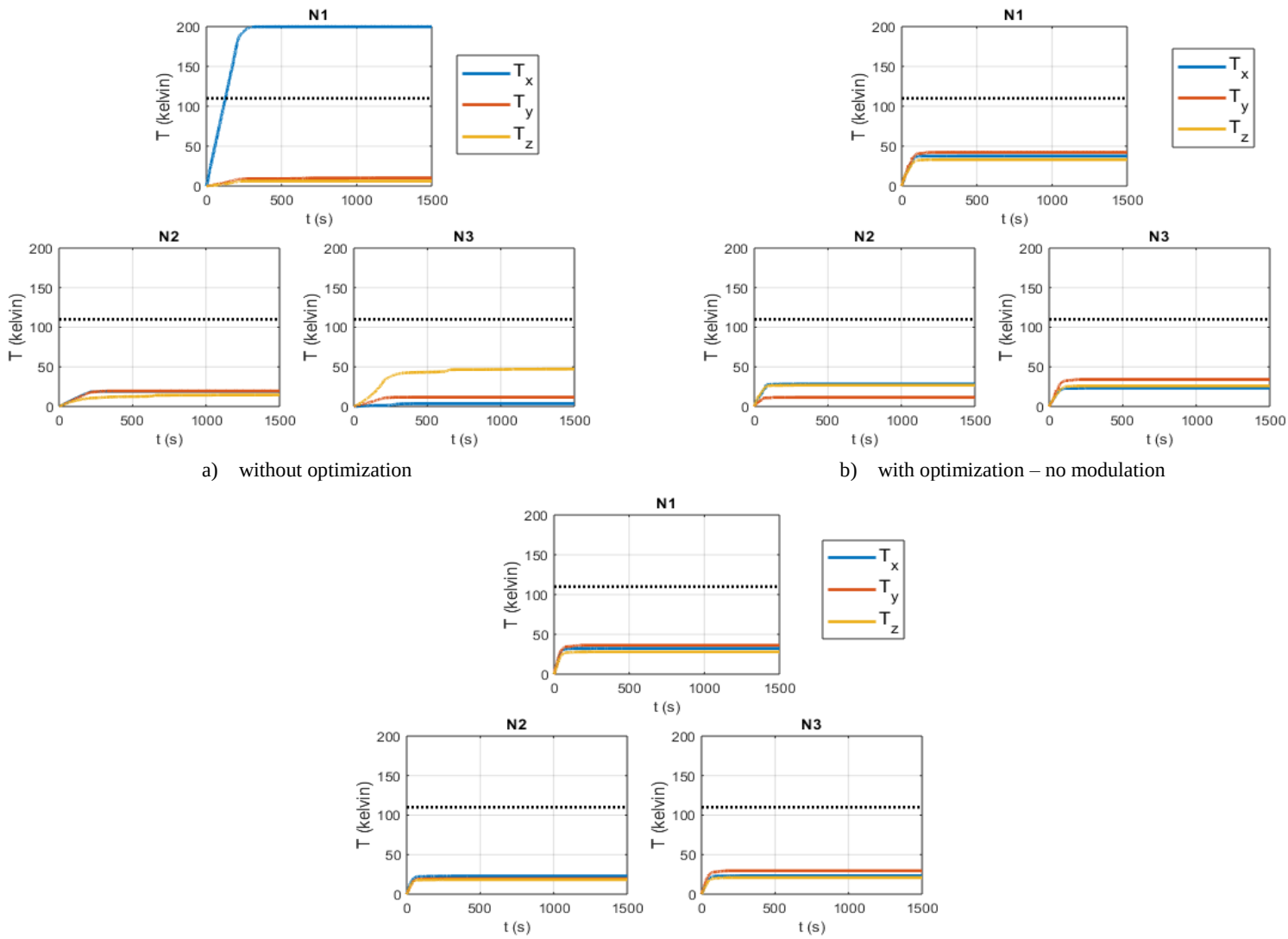

a) without optimization

b) with optimization – no modulation

c) with optimization & modulation

Figure 37. 3-spacecraft reconfiguration with thermal optimization simulation results – electromagnet temperature

To better understand the results, Table 15 shows the maximum, average and L2 norm of temperatures of all the electromagnets at terminal time. All of these parameters are evidently higher in the first scenario. Moreover, the maximum temperature surpasses the critical value, which can cause a failure in the system. The thermal indications significantly fall in the second and third simulations minimizing the chance of overheating faults. This confirms that improving the dipole inversion process is a promising approach to tackle overheating problems in EMFF. As for the advantages of applying modulation, marginal improvements can be observed in all three indicators.

Table 15. Summary of thermal buildup results

Simulation Scenario	Average temperature (k)	Maximum temperature (k)	L2-Norm of temperatures (k)
- Without optimization	36.9	199.8	201.3
- With optimization **- Without modulation**	29.2	42.3	91.4
- With optimization **- With modulation**	25.7	36.3	79.0

Unfortunately, adopting this approach to enhance the thermal distribution in the system translates into additional complexity and computation time. Optimizing the dipole inversion process requires more computations than simply finding a valid solution, especially when modulation takes place and additional decoupled sets of magnetic interactions exist. Table 16 shows the computation time for several iterations of the dipole inversion process for each of the three simulations.

Table 16. Computation time of the thermal optimized dipole inversion process

Iteration:		**1**	**2**	**3**	**4**	**5**
Computation time (s)	**- Without optimization**	0.178	0.017	0.019	0.014	0.010
	- With optimization **- Without modulation**	0.244	0.085	0.065	0.066	0.057
	- With optimization **- With modulation**	0.360	0.291	0.247	0.210	0.251

5.3. Chapter Summary

This chapter investigated optimizing the dipole inversion process of the control policy to tackle two EMFF related problems. Section 5.1 modified the inversion problem to account for the angular momentum accumulation and reaction wheel saturation problem. Section 5.2, on the other hand, adjusted the same process but for the purpose of mitigating electromagnet overheating and alleviating the thermal buildup problem. Promising results with closed-loop simulations were obtained for both objectives, proving the validity of the proposed concepts. In general, better results can also be obtained when modulation of alternating magnetic moments is allowed. Nonetheless, such improvements come at the cost of increased complexity and computation times.

Chapter 6. Optimal Trajectory Generation

The multi-agent and coupled nature of EMFF makes trajectory generation and path planning a crucial part of operating a formation. A feasible trajectory should avoid any collisions with a decent safety margin while satisfying initial conditions and terminal requirements. In addition to collision avoidance, trajectories can be optimized to enhance specific aspects of EMFF and compensate for its shortcoming. While the study so far assumed a pre-defined trajectory for each spacecraft in the formation, this chapter examines the procedure for generating safe and optimal trajectories.

Prior to proceeding with the optimal trajectory generation process, it is first important to define a criterion of optimality. As explored in previous sections, one of the main problems in EMFF is angular momentum accumulation due to the continuous generation of electromagnetic torques. Equation. (14) shows that these electromagnetic torques are inversely proportional to the third power of the relative distance. This property makes angular momentum buildup sensitive to the path the satellites are following. Therefore, minimizing the accumulated angular momentum is a suitable criterion of optimality for generating trajectories. The remainder of this chapter formulates and investigates this trajectory optimization problem.

Trajectory optimization can be thought of as the optimal control problem of finding a state-control pair that minimizes a target cost function J, while satisfying a set of constraints. In a conventional trajectory optimization problem, these constraints can correspond to the dynamics of the system, boundary conditions, path restrictions, and state-control limitations. This problem can be represented by Eq. (90) [34]:

$$\underset{\mathbf{t_o},\,\mathbf{t_f},\,\mathbf{x(t)},\,\mathbf{u(t)}}{\textbf{minimize}} : J = E\left(t_o, t_f, x(t_f)\right) + \int_{t_o}^{t_f} F\big(t, x(t), u(t)\big)dt$$

$$\begin{aligned} \textbf{subject to}: \quad & \dot{x}(t) = f(x(t), u(t), t) && (system\ dynaics) \\ & g^L \le g\left(t_o, t_f, x(t_o), x(t_f)\right) \le g^U && (boundary\ constraints) \\ & h^L \le h\big(t, x(t), x(t)\big) \le h^U && (path\ constraints) \end{aligned} \tag{90.}$$

Where $x(t)$ are the states, $u(t)$ are the controls, and $\{\mathrm{t_o}, \mathrm{t_f}\}$ are the initial and terminal time respectively.

For FF problems, the interdependencies and coupling between different spacecrafts in addition to the nonlinearities of the dynamics make it almost impossible to find an analytical solution to Eq. (90). Fortunately, numerical optimization methods have reached a high level of maturity in the last couple of decades. This enabled several studies to successfully develop trajectory optimization techniques for FF applications [18, 35, 36].

In general, numerical optimization methods fall into two categories: direct and indirect methods. Indirect methods first construct the sufficient and necessary conditions for optimality using the calculus of variations, then discretize and numerically solve these conditions [34]. Direct methods, on the other hand, do not require establishing the conditions for optimality. They directly discretize the trajectory optimization problem into a parameter optimization problem, then solve the parameter optimization problem using nonlinear programming (NLP). While indirect methods can yield more accurate results, direct methods have a larger region of convergence and are less sensitive to the solution's initial guess [34, 35]. This along with the feature that they do not require derivation of optimality conditions, make direct methods easier to adapt and implement in most cases.

One class of direct trajectory optimization are pseudo-spectral methods. Pseudo-spectral methods rely on global high order polynomial interpolation and collocation to parametrize the trajectory optimization problem [37]. Pseudo-spectral optimal control has been verified through different flight implementations such as the minimum-time rotational maneuver for NASA's space telescope TRACE and the zero-propellant maneuver for the International Space Stations [38].

Pseudo-spectral trajectory optimization is used in this chapter to achieve minimum angular momentum trajectories for Electromagnetic Satellite Formations. Section 6.1 reviews the basic mathematical concepts of pseudo-spectral optimal control. Section 6.2 shows how these concepts are applied to the optimization problem at hand. Finally, section 6.3 presents simulation results for using trajectory optimization for EMFF angular momentum management.

6.1. Overview of Pseudo-spectral Optimal Control

Pseudo-spectral optimal control relies on using global high-order orthogonal polynomials to approximate the states and controls of the optimal control problem in Eq. (90). The reason such polynomials are used for interpolation is that they achieve an exponential convergence rate with the order of the polynomials [34]. Additionally, this interpolation method enables easy and accurate numerical approximation of derivatives and integrals. The main shortcoming of using global polynomials however resides in their inability to represent discontinuities in the controls, making them less suitable for applications where non-smooth controls are admissible. This section reviews how pseudo-spectral methods can be used to discretize optimal control problems.

6.1.1. Interpolating functions using orthogonal polynomials

First, for simplficiation purposes, the physical time domain $\mathrm{t} \in [\mathrm{t_o}, \mathrm{t_f}]$ is mapped into a computational domain $t^c \in [-1,1]$ as follows:

$$t^c = \left(\frac{2}{t_f - t_o}\right) t - \left(\frac{t_f + t_o}{t_f - t_o}\right). \tag{91.}$$

Then, Considering a function $y(t^c)$ in the domain $t^c \in [-1,1]$, it can be approximated by an N_c degree polynomial $y(t^c)^{N_c}$ using Lagrange's interpolation formula [38]:

$$y(t^c) \approx y(t^c)^{N_c} = \sum_{i=0}^{N_c} y(t_i^c) L_i(t^c) \qquad -1 \leq \mathrm{t_c} \leq 1. \tag{92.}$$

Where $L_i(t^c)$ correspond to the ith degree Lagrange interpolating polynomial:

$$L_i(t^c) = \prod_{j=0}^{N_c} \frac{t^c - t_i^c}{t_j^c - t_i^c}. \tag{93.}$$

Equations (92) and (93) show that the interpolation formula highly depends on interpolation points $\{t^{N_c}: t_0^c, \dots, t_{N_c}^c\}$ which can be referred to as "cardinal points". Several methods in the literature discuss the selection of these cardinal points using Legendre polynomials to avoid the Runge Phenomenon and minimize approximation errors [37, 38]. Three methods of

selecting cardinal points through Legendre polynomials exist: Gauss points, Gauss-Radau points, and Gauss-Lobatto points. Gauss-Lobatto points are unique in that they use both the initial time $t^c = -1$ and the terminal time $t^c = 1$ as cardinal points. This makes them simpler to use in Boundary Value Problems (BVP) where initial and target states are defined, and thus are used for the remainder of this study. Denoting $P_{N_c}(t^c)$ as the N_c degree Legendre polynomial, Legendre-Gauss-Lobatto points are defined as the roots of $\dot{P}_{N_c}(t^c)$ along with points -1 and 1, as indicated by Eq. (94).

$$t_0^c = -1$$
$$\dot{P}_{N_c}(t_r^c) = 0, \quad r = 1, \dots, N_c - 1 \tag{94.}$$
$$t_{N_c}^c = 1\,.$$

Defining vectors $y^{N_c} = [y(t_0^c), \dots, y(t_N^c)]$ and $\frac{dy^{N_c}}{dt^c} = \left[\frac{dy}{dt^c}|_{t_0^c}, \dots, \frac{dy}{dt^c}|_{t_{N_c}^c}\right]$ as the values of function $y(t^c)$ and its derivative at the collocation points, the relationship between these two vectors can be simply represented by a matrix multiplication as [39]:

$$\frac{dy^{N_c}}{dt^c} = [D]y^{N_c}\,, \tag{95.}$$

$$[D] = D_{ij} := \begin{cases} \frac{P_{N_c}(t_i^c)}{P_{N_c}(t^c{}_j)} \cdot \frac{1}{(t^c{}_i - t^c{}_j)} & i \neq j \\ -\frac{N_c(N_c+1)}{4} & i = j = 0 \\ \frac{N_c(N_c+1)}{4} & i = j = 0 \\ 0 & otherwise \end{cases} \qquad \begin{matrix} i = 0, \dots, N_c \\ j = 0, \dots, N_c \end{matrix} \tag{96.}$$

The same concept can be extended to second-order derivatives as:

$$\frac{d^2y^{N_c}}{dt^{c^2}} = [D]^2 y^{N_c}\,. \tag{97.}$$

As for the derivatives with respect to the physical time t, they should be scaled by a factor of $\left(\frac{2}{t_f - t_o}\right)$:

$$\dot{y}^{N_c} = \frac{dy^{N_c}}{dt} = \left(\frac{2}{t_f - t_o}\right)\frac{dy^{N_c}}{dt^c} = \left(\frac{2}{t_f - t_o}\right)[D]y^{N_c} . \tag{98.}$$

$$\ddot{y}^{N_c} = \left(\frac{2}{t_f - t_o}\right)^2 [D]^2 y^{N_c} . \tag{99.}$$

Similarly, defining a vector of integrals $Y_\tau^{N_c} = \left[\int_{-1}^{t_1^c} y(\tau)dt^c , \dots , \int_{-1}^{t_{N_c}^c} y(\tau)dt^c\right]$, the relationship between this vector and y^{N_c} becomes [40]:

$$Y_\tau^{N_c} = [W]y^{N_c} , \tag{100.}$$

$$[W] = W_{ij} \coloneqq \frac{\omega_i}{2}\left[1 + \tau_j + \sum_{k=1}^{N_c} P_k(t_i^c)\{P_{k+1}(t_j^c) - P_{k-1}(t_j^c)\}\right] \quad \begin{matrix} i = 1, \dots , N_c \\ j = 0, \dots , N_c \end{matrix} . \tag{101.}$$

Where:

$$\omega_i = \int_{-1}^{1} L_i(t^c)d\tau = \frac{2}{N_c(N_c + 1)}\frac{1}{P_{N_c}(t_i^c)^2} . \tag{102.}$$

The time integrals with respect to physical time $\int y\, dt$ can then be inferred as:

$$\int y\, dt = \left(\frac{t_f - t_o}{2}\right)\int y\, dt^c . \tag{103.}$$

6.1.2. Applying Pseudo-spectral optimal control:

Going back to the optimal control problem of Eq. (90), by applying the domain transformation $t \to t^c$, the problem is redefined:

$$\underset{\mathbf{t_o}, \mathbf{t_f}, \mathbf{x(\tau)}, \mathbf{u(\tau)}}{\textbf{minimize}} : J = E\left(t_o, t_f, x(1)\right) + \left(\frac{t_f - t_o}{2}\right)\int_{-1}^{1} F\left(t^c, x(t^c), u(t^c)\right)dt^c$$

$$\textbf{subject to}: \quad \frac{dx(t^c)}{dt^c} = \left(\frac{t_f - t_o}{2}\right) f(x(t^c), u(t^c), t^c) \qquad (system\ dynamics) \tag{104.}$$

$$g^L \le g\left(x(-1), x(1)\right) \le g^U \qquad (boundary\ constraints)$$

$$h^L \le h\left(\tau, x(\tau), x(\tau)\right) \le h^U \qquad (path\ constraints)$$

Applying the interpolation formula in Eq. (92) using the Legendre-Gauss-Lobatto points on the states $x(t^c)$ and controls $u(t^c)$, the entire trajectory can be described by the states and controls at cardinal times t_i^c. Denoting X^{N_c} and U^{Nc} to describe these values as:

$$X^{N_c} = \begin{bmatrix} x(t_0^c)^T \\ x(t_1^c)^T \\ \vdots \\ x\left(\mathrm{t}_{\mathrm{N_c}}^{\mathrm{c}}\right)^T \end{bmatrix}. \tag{105.}$$

$$U^{N_c} = \begin{bmatrix} u(t_0^c)^T \\ u(t_1^c)^T \\ \vdots \\ u\left(\mathrm{t}_{\mathrm{N_c}}^{\mathrm{c}}\right)^T \end{bmatrix}. \tag{106.}$$

The dynamics and constraints of the optimal control problem are then enforced at the cardinal points. To do so, the dynamic equation f can be discretized to f^{N_c} as:

$$f^{N_c}(X^{N_c}, U^{N_c}) = \begin{bmatrix} f(x(t_0^c), u(t_0^c), t_0^c)^T \\ f(x(t_1^c), u(t_1^c), t_1^c)^T \\ \vdots \\ f\left(x\left(\mathrm{t}_{\mathrm{N_c}}^{\mathrm{c}}\right), u\left(\mathrm{t}_{\mathrm{N_c}}^{\mathrm{c}}\right), \mathrm{t}_{\mathrm{N_c}}^{\mathrm{c}}\right)^T \end{bmatrix}. \tag{107.}$$

The same concept can be applied to all the constraints functions.

Taking all the previous steps into consideration, the optimal control problem can finally be transferred into a parameter optimization problem as shown in Eq. (108). The Covector Mapping Principle (CMP) describes the equivalency of this problem with regards to the original optimal control statement [38].

$$\underset{\mathbf{t_o}, \mathbf{t_f}, \mathbf{X^{N_c}}, \mathbf{U^{N_c}}}{\textbf{minimize}} : J = E\left(t_o, t_f, x(1)\right) + \left(\frac{t_f - t_o}{2}\right) \sum_{k=0}^{N_c} F\left(\mathrm{t}_{\mathrm{k}}^{\mathrm{c}}, x(\mathrm{t}_{\mathrm{k}}^{\mathrm{c}}), u(\mathrm{t}_{\mathrm{k}}^{\mathrm{c}})\right) \cdot \omega_k$$

$$\textbf{subject to}: \quad [D]X^{N_c} = \left(\frac{t_f - t_o}{2}\right) f^{N_c}(X^{N_c}, U^{N_c}) \qquad (system\ dynamics) \tag{108.}$$

$$g^L \leq g\left(x(-1), x(1)\right) \leq g^U \qquad (boundary\ constrints)$$

$$h^L \leq h^{N_c}(X^N, U^N) \leq h^U \qquad (path\ constraints)$$

6.2. Trajectory Generation for EMFF torque optimization

Following the preliminaries formulated in the previous section, this section constructs the trajectory optimization problem associated with minimizing angular momentum buildup in EMFF. First, defining vectors $\vec{p}\,(t^c)$ and $\vec{\mu}\,(t^c)$ that concatenate the relative positions and control magnetic moments of all the N spacecrafts of the formations at time t^c as:

$$\vec{p}\,(\tau) = \begin{bmatrix} \vec{p}_1\,(t^c) \\ \vec{p}_2\,(t^c) \\ \vdots \\ \vec{p}_N\,(t^c) \end{bmatrix}, \tag{109.}$$

$$\vec{\mu}\,(\tau) = \begin{bmatrix} \vec{\mu}_1\,(t^c) \\ \vec{\mu}_2\,(t^c) \\ \vdots \\ \vec{\mu}_N\,(t^c) \end{bmatrix}. \tag{110.}$$

To describe the positions and control at all the cardinal or discretization points $\{t^{N_c}: t_0^c, \dots, t_{N_c}^c\}$, matrices P^{N_c} and U^{N_C} are defined as:

$$P^{N_c} = \begin{bmatrix} \vec{p}\,(t_0^c)^T \\ \vec{p}\,(t_1^c)^T \\ \vdots \\ \vec{p}\,\left(t_{N_c}^c\right)^T \end{bmatrix}. \tag{111.}$$

$$U^{N_c} = \begin{bmatrix} \vec{\mu}\,(t_0^c)^T \\ \vec{\mu}\,(t_1^c)^T \\ \vdots \\ \vec{\mu}\,\left(t_{N_c}^c\right)^T \end{bmatrix}. \tag{112.}$$

As described in the previous section, the entire trajectory can then be interpolated from P^{N_c} and U^{N_C}. Concurrently, constraints are enforced at cardinal points as an approximation for the entire trajectory. A matrix function F^{N_c} is introduced to represent the translational dynamics:

$$F^{N_c} = \begin{bmatrix} \left[\vec{a}_M\left(\vec{p}\,(t_0^c), \vec{\mu}\,(t_0^c)\right) + \vec{O}\left(\vec{p}\,(t_0^c), t_0^c\right)\right]^T \\ \left[\vec{a}_M\left(\vec{p}\,(t_1^c), \vec{\mu}\,(t_1^c)\right) + \vec{O}\left(\vec{p}\,(t_1^c), t_1^c\right)\right]^T \\ \vdots \\ \left[\vec{a}_M\left(\vec{p}\,(t_{N_c}^c), \vec{\mu}\,(t_{N_c}^c)\right) + \vec{O}\left(\vec{p}\,(t_{N_c}^c), t_{N_c}^c\right)\right]^T \end{bmatrix}. \tag{113.}$$

Where $\vec{a}_M$ corresponds to accelerations resulting from the electromagnetic forces and $\vec{0}$ corresponds to the orbital dynamics.

The second derivatives of positions at cardinal points are evaluated using matrix multiplication as $[D]^2 P^{N_c}$. Consequently, the system dynamics are enforced by setting the below constraint:

$$[D]^2 P^{N_c} = \left(\frac{t_f - t_o}{2}\right)^2 F^{N_c} . \tag{114.}$$

The scaling factor $\left((t_f - t_o)/2\right)^2$ is important to compensate for the time scaling as presented in Eq. (91).

As for path constraints, they are enforced at each time step independently. The only path constraint considered in this is collision avoidance which is imposed by setting a minimum distance between different satellites at the same time as in Eq. (115):

$$\left\|\vec{p}_i\,(t_k^c) - \vec{p}_j\,(t_k^c)\right\| \geq d_{min} \qquad for \quad \begin{matrix} i = 1, 2, \dots, N \\ j = 1, 2, \dots, N\ , i \neq j\ . \\ k = 0, 1, \dots, N_c \end{matrix} \tag{115.}$$

Boundary Constraints are also applied as in Eq. (116) for initial conditions, Eq. (117) for terminal conditions, and Eq. (118) as a bound on terminal time. Where P_o, P_f, V_o and V_f are the initial and target positions and velocities, and $\vec{v}\,(t^c)$ represents the velocity vector of all spacecrafts at time t^c. The notation $D_{(0,:)}$ and $D_{(N_c,:)}$ symbolize the 0th and N_c rows of the differentiation matrix $[D]$.

$$\begin{gathered} \vec{p}\,(\tau_0 = -1) = P_o \\ \vec{v}\,(\tau_0 = -1) = \left(\frac{t_f - t_o}{2}\right)[D_{(0,:)}]P^{N_c} = V_o \end{gathered} \tag{116.}$$

$$\begin{gathered} P(\tau_f = -1) = P_f \\ V(\tau_f = -1) = \left(\frac{t_f - t_o}{2}\right)[D_{(N_c,:)}]P^{N_c} = V_f \end{gathered} \tag{117.}$$

$$t_f \leq T_{max}\ . \tag{118.}$$

6.2.1. Cost Function Design

A crucial part of designing the optimal trajectory problem is constructing an appropriate cost function that represents the optimality criteria. In this study, the criteria consist of three parts. First, it is intuitive to consider minimizing the overall time of a trajectory. Also, as the pseudo-spectral approach cannot incorporate discontinuities, a control smoothing term must be incorporated in the cost function. Finally, the main optimization criterion for this study is angular momentum buildup. Taking these criteria into account, a cost function can be formulated as:

$$J = \int_{t_o}^{t_f} \left\{1 + \mathrm{w}_1 \, \dot{\vec{\mu}}\,(t)^T \, \dot{\vec{\mu}}\,(t)\right\} dt + w_2 \left\| \int_{t_o}^{t_f} \vec{\tau}\left(\vec{p}\,(t), \vec{\mu}\,(t)\right) dt \right\|^2 . \qquad (119.)$$

The unity term within the first integration corresponds to the time optimality criteria, while the quadratic term $\dot{\vec{\mu}}\,(t)^T \, \dot{\vec{\mu}}\,(t)$ penalizes variations in control. The second part of the cost function integrates electromagnetic torques $\vec{\tau}$ as an indication of angular momentum buildup. Integrating torques does not directly correspond to the angular momentum as it does not account for inertias. Nonetheless, it is a fairly good indicator especially if the rotational inertias of all the spacecrafts are similar. Finally, $[w_1]$ and w_2 are weighting factors that are used to tune the optimality criterion.

Transforming the cost function from physical time t to computational time t^c, it becomes:

$$\begin{aligned} J &= \left(\frac{t_f - t_o}{2}\right) \int_{-1}^{1} \left\{1 + w_1 \left(\frac{2}{t_f - t_o}\right)^2 \dot{\vec{\mu}}\,(t^c)^T \, \dot{\vec{\mu}}\,(t^c)\right\} dt^c \\ &\qquad + w_2 \left(\frac{t_f - t_o}{2}\right)^2 \left\| \int_{-1}^{1} \vec{\tau}\left(\vec{p}\,(t^c), \vec{\mu}\,(t^c)\right) dt^c \right\|^2 \\ &= \left(\frac{t_f - t_o}{2}\right) + w_1 \left(\frac{2}{t_f - t_o}\right) \int_{-1}^{1} \left\{\dot{\vec{\mu}}\,(t^c)^T \, \dot{\vec{\mu}}\,(t^c)\right\} dt^c \\ &\qquad + w_2 \left(\frac{t_f - t_o}{2}\right)^2 \left\| \int_{-1}^{1} \vec{\tau}\left(\vec{p}\,(t^c), \vec{\mu}\,(t^c)\right) dt^c \right\|^2 \; F^I : \{\hat{I}, \hat{J}, \hat{K}\} . \end{aligned} \qquad (120.)$$

Upon discretization following the pseudo-spectral approach, the cost function is modified as:

$$J = \left(t_f - t_o\right) + w_1 \left(\frac{2}{t_f - t_o}\right) \sum_{i=0}^{N_c} \left\{ \dot{\vec{\mu}}\left(t_i^c\right)^T \dot{\vec{\mu}}\left(t_i^c\right) \right\} \cdot \omega_i + w_2 \left(\frac{t_f - t_o}{2}\right)^2 \left\| \sum_{i=0}^{N_c} \vec{\tau}\left(\vec{p}\left(t_i^c\right), \vec{\mu}\left(t_i^c\right)\right) \cdot \omega_i \right\|^2 . \tag{121.}$$

While quite challenging to represent, all the derivative and integrals can be calculated using linear algebra and the guidelines of section 6.1.1.

Taking all into consideration, the trajectory optimization problem to minimize angular momentum buildup in EMFF can be posed as follows:

$$\underset{\mathbf{t_o}, \mathbf{t_f}, \mathbf{x(t^c)}, \mathbf{u(t^c)}}{\textbf{minimize}} : \quad \mathrm{J} = \left(t_f - t_o\right) + w_1 \left(\frac{2}{t_f - t_o}\right) \sum_{i=0}^{N_c} \left\{ \dot{\vec{\mu}}\left(t_i^c\right)^T \dot{\vec{\mu}}\left(t_i^c\right) \right\} \cdot \omega_i + w_2 \left(\frac{t_f - t_o}{2}\right)^2 \left\| \sum_{i=0}^{N_c} \vec{\tau}\left(\vec{p}\left(t_i^c\right), \vec{\mu}\left(t_i^c\right)\right) \cdot \omega_i \right\|^2$$

subject to:

$$[D]^2 P^{N_c} = \left(\frac{t_f - t_o}{2}\right)^2 F^{N_c} \qquad (system\ dynamics)$$

$$P(t_0^c = -1) = P_o$$
$$V(t_0^c = -1) = \left(\frac{t_f - t_o}{2}\right) \left[D_{(0,:)}\right] P^{N_c} = V_o \tag{122.}$$

$$P\left(t_f^c = -1\right) = P_f$$
$$V\left(t_f^c = -1\right) = \left(\frac{t_f - t_o}{2}\right) \left[D_{(N_c,:)}\right] P^{N_c} = V_f$$

$$t_f \leq T_{max} \qquad (boundary\ constraints)$$

$$\left\| \vec{p}_i\left(t_k^c\right) - \vec{p}_j\left(t_k^c\right) \right\| \geq d_{min} \qquad \begin{matrix} i = 1, 2, \dots, N \\ for\ \ j = 1, 2, \dots, N\ , i \neq j \\ k = 0, 1, \dots, N_c \end{matrix} \qquad (path\ constraints)$$

6.2.2. Earth Magnetic Field AMM

Section 3.4 explained an approach for managing the buildup of angular momentum in EMFF using earth's magnetic field. The geomagnetic field was used to generate torques that can desaturate the formation's reaction wheels. This approach can be augmented with trajectory generation to refine the entire angular momentum optimization process and intensify the reduction

in accumulated angular momentum. As such, the trajectory optimization problem needs to be adjusted to take this new integrated technique into account.

The main shortcoming of using earth's magnetic field was that it cannot be used to generate parallel desaturating torques, and thus, cannot counter angular momentum buildup in parallel directions of the geomagnetic field. Therefore, the optimal trajectory generation process is revised to find trajectories that would minimize angular momentum buildup in directions that cannot be undermined using the geomagnetic approach.

First, a vector $B^N(t^c)$ is defined to concatenate the directions of earth's magnetic field at the location of all the N spacecrafts of the formation as follows:

$$B^N(t^c) = \begin{bmatrix} \vec{b}_e\left(t^c, \vec{p}_1\right) \Big/ \left\|\vec{b}_e\left(t^c, \vec{p}_1\right)\right\| \\ \vec{b}_e\left(t^c, \vec{p}_2\right) \Big/ \left\|\vec{b}_e\left(t^c, \vec{p}_2\right)\right\| \\ \vdots \\ \vec{b}_e\left(t^c, \vec{p}_N\right) \Big/ \left\|\vec{b}_e\left(t^c, \vec{p}_N\right)\right\| \end{bmatrix}. \tag{123.}$$

The cost function in Eq. (121) is then modified to only consider angular momentum accumulation parallel to B^{N_c} as follows:

$$\begin{aligned} J = \left(t_f - t_o\right) + w_1 \left(\frac{2}{t_f - t_o}\right) \sum_{i=0}^{N_c} \left\{\dot{\vec{\mu}}\left(t_i^c\right)^T \dot{\vec{\mu}}\left(t_i^c\right)\right\} \cdot \omega_i \\ + w_2 \left(\frac{t_f - t_o}{2}\right)^2 \left[dot\left(B^N\left(t_f^c\right), \sum_{i=0}^{N_c} \vec{\tau}\left(\vec{p}\left(t_i^c\right), \vec{\mu}\left(t_i^c\right)\right) \cdot \omega_i\right)\right]^2 . \end{aligned} \tag{124.}$$

6.3. Testing & results

To examine the effectiveness of trajectory optimization in alleviating the buildup of angular momentum, the concepts presented in this chapter are tested on a four-spacecraft formation in LEO. All the satellites start from different positions and then align in the orbit along-track direction as shown in Figure 38. Exact parameters of the orbit and reconfiguration problem can be seen in Table 17, where the presented relative positions are expressed in the orbital coordinate frame F^O.

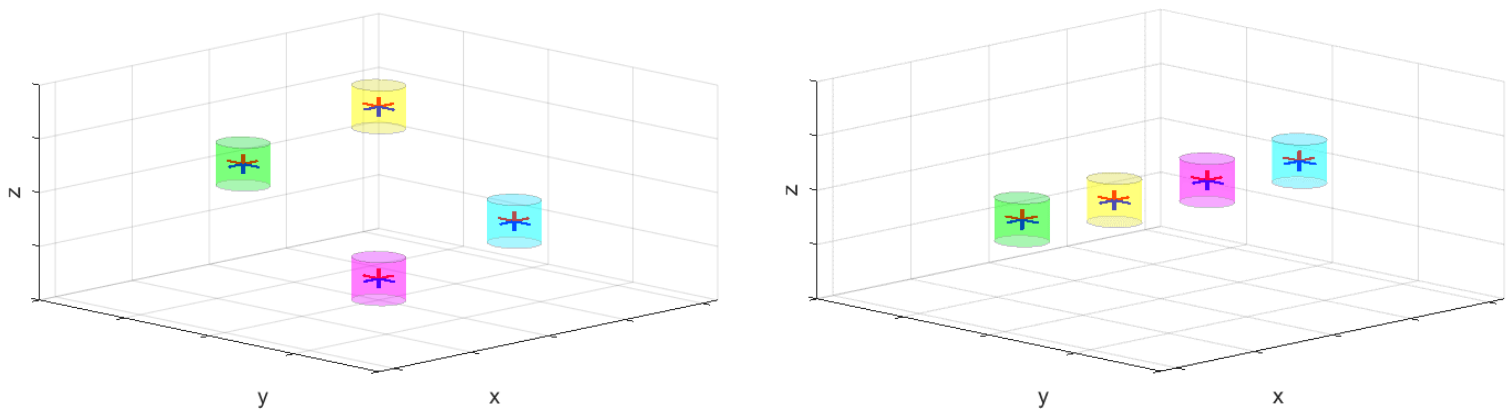

a) Initial configuration b) Final configuration

Figure 38. Initial and final configurations for the trajectory generation problem

Table 17. Parameters for the trajectory generation problem

Orbit Type	Circular LEO
Altitude	900 km
Orbit inclination	0°
Initial relative positions (m)	$p_1 = \{0, -8, 0\}$ $p_2 = \{0, 8, 0\}$ $p_3 = \{0, 0, -8\}$ $p_4 = \{0, 0, 8\}$
Final relative positions (m)	$p_1 = \{9, 0, 0\}$ $p_2 = \{-9, 0, 0\}$ $p_3 = \{3, 0, 0\}$ $p_4 = \{-3, 0, 0\}$

As a benchmark, a straight-line trajectory from starting to terminal positions is considered for each satellite. The optimal trajectory method presented in this chapter is then applied twice. The first time uses the formulation in Eq. (122) which minimizes torque accumulation in all

directions. The second iteration employs the modification in Eq. (124) to incorporate the geomagnetic angular momentum management algorithm. For the cost function, the weighing values were selected as $w_1 = 3 \times 10^{-5}$ and $w_2 = 1.5 \times 10^4$. For both approaches, interpolating polynomials of order $N_C = 10$ were used to approximate states and controls.

The results of the trajectory optimization process are displayed in Figure 39 to Figure 41. Figure 39 shows a 3D plot of the reference trajectories for the three cases. Figure 40 and Figure 41 respectively show x-y and x-z planar views in the orbital coordinate frame.

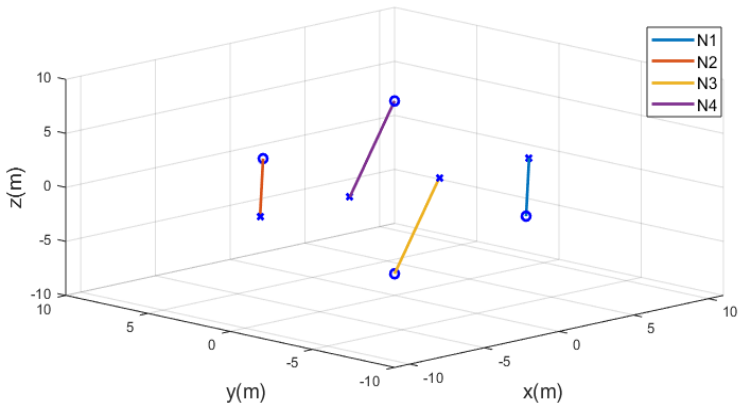

a) Straight line trajectory

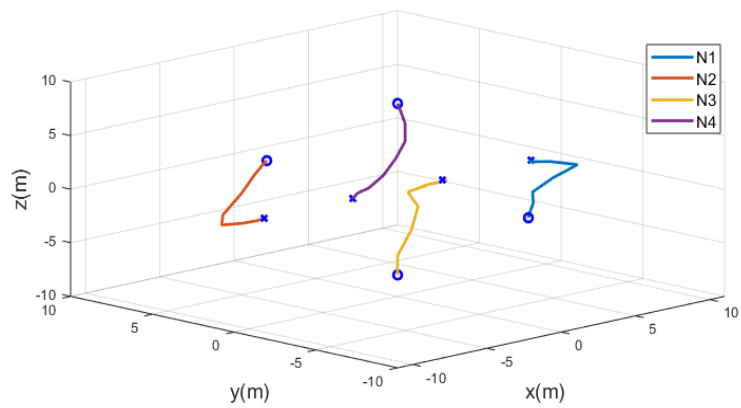

b) Optimal trajectory - 1

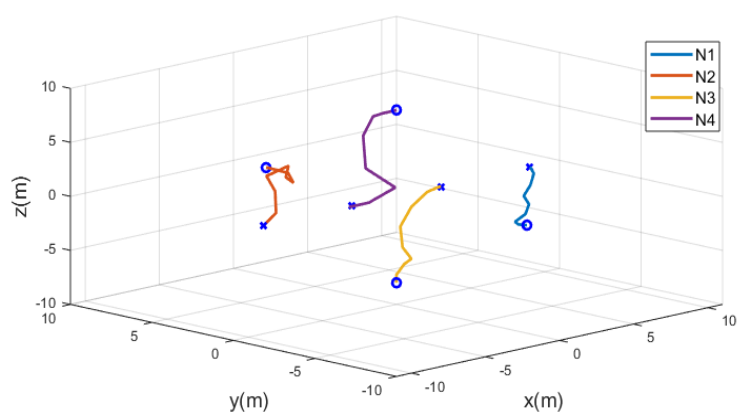

c) Optimal trajectory - 2

Figure 39. 3D view of the results of trajectory optimization

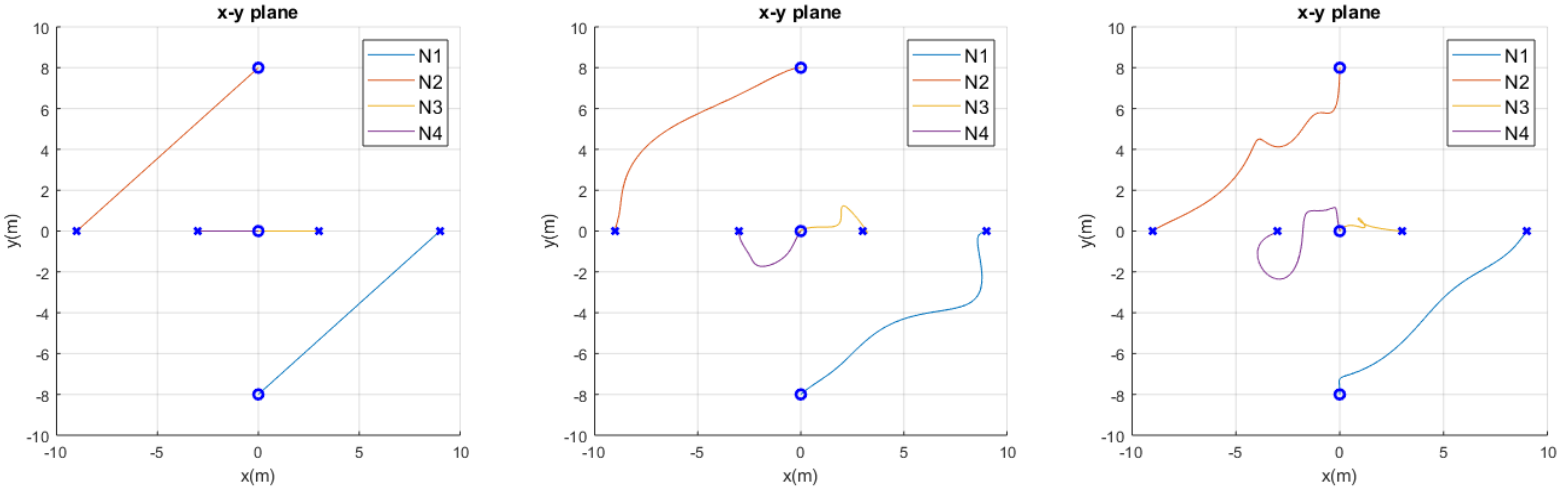

Figure 40. x-y planar view of the results of trajectory optimization

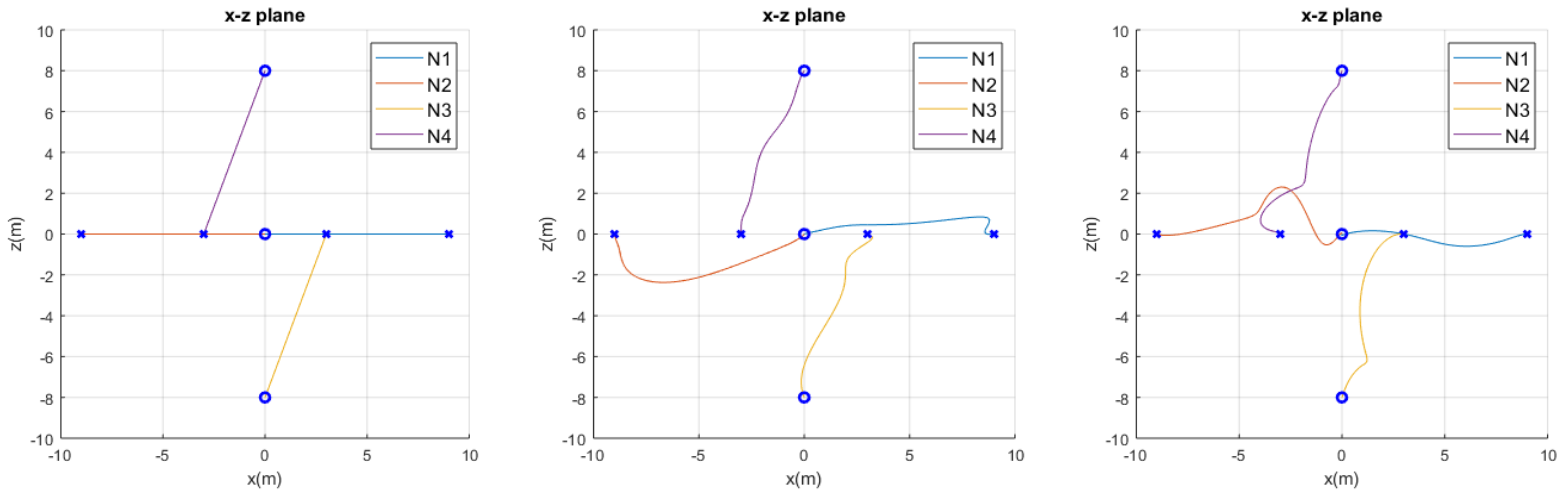

Figure 41. x-z planar view of the results of trajectory optimization

To check the difference in angular momentum accumulation, each of the trajectories was simulated using the guidelines and control policy of chapter 3. Results in terms of relative position and attitude are shown in Figure 42 and Figure 43. For each of the three simulations, satellites eventually converge to the desired final position while maintaining a stable attitude. More importantly for the purpose of this simulation, Figure 44 shows the profile of torques generated on each satellite due to intra-formation electromagnetic interactions. These torques are shown in each satellite's respective body-fixed frame. Subsequently, these torques along with other external torques accumulate in the reaction wheels leading to angular momentum buildup. Figure 45

demonstrates the accumulated angular momentum in the spacecrafts for the three simulation scenarios. It must be noted that the geomagnetic angular momentum managements algorithm of section 3.4 was applied in all the simulations to augment the optimization objectives.

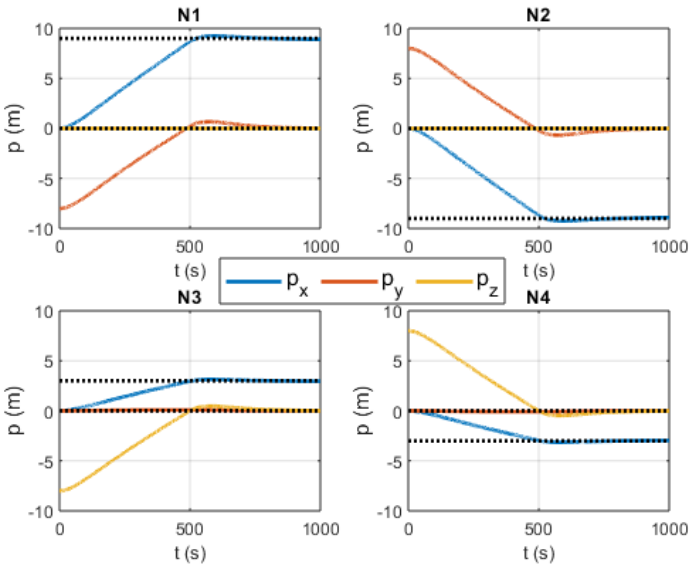

a) Straight line trajectory

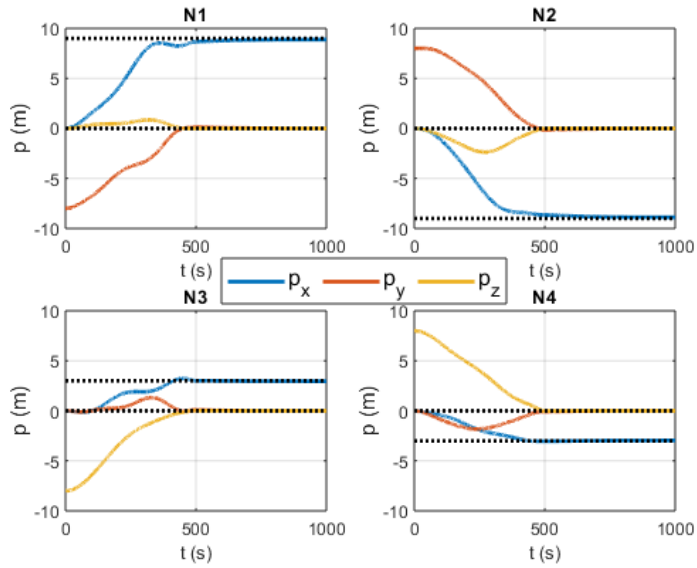

b) Optimal trajectory - 1

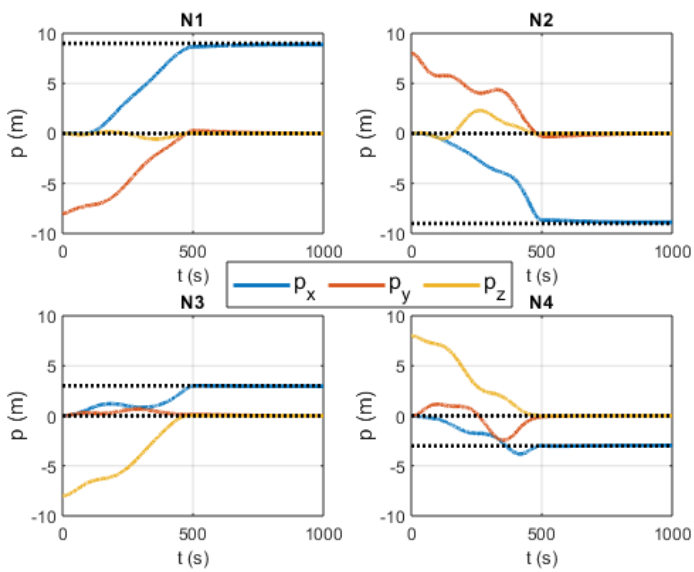

c) Optimal trajectory - 2

Figure 42. Simulation results for the optimal trajectories – relative position

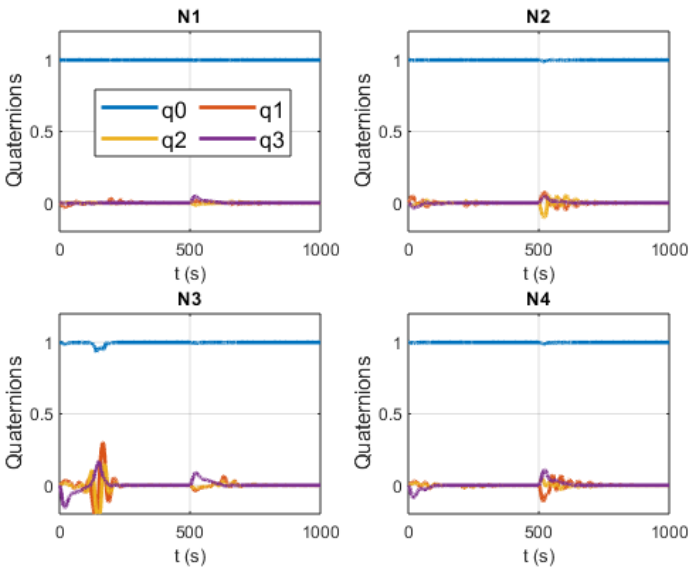

a) Straight line trajectory

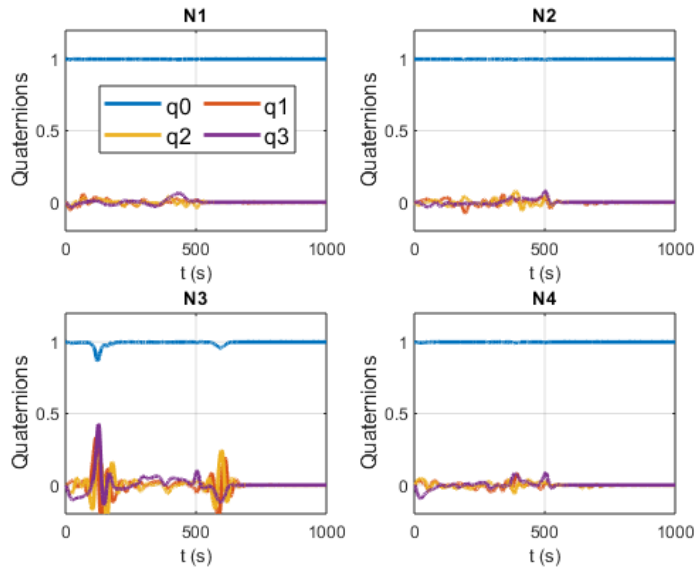

b) Optimal trajectory - 1

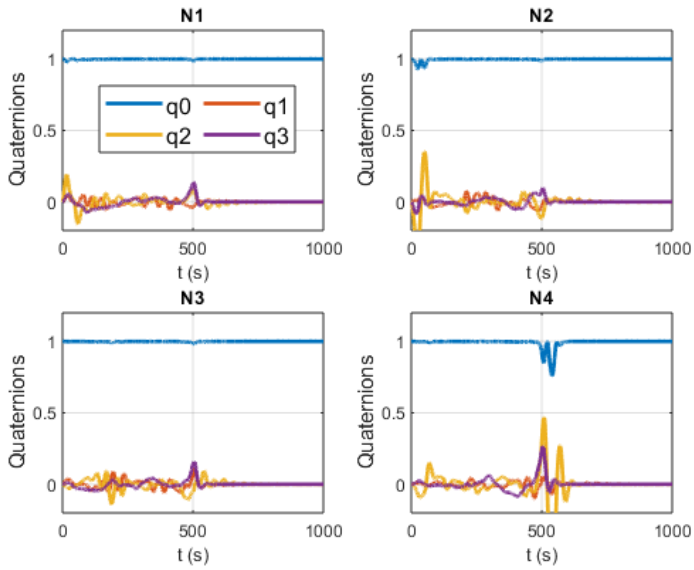

c) Optimal trajectory - 2

Figure 43. Simulation results for the optimal trajectories – attitude

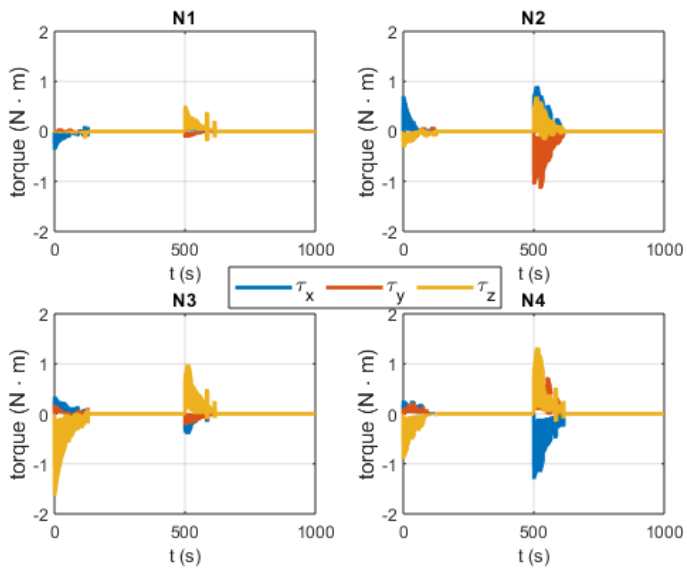

a) Straight line trajectory

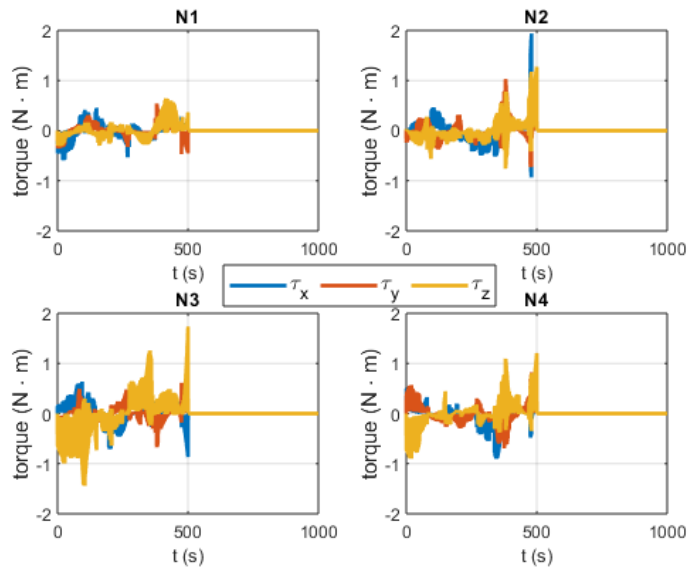

b) Optimal trajectory - 1

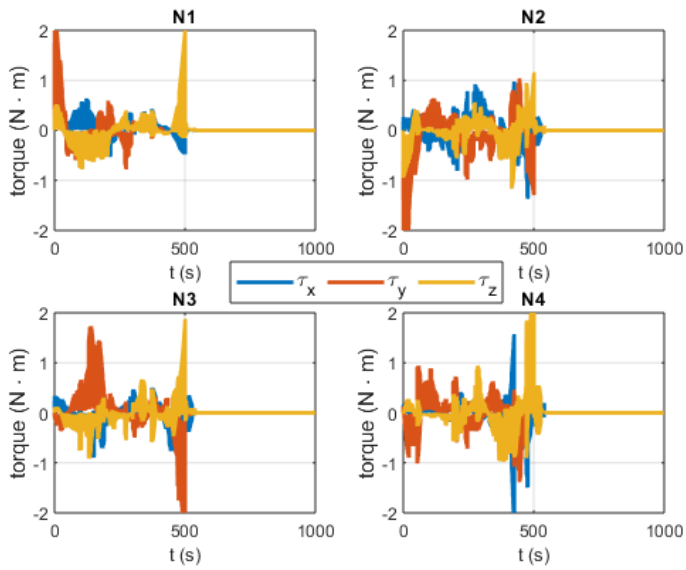

c) Optimal trajectory - 2

Figure 44. Simulation results for the optimal trajectories – electromagnetic torques

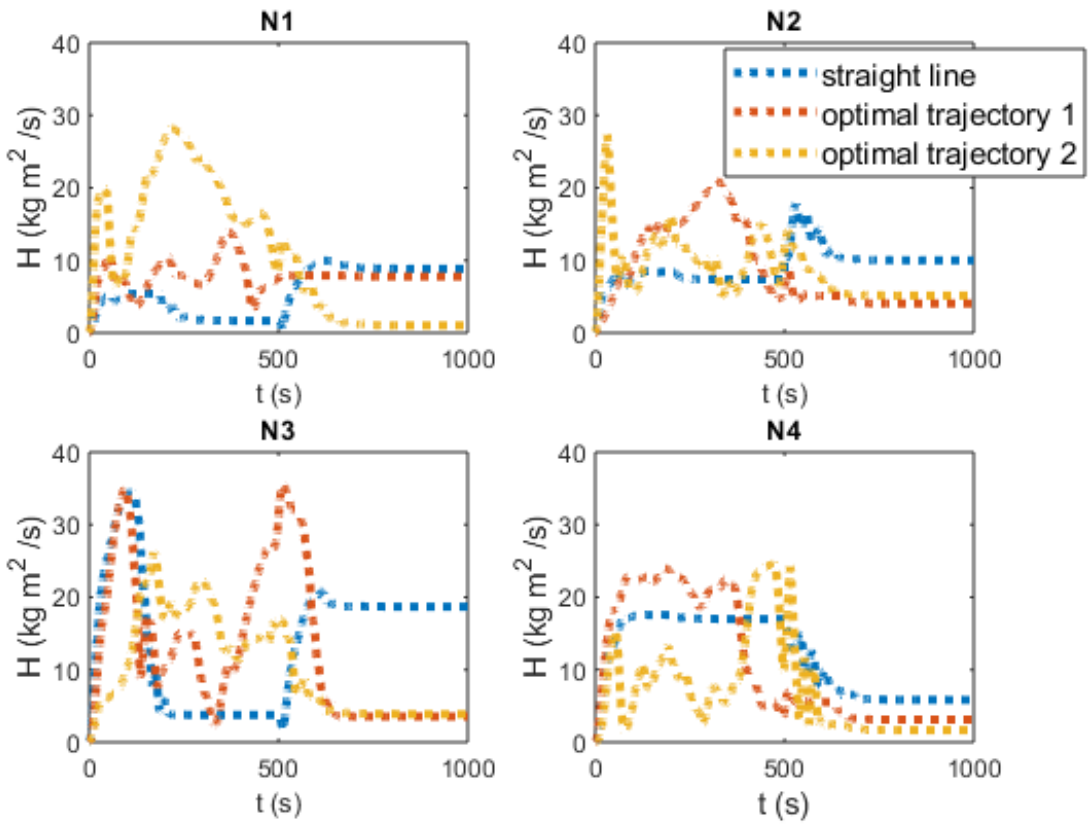

Figure 45. Comparison of angular momentum accumulation between three trajectories

Table 18. Terminal reaction wheel's angular momentum for three trajectories

Spacecraft:		**N1**	**N2**	**N3**	**N4**	**Total**
Terminal Angular Momentum ($\mathbf{kg \cdot m^2/s}$):	**- Straight-line trajectory**	8.84	10.00	18.70	5.83	43.38
	- Optimal trajectory - 1	7.75	4.03	3.53	3.12	18.45
	- Optimal trajectory - 2	1.02	5.15	3.88	1.68	11.72

As observed in the above figures, the accumulated angular momentum for all spacecrafts falls considerably for the optimized trajectories. This validates the idea that paths and trajectories significantly affect the rotational behavior in EMFF due to the dependency of electromagnetic torques on separation distances. Furthermore, angular momentum is further reduced when external

factors such as the geomagnetic field are taken into account in the design of trajectories, as indicated by the yellow lines of Figure 45. For easier comparison, Table 18 shows the angular momentum at terminal time for the three scenarios. The total angular momentum falls to less than the third when optimal trajectories are adopted. Therefore, it can be inferred that enhanced trajectory design effectively reduces torque accumulation and alleviates reaction wheel saturation problems.

Table 19. Angular momentum buildup results with trajectory optimization for several reconfiguration problems

Simulation Case:		**1**	**2**	**3**
Initial Relative Positions (m):		$p_1 = \{-8, 0, 0\}$ $p_2 = \{8, 0, 0\}$ $p_3 = \{0, 0, -8\}$ $p_4 = \{0, 0, 8\}$	$p_1 = \{-8, 0, 0\}$ $p_2 = \{8, 0, 0\}$ $p_3 = \{0, -8, 0\}$ $p_4 = \{0, 8, 0\}$	$p_1 = \{-8, 0, 0\}$ $p_2 = \{8, 0, 0\}$ $p_3 = \{0, 0, -8\}$ $p_4 = \{0, 0, 8\}$
Final Relative Positions (m):		$p_1 = \{0, -8, 0\}$ $p_2 = \{0, 8, 0\}$ $p_3 = \{-8, 0, 0\}$ $p_4 = \{8, 0, 0\}$	$p_1 = \{0, -8, 0\}$ $p_2 = \{0, 8, 0\}$ $p_3 = \{8, 0, 0\}$ $p_4 = \{-8, 0, 0\}$	$p_1 = \{0, 9, 0\}$ $p_2 = \{0, -9, 0\}$ $p_3 = \{0, 3, 0\}$ $p_4 = \{0, -3, 0\}$
Terminal Total Angular Momentum ($\mathbf{kg \cdot m^2/s}$):	**- Straight-line trajectory**	49.28	36.32	26.54
	- Optimal trajectory - 1	23.43	24.44	28.17
	- Optimal trajectory - 2	21.63	19.77	18.56

In order to further authenticate the concept, the proposed trajectory optimization approaches were tested for several other formation reconfiguration problems. The results for three additional cases are presented in Table 19. The first case reconfigures the formation into the orbital plane, the second performs a simple maneuver in the orbital plane, and the final one aligns the satellites in the orbit radial direction. For all the tested cases, trajectory optimization can effectively reduce the total accumulated angular momentum. However, the extent of this reduction differs from case to case. For instance, in the previous detailed example and in case 1 of Table 19, the minimization in angular momentum is substantial compared to the other two cases. Moreover, the differences between the two trajectory techniques of Eq. (122) and (124) differ based on the specific scenario. The second trajectory optimization approach always reduces angular buildup,

but the same does not apply to the first approach as manifested in case 3. That is because the first approach does not incorporate external torques in the trajectory generation process, and thus cannot fully represent the simulated dynamics of the formation.

Chapter 7. Conclusion

7.1. Summary & Results

Developing fully propellant-less means of controlling satellite formations is a key research area for expanding the applicability of formation flying technologies. Electromagnetic Formation Flying (EMFF) is at the forefront of achieving this propellant-less goal by harnessing intra-formation magnetic interactions. This study aimed to employ the concept of modulating magnetic fields along with enhanced guidance and control techniques to improve EMFF operation with regards to three criteria:

- EMFF control under minimal availability of superconducting electromagnets.
- Preventive thermal management of EMFF electromagnets.
- Angular momentum management for EMFF.

Chapter 2 reviewed the equations of motion associated with EMFF. Chapter 3 utilized these equations to develop effective control strategies for the relative motion of satellites in an orbiting formation. Chapter 4 tackled the first main objective of this study by investigating the use of the phase and frequency modulation in controlling formations under the reduction or fault of several electromagnets. Chapter 5 also took benefit of modulation and augmented it with numerical optimization methods; to optimize magnetic interactions and alleviate the problems of heating and angular momentum buildup. Chapter 6 adopted a different approach to EMFF angular momentum management in which optimal trajectory generation was examined to minimize torque accumulation during formation reconfiguration.

For all the aforementioned conceptions, closed-loop simulations were carried out to analyze their validity. All in all, simulation results demonstrate the appropriateness of the proposed ideas in targeting this study's objectives and show their potential in enhancing EMFF performance. While it is challenging to prove the absolute efficacy of the suggested approaches for all possible EMFF configurations, the promising results obtained in this study identify the potential of these approaches in being key contributions towards the fully propellant-less formation ambition.

7.2. Future Work

Despite being tested with simple experiments, the bulk the work on EMFF is still at a conceptual level that requires experimental verification prior to functional deployment. The same applies to the work presented in this thesis. Developing a 2D EMFF testbed to test the application of magnetic fields' modulation in the formation guidance and control processes would, without doubt, enforce the results obtained from simulation. Needless to say, new complexities would arise when considering an experimental setup. Most notably, the operation and thermal management of HTS electromagnets in addition to dynamic model uncertainties would represent major challenges to any hardware implementation of EMFF.

Furthermore, a lot of factors contribute to the behavior of an electromagnetic formation. Aspects like the number of satellites, formation geometry, and the reference orbit can all play a role in the effectiveness of the ideas proposed in this thesis. This study focused on cases with some intuitive configurations for formation flying missions and obtained very promising results. Nonetheless, there is still an almost infinite number of possible EMFF cases, some of which might exhibit different results and require further inspection. Unfortunately, it would be very challenging for any study to consider and evaluate all the potential configurations. Therefore, for any follow up work that would utilize this study's concepts, it would be more feasible to first define a limited scope of configurations based on specific mission requirements prior to evaluating the appropriateness of the suggested methods.

Publications List

- A. Ayyad and T. Hashimoto, Phase and Frequency Modulation of Alternating Magnetic Moments for Electromagnetic Formation Flying, International Symposium on Space Technology and Science, 2019-d-033, 2019.

- A. Ayyad and T. Hashimoto, Optimal Trajectory Generation for Electromagnetic Formation Flying, 29th. Workshop on Astrodynamics and Flight Mechanics, A-15, 2019. (to be published)

References

[1] S. Chung, S. Bandyopadhyay, R. Foust., G. Subramanian and F. Hadaegh, "Review of Formation Flying and Constellation Missions Using Nanosatellites," *Journal of Spacecraft and Rockets,* vol. 53, no. 3, pp. 567-578, 2016.

[2] G. D. Mauro, M. Lawn and R. Bevilacqua, "Survey on Guidance Navigation and Control Requirements for Spacecraft Formation-Flying Missions," *Journal of Guidance, Control, and Dynamics,* vol. 41, no. 3, pp. 581-602, 2018.

[3] G. Skinnr, B. Dennis, J. Krizmanic and E. Kontar, "Science enabled by high precision inertial formation flying," *International Journal of Space Science and Engineering,* vol. 1, no. 4, pp. 331-348, 2013.

[4] European Space Agency, "About Proba-3," [Online]. Available: https://m.esa.int/Our_Activities/Space_Engineering_Technology/Proba_Missions/About_Proba-3. [Accessed 09 08 2019].

[5] P. R. Lawson, O. P. Lay, K. J. Johnston and C. A. Beichman, "Terrestrial Planet Finder Interferometer Science Working Group Report," Jet Propulsion Laboratory , Pasadena, California, 2007.

[6] European Space Agency, "XEUS 2 Fact Sheet," [Online]. Available: http://sci.esa.int/xeus-2/31591-fact-sheet/. [Accessed 09 09 2019].

[7] Nanosats Database, "AAReST MirrorSat 1," [Online]. Available: https://www.nanosats.eu/sat/aarest-mirrorsat1. [Accessed 09 08 2019].

[8] V. Kapila, S. A. J, J. M. Buffington and Q. Yan, "Spacecraft Formation Flying: Dynamics and Control," *Journal of Guidance, Control, and Dynamics,* vol. 23, no. 3, pp. 561-564, 2000.

[9] R. C. Foust, Y. K. Nakka, A. Saxena, S. Chung and F. Hadaegh, "Automated Rendezvous and Docking Using Tethered Formation Flight," in *9th International Workshop on Satellite Constellations and Formation Flying*, Boulder, Colorado, USA, 2017.

[10] D. Jones and H. Schaub, "Collinear Three-Craft Coulomb Formation Stability Analysis and Control," *Journal of Guidance, Control, and Dynamics,* vol. 37, no. 1, pp. 224-232, 2014.

[11] S. Tsujii, M. Bando and H. Yamakawa, "Spacecraft Formation Flying Dynamics and Control Using the Geomagnetic Lorentz Force," *Journal of Guidance, Control, and Dynamics,* vol. 36, no. 1, pp. 136-148, 2013.

[12] Y. Lvovsky, E. W. Stautner and T. Zhang, "Novel technologies and configurations of superconducting magnets for MRI," *Superconductor Science and Technology,* vol. 26, no. 9, p. 093001, 2013.

[13] M. Ono, S. Koga and H. Ohtsuki, "Japan's superconducting Maglev train," *IEEE Instrumentation & Measurement Magazine,* vol. 5, no. 1, pp. 9-15, 2002.

[14] S. Sakai, R. Kaneda, H. Saito and T. Hashimoto, "Electromagnetic formation flight for LEO satellites," in *Proceedings of the 17th Workshop on JAXA Astrodynamics and Flight Mechanics*, Sagamihara, Kanagawa, Japan, 2008.

[15] D. Kwon, "Propellantless formation flight applications using electromagnetic satellite formations," *Acta Astronautica*, vol. 67, no. 9-10, pp. 1189-1201, 2010.

[16] S. Schweighart, "Electromagnetic Formation Flight Dipole Solution Planning, Ph.D. Thesis," Massachusetts Inst. of Technology, 2005.

[17] L. Elias, D. Kwon, R. Sedwick and D. Miller, "Electromagnetic Formation Flight Dynamics Including Reaction Wheel Gyroscopic Stiffening Effects," *Journal of Guidance, Control, and Dynamics*, vol. 30, no. 2, pp. 499-511, 2007.

[18] U. Ahsun, "Dynamics and Control of Electromagnetic Satellite Formations, Ph.D. Thesis," Massachusetts Inst. of Technology, 2007.

[19] H. Huang, Y. Zhu, L. Yang and Y. Zhang, "Stability and shape analysis of relative equilibrium for three-spacecraft electromagnetic formation," *Acta Astronautica*, vol. 94, no. 1, pp. 116-131, 2014.

[20] J. Zhang, C. Yuan, D. Jiang and D. Jin, "Adaptive Terminal Sliding Mode Control of Electromagnetic Spacecraft Formation Flying in Near-Earth Orbits," *Advances in Mechanical Engineering*, vol. 6, pp. 512-583, 2014.

[21] D. Kwon, R. Sedwick, S. Lee and J. Ramirez-Riberos, "Electromagnetic Formation Flight Testbed Using Superconducting Coils," *Journal of Spacecraft and Rockets*, vol. 48, no. 1, pp. 124-134, 2011.

[22] A. Porter, D. Alinger, R. Sedwick, J. Merk, R. Opperman, A. Buck, G. Eslinger, P. Fisher, D. Miller and E. Bou, "Demonstration of Electromagnetic Formation Flight and Wireless Power Transfer," *Journal of Spacecraft and Rockets*, vol. 51, no. 6, pp. 1914-1623, 2014.

[23] M. Neave, "Dynamic and Thermal Control of an Electromagnetic Formation Flight Testbed, Ph.D. Thesis," Massachusetts Inst. of Technology, 2003.

[24] J. Schwartz, "Quench in high temperature superconductor magnets," in *Workshop on Accelerator Magnet, Superconductor, Design and Optimization*, Geneva, Switzerland, 2013.

[25] A. Buck, "Path Planning and Position Control and of an Underactuated Electromagnetic Formation Flight Satellite System in the Near Field, Master's Thesis," Massachusetts Institute of Technolog, 2013.

[26] C. Zhang and X. Huang, "Angular-Momentum Management of Electromagnetic Formation Flight Using Alternating Magnetic Fields," *Journal of Guidance, Control, and Dynamics*, vol. 39, no. 6, pp. 1292-1302, 2016.

[27] Y. Zhang, L. Yang, Y. Zhu, H. Huang and W. Cai, "Angular-Momentum Management of Spacecraft Electromagnetic Docking Considering the Earth's Magnetic Field," *Journal of Guidance, Control, and Dynamic*, vol. 36, no. 3, p. 860–869, 2013.

[28] R. Youngquist, M. Nurge and S. Starr, "Alternating Magnetic Field Forces for Satellite Formation Flying," *acta astronautica*, vol. 84, pp. 197-205, 2013.

[29] S. A. Schweighart and R. J. Sedwick, "High-Fidelity Linearized J Model for Satellite Formation Flight," *Journal of Guidance, Control, and Dynamics,* vol. 25, no. 6, pp. 1073-1080, 2002.

[30] H. Schaub and J. Junkins, Analytical Mechanics of Space Systems, Reston, Virginia, USA: American Institute of Aeronautics and Astronautics, 2002.

[31] S. Poedts and H. Goedbloed, Principles of Magnetohydrodynamics: With Applications to Laboratory and Astrophysical Plasmas, Cambridge: Cambridge University Press, 2004.

[32] R. Kristiansen and P. J. Nicklasson, "Spacecraft formation flying: A review and new results on state feedback control," *Acta Astronautica,* vol. 65, p. 1537–1552, 2009.

[33] R. Mukherjee and D. Chen, "Asymptotic Stability Theorem for Autonomous Systems," *Journal of Guidance, Control, and Dynamics,* vol. 16, pp. 961-963, 1993.

[34] M. Kelly, "An Introduction to Trajectory Optimization: How to Do Your Own Direct Collocation," *SIAM Review,* vol. 59, no. 4, pp. 849-904, 2017.

[35] G. Huntington and A. Rao, "Optimal Reconfiguration of Spacecraft Formations Using the Gauss Pseudospectral Method," *JOURNAL OF GUIDANCE,CONTROL, AND DYNAMICS,* vol. 31, no. 3, pp. 689-698, 2008.

[36] B. Wu, D. Wang, E. Poh and G. Xu, "Nonlinear Optimization of Low-Thrust Trajectory for Satellite Formation: Legendre Pseudospectral Approach," *Journal of Guidance, Control, and Dynamics,* vol. 32, no. 4, pp. 1371-1381, 2009.

[37] D. Garg, M. Patterson, W. Hager, A. Rao, D. Benson and G. Huntington, "An overview of three pseudospectral methods for the numerical solution of optimal control problems," *Advances in the Astronautical Sciences,* vol. 135, pp. 1-17, 2009.

[38] M. Ross and M. Karpenko, "A review of pseudospectral optimal control: From theory to flight," *Annual Reviews in Control,* vol. 36, no. 2, pp. 182-197, 2012.

[39] G. Elnagar, M. Kazemi and M. Razzaghi, "The Pseudospectral Legendre Method for Discretizing Optimal Control Problems," *IEEE Transactions on Automatic Control,* vol. 40, no. 10, pp. 1793-1796, 1995.

[40] O. Axelsson, "Global integration of differential equations through Lobatto quadrature," *BIT,* vol. 4, no. 2, pp. 69-86, 1964.